GENOMICS-GUIDED PERSONALIZED MEDICINE IN THE TREATMENT OF COMPLEX CANCER PHENOTYPES

by

Nader N. El-Chaar

A dissertation submitted to the faculty of
The University of Utah
in partial fulfillment of the requirements for the degree of

Doctor of Philosophy

Department of Oncological Sciences

The University of Utah

December 2014

The University of Utah Graduate School

STATEMENT OF DISSERTATION APPROVAL

The dissertation of **Nader N. El-Chaar**

has been approved by the following supervisory committee members:

Andrea Bild	, Chair	**10.03.2014** Date Approved
Philip Moos	, Member	**10.03.2014** Date Approved
Adam Cohen	, Member	**10.03.2014** Date Approved
Donald Ayer	, Member	**10.03.2014** Date Approved
Rodney Stewart	, Member	**10.03.2014** Date Approved

and by **Bradley R Cairns** , Chair/Dean of the Department/College/School of **Oncological Sciences**

and by David B. Kieda, Dean of The Graduate School.

ABSTRACT

Complex cancer phenotypes are defined by their aggressive nature and lack of known or accessible therapeutic targets. My dissertation focuses on the use of a personalized medicine approach for the identification of novel therapies against two complex cancer phenotypes: Basal-like/Claudin-low breast cancer and RAS-active nonsmall cell lung cancer.

RAS-active cancer is characterized by the activation of the complex signaling network of RAS, which lacks effective therapeutics capable of inhibiting the RAS protein itself or the overall pathway. Further complicating treatment is the ability of the RAS pathway to be activated independent of the presence of an activating mutation in the RAS protein. To broadly characterize pathway activation independent of RAS protein mutation, I used a gene-expression-based biomarker for RAS network activity in nonsmall cell lung cancer (NSCLC) cell lines, and identified RAS activation in both RAS-mutant and wild-type lines. I then screened for drugs whose efficacy significantly correlated to RAS network activity and showed that EGFR and MEK co-inhibition is an effective treatment personalized against RAS-active NSCLC. Finally, I demonstrated that EGFR and MEK co-inhibition induced apoptosis and blocked both EGFR-RAS-RAF-MEK-ERK and EGFR-PI3K-AKT-RPS6 nodes simultaneously in RAS-active, but not RAS-inactive NSCLC.

Secondly, I identified a novel compound effective against Basal-like and Claudin-low breast cancer (BL-CL). BL-CL is a molecular subtype of breast cancer characterized by an aggressive, recurrent and nonluminal nature, epitomized by the lack of known therapeutic targets and poor patient prognosis. Using high-

throughput screening of a marine invertebrate compound library and sequential purification of crude fractions, I identified a previously uncharacterized sulfated sterol, Topsentinol L Trisulfate (TLT), purified from a marine sponge, and showed that it inhibits AMPK and CHK1 but activates p38. Furthermore, I indentified the potential use of known AMPK and CHK1 inhibitors, alone or in combination, as an effective therapy against BL-CL. Lastly, sensitivity to TLT was projected against various human tumors by generating a gene-expression signature that predicted breast and bladder cancer as the cancer types most receptive to TLT therapy.

This work describes the identification of novel treatments personalized against BL-CL and RAS-active NSCLC, providing a framework for future pre-clinical studies.

“Luck’s the word those with poor hearts use for ka...” - Stephen King

TABLE OF CONTENTS

LIST OF TABLES

ACKNOWLEDGEMENTS

Graduate school is an all-encompassing endeavor. It pushes you to the limit spiritually, emotionally and physically. It would have been impossible for me to get through it without the wonderful support of friends, mentors and colleagues. I would have not had the confidence in myself to make it through to the end were it not for the unwavering support from Raya Saab. I was blessed to have had my first scientific experience in your lab. You took me in when I didn't know how to use a pipette, and taught me everything firsthand. The support, encouragement and the unwavering belief you have in me helped me push through this PhD. I am also grateful for Andrea Bild; I consider you my friend as much as my mentor. You constantly pushed me to my limits, making me dig deep to find out that I can achieve a lot more than I thought I could. I am forever thankful for letting me express myself scientifically, allowing me to challenge your thoughts and ideas with my own. Philip Moos, whom I considered my second mentor; I have learned so much from you over the years and you have been a constant source of support for me. I also want to acknowledge Adam Cohen, who always brought a much-needed clinical aspect to my research. Thank you for letting me have a firsthand experience in an oncology clinic shadowing you for a year. I learned so much from you; it was one of the highlights of my graduate education. Anthea Letsou and the HHMI Med-to-Grad program; I loved every minute of it and became a much better translational scientist because of it. My committee members, past and present: Rodney Stewart, Donald Ayer, Riccardo Baron, David Jones; thank you for your input. My labmates throughout the years, you've made this experience a lot easier.

Stephen Piccolo, I cannot thank you enough for all the computational help you have given me. Mumtahena Rahman, you are so kind and supportive I never felt like I was suffering through anything alone. Laurie Jackson, thank you for all the experimental advice you have given me over the years, and all the delicious cakes you have made! Shelley Macneil, your happy and relaxed attitude that you brought really helped to change the mood of the lab.

I want to dedicate this paragraph to my family, who had to bare the pain of having a member thousand of miles away. My wonderful mother, Mary El-Chaar; I decided to become a scientist because of you. It all started back when I was in fourth grade when you told me that I would make an excellent scientist. Your foresight has made me the person I am today, and I am forever grateful for the sacrifices you have made; I know it wasn't easy for you to let me go. My father, Nassib El-Chaar, who is the most hardworking and loving person I know in this entire world. I remember one day when you told me you were selling your beloved Range Rover to pay for my high school fees. I will never forget that, and I vow to buy you a brand new Range Rover one day. My siblings, who I always wanted to make proud with my work. My best friends, Majed El Saadi and Nour Halabi; you were always there to cheer me up. My grandfather, the rock of the family; I owe so much to you. You put me through college, and you are always there when I need you. My grandmother, Salwa El-Chaar; you hold an everlasting special place in my heart. Every time I hear your voice on the phone, I feel like I don't have a worry in the world. Last but not least, Laura "Lalis" Castillo. Thank you for putting up with years and years of my moodiness following bad days in lab. I would not have been able to complete this PhD without your loving support. You never ceased to put things into perspective and give me the push I needed. Your unwavering belief in my abilities and your confidence in me were at times the one thing that kept me going. You have made me a better person spiritually, emotionally and intellectually.

CHAPTER 1

INTRODUCTION

1.1 Overview

My dissertation work investigates the use of personalized medicine in the treatment of complex cancer phenotypes. I identify two separate therapies personalized against RAS-active nonsmall cell lung cancer and Basal-like/ Claudin-low breast cancer. As such, my dissertation necessitates an introduction to personalized medicine and its application in cancer therapy and research. Afterwards, I introduce the first complex phenotype addressed in my dissertation, RAS-active NSCLC, by discussing lung cancer epidemiology and subtypes, while linking the RAS pathway to the complicated pathology and treatment difficulty. Lastly, I provide the necessary background on Basal-like and Claudin-low breast cancer (BL-CL), the second complex cancer phenotype addressed in my dissertation work. I provide the reader with the necessary information on breast cancer epidemiology, the different subtypes of the cancer, and a section focusing on BL-CL, as well as the proteins and pathways targeted and discussed in Chapter 3. The following introduction provides the reader with a framework in which to discuss the necessity of novel therapeutic treatment against these cancer phenotypes. This facilitates a transition to the importance of personalized medical approaches in cancer drug discovery and the findings in Chapters 2 and 3, highlighting the purpose of my dissertation work.

1.2 Personalized Medicine in Cancer

Personalized medicine is a vague term that has been subjected to an evolving definition with the changing landscape of clinical practice and research [1]. The United States National Institutes of Health (NIH), as well as the Food and Drug Administration (FDA) view it as the capacity to use the genetic or genomic profile of an individual to guide medical decisions in regards to the prevention, diagnosis, and treatment of diseases [2]. However, it is becoming readily apparent

that personalized medicine is not exclusively attributed to patient individuality. Instead, personalized medicine refers to the idea that molecular information optimizes the accuracy with which patients are categorized and treated [3]. It describes the medical method of classifying individuals into subpopulations based on patient similarities in susceptibility to a particular disease or response to a particular treatment. Therefore, the impact of personalized medicine depends on molecular biomarkers that classify patients to such subpopulation [1-4]. Thus, it can be argued that personalized medicine is in fact a misnomer. Genome or precision medicine, are two terms that encompass the current practice of incorporating genomic information to guide precise medical intervention [3,4].

The ultimate goal of personalized medicine is to provide the most effective treatment to the right person at the right time, based on molecular assessment of guidance towards precise treatment strategy [1-4]. This is particularly important in the treatment of cancer, due to the highly heterogeneous and genomically diverse nature of the disease that leads to cancer-distinct differences in clinical behavior and treatment response [5-8]. Central to incorporating personalized medicine in oncology is the acceptance of cancer as a collective phenotypic consequence of somatically acquired genetic, genomic and epigenetic modifications. Fortunately, with the collaborative consortiums like The Cancer Genome Atlas (TCGA) leading the cataloguing process of cancer genomic alternations in patient samples, it has become a feasible option [9,10]. It is expected that the generation of such comprehensive catalogs of somatic alterations and changes in epigenetic and transcriptional states in cancer genomes will improve our capacity to tailor and guide the development of therapeutics against the proper patient subpopulation. The incorporation of personalized medicine in cancer can no longer be considered a fantasy. It is now a realistic option for cancer therapy [2,3,8,10]. Work documented in this dissertation explores the personalization of novel compounds and clinically-

available drugs against particular molecular subtypes of breast and lung cancer. Such work would not have been possible without the advent of cancer genomics.

1.2.1 Cancer Genomics: The Guide for Personalized Medicine

The fundamental role of the genome in cancer development and progression first became apparent in the studies performed by David von Hansemann and Theodor Boveri. In the late nineteenth and early twentieth centuries, they discovered that dividing cancer cells showed peculiar chromosomal aberrations. This finding culminated in the proposal that cancer is a result of aberrant clones of cells, caused by abnormalities of hereditary material. Further studies identified DNA as the molecular substrate of inheritance, leading to the seminal discovery of the genomic nature of cancer [11]. However, due to the inherent genomic diversity of cancer, the changes involved in the molecular landscape of the disease are variable and numerous. Therefore, a systematic approach to catalogue such changes in the genome of the cancer cell was required to provide a more detailed understanding of the molecular nature of cancer [12].

With the availability of the human genome sequence, the field of cancer genomics emerged to investigate large-scale molecular differences between normal and cancer cells [12]. Cancer genomics involves the systematic analysis of the cancer cell genome with the purpose of describing recurrent aberrations in specific cancer types on a genetic or pathway level [9,10,12]. Such studies are required to address the molecular heterogeneity arising within histology-specified cancer types that add further complexity to the observed differences in clinical behavior and treatment response. More importantly, the successful incorporation of personalized medicine to cancer therapy predicated the identification of molecular biomarkers that classify tumors based on their ability to respond to a particular treatment. Therefore, knowledge of the molecular profile of cancer is necessary to

understand cancer behavior and guide selection of therapy for the patient [8,10,12]. This is possible through the use of cancer genomics.

Cancer genomics describes the molecular landscape of tumors. This information can then be incorporated into personalized medical approaches to identify molecular changes that can predict patient outcome, and provide information on treatment sensitivity. Chapter 2 and 3 describes the utilization of cancer genomics to classify breast and nonsmall cell lung cancer (NSCLC) into molecular subtypes, with the purpose of identifying personalized treatment options. Cancer genomics has been successfully integrated in various personalized medical approaches in the context of cancer prevention, treatment optimization, and patient prognosis prediction, as described in the next section.

1.2.2 Personalized Medicine Approaches in Cancer

Genomics permitted access into the molecular profiles of cancer that contribute to the heterogeneity inherent in the disease. This laid the foundation for the investigation and exploitation of molecular weaknesses in cancer. Moreover, since cancer genomics was readily available, personalized investigation was possible through molecular biomarkers [8,13]. Personalized medicine in cancer has been used to tailor treatment strategies according to individual genetic, genomic or proteomic tumor profiles. This is accomplished using a molecular biomarker that identifies a particular patient population or a tumor phenotype responsive to a specific treatment [2,8]. Indeed, the effectiveness of this approach is apparent in the clinical success of trastuzumab, a direct HER2 inhibitor in the form of a monoclonal antibody, and erlotinib, a small molecule inhibitor of EGFR. The success of trastuzumab and erlotonib was achieved as a result of tailoring the therapeutics to patients whose tumors expressed the respective molecular biomarkers of HER2 overexpression or an EGFR activating mutation. These molecular biomarkers

effectively guided targeted therapy by identifying the subpopulation of cancer patients responsive to the treatment [8,14,15]. Furthermore, biomarkers have also been used to identify patient populations and tumor phenotypes resistant to a particular treatment. For example, colorectal cancer patients suffering from a tumor with an activating KRAS mutation exhibit resistance to EGFR inhibition therapy [16]. This methodical, molecular-guided personalized cancer therapy is in stark contrast to the historical approach of chemotherapy implementation, whereby universally toxic agents were used in various combinations to identify the optimal treatment [17]. Personalized cancer therapy provides a methodical strategy to identify key molecular biomarkers and link them to the optimal treatment regimen.

Personalized medicine in cancer is also used preventatively, as a method to forecast disease risk prior to the appearance of clinical symptoms. This is possible through the identification of oncogenes that increase the risk of cancer occurrence and applying the proper tests to screen for them in the clinic. The clinical value of BRCA1 and BRCA2 tests and their importance as genetic guides towards cancer prevention highlight the significance of this aspect of personalized medicine [2,18]. Indeed, the greatest risk factor for both breast and ovarian cancer is the inheritance of a mutation in either of the breast cancer susceptibility genes BRCA1, BRCA2 or both [19]. Women carrying such mutations have a collective lifetime risk of invasive breast cancer (up to 70 years of age) of 55-85% and of invasive epithelial ovarian cancer of 15-65%. For these women, prophylactic bilateral total mastectomy reduces the incidence and risk of breast cancer associated with these mutations significantly [20]. However, BRCA1/2 mutations are found in only a small fraction (5–10%) of all breast cancers [21]. Therefore, the ability to assess the population for these mutations is crucial in order to recommend and tailor such a highly morbid procedure as a total mastectomy to the most beneficial group. In this light, the ability to personalize cancer prevention interventions is essential.

Personalized medicine is also capable of predicting patient prognosis, cancer recurrence and treatment outcomes based on molecular tumor profiles [2,22,23]. Indeed, one such example is the incorporation of Oncotype DX, a clinically-available multigene diagnostic with prognostic and predictive significance. Oncotype DX is a multiplex PCR-based assay that analyzes the expression of 21 genes and quantifies the probability of cancer recurrence (prognostic significance) and assesses the likely benefit of particular chemotherapeutic interventions (predictive significance). This diagnostic is tailored to women with hormone receptor positive, lymph node negative early stage breast cancer (stages I and II) [23,24]. Through the use of this diagnostic test, a personalized assessment of the probability of cancer recurrence and potential benefit from chemotherapy is possible.

Furthermore, another clinically-available test, Mammaprint, assess tumors molecularly to provide a personalized prognosis of breast tumor metastasis. Mammaprint is a genomic diagnostic test that examines the expression of 70 genes using microarray analysis. It has been shown to be a successful prognostic test, independent of conventional pathological and clinical markers such as tumor size and hormone/HER2 receptor status. It is currently used in the clinic to personalize assessment of potential distant metastases in lymph node negative breast cancer patients of all ages with tumors small than 5 cm and independent of hormone receptor status [6,22,24].

Through the incorporation of cancer genomics, personalized medicine has been able to change the landscape of cancer prevention, therapy and research. As such, the goal of my dissertation is to incorporate cancer genomics and personalized medicine approaches to identify treatments for complex cancer phenotypes. A complex cancer phenotype is defined here as an aggressive subtype of cancer that is characterized by deregulated signaling in unknown oncogenic pathways or known complicated networks that lack available therapeutic targets.

In this dissertation, I address two such cancers, RAS-driven nonsmall cell lung cancer, with its aberrant signaling in the complex branching RAS pathway, and Basal-like/Claudin-low breast cancer, which lacks an identified driver oncogenic signaling pathway. The next section will provide background information on the former complex cancer phenotype, laying the foundation for the work described in Chapter 2 that identifies a novel personalized treatment strategy effective against the disease.

1.3 RAS-active Nonsmall Cell Lung Cancer

Lung cancer is the leading neoplasm in incidence and mortality worldwide. Every year, more patients die of lung cancer than breast, colorectal and prostate cancers combined [25]. Approximately 85% of all lung cancers are caused by the carcinogens found in tobacco smoke, with the remainder 15% of lung cancer cases occurring in lifetime “never smokers” (those who have smoked less than 100 cigarettes in their lifetime) [26]. In the US, an estimated 224,210 cases of lung cancer are expected in 2014. Lung cancer is responsible for more deaths than any other type of cancer in both men and women. An estimated 159,260 deaths that account for roughly 27% of all cancer mortality are expected to occur in 2014. The 5-year survival rate of lung cancer has not improved significantly since 1975, going up from 12% in 1975 to 18% in 2009 [27], highlighting the desperate need for novel therapeutics that can treat lung cancer.

Lung cancer occurs in two general types, nonsmall-cell lung cancer (NSCLC) and small-cell lung cancer (SCLC), making up 85% and 15% of all cases, respectively [28]. Three separate subtypes exist within NSCLC: adenocarcinoma, squamous cell carcinoma, and large cell carcinoma, comprising 40%, 30% and 15% of all lung cancer cases, respectively [29]. Smoking is associated with causing all major histological types of lung cancer, although the connection is stronger for

SCLC and squamous cell carcinoma. In comparison, adenocarcinoma is the most common form of lung cancer to occur in never smokers [30,31]. Adenocarcinoma tumors have glandular histology and arise in more distal airways, expressing genes consistent with their origin in the distal lung. Squamous cell carcinoma tumors occur in more proximal airways and are associated with chronic inflammation. This subtype is characterized by squamous differentiation, similar to the pseudostratified columnar epithelium that lines the trachea and upper airways where these tumors form. Lastly, large cell carcinomas are part of a NSCLC subtype that is diagnosed by exclusion. This occurs when tumor cells do not display morphological features diagnostic of adenocarcinoma, squamous cell carcinoma or SCLC. It is uncertain whether large cell carcinomas are genetically distinct from adenocarcinoma or squamous cell carcinoma. These tumors tend to be large, partially necrotic and composed of undifferentiated cells [32,33].

Adding further complexity to NSCLC are the vast molecular differences observed among these diverse types and subtypes of lung cancer [32,33]. Genomic studies have revealed the molecular landscape of lung cancer and described the numerous somatic alterations observed in NSCLC. These modifications encompass protein kinases, epigenome modulators, transcription and splicing factors, as well as cellular immunity genes. Among the various altered genes in NSCLC with relevant preclinical and clinical evidence identified from patient tumours is KRAS, a member of the highly oncogenic RAS protein family [32,34]. KRAS mutations are found in 17% of all lung cancer cases [35,36]. The survival rate for KRAS-positive lung cancer patients is even worse than the other lung cancer patients [37]. KRAS mutations occur in 25% of all NSCLC, but are evidently rare in SCLC [26]. Furthermore, RAS can be activated without the acquisition of an activating mutation [38]. Therefore, it is necessary to accurately classify the lung cancers with activated RAS independent of mutation status. In the work described

in this dissertation, RAS-active NSCLC is characterized genomically, with the use of a RAS gene-expression signature that classifies RAS activation based on global pathway activity and transcription. RAS-active NSCLC is defined as a molecular subtype of NSCLC characterized by an activated RAS pathway, independent of RAS mutation status and NSCLC histological subtypes (adenocarcinoma, large cell carcinoma, squamous cell carcinoma). In the following section, I provide an elaboration on the RAS pathway, and its role in carcinogenesis and NSCLC to present the reader with the required background knowledge on the importance of this pathway.

1.3.1 The RAS Pathway

RAS proteins are key regulators of cell growth and differentiation, with crucial roles in the development and maintenance of tumors. In humans, four different RAS proteins exist: HRAS, NRAS, KRAS-4A, and KRAS-4B, with the latter two being alternative splice variants of the KRAS gene [36,39]. The protein products of these genes are widely expressed, with KRAS in particular being expressed in almost all cell types. The KRAS gene is found mutated frequently in particular forms of cancer, such as pancreatic, colon and lung carcinomas, the latter of which is of significance for the body of work described in this dissertation. Mutated NRAS on the other hand is often found in melanomas and some leukemias, while mutated HRAS is less frequent but observed in bladder, breast, and thyroid carcinomas [39,40]. Knockdown studies have indicated that singular or combinatorial inhibition of HRAS and NRAS do not severely hinder normal development in mice, whereas KRAS is essential [41].

While some differences exist in the roles and functions of the proteins, HRAS, NRAS and KRAS are highly homologous GTPases, sharing 90% amino acid identity and localizing to the cytosolic part of the plasma membrane where they

cycle through “on” (GTP-bound) and “off” (GDP-bound) states [42]. The prominent structural differences between these RAS proteins occur in the short hypervariable region immediately before the C-terminus [39]. However, they share similar RAS GTPase characterstics. Purified RAS possesses a low level of intrinsic GTPase activity *in vitro* [42], highlighting the inefficiency of RAS as a GTPase working alone. In the cell, RAS is aided by GTPase activating proteins (GAPs) which catalyze the GTP to GDP exchange and guanine exchange factors (GEFs), which catalyze GDP to GTP exchange [35,36,38,42-45]. The most common mutations that target the RAS genes occur in codons 12, 13 and 61; all of which function to impair hydrolysis of the GTP bound in the active site of RAS, by either preventing RAS association with its GAPs (codons 12 or 13 mutations) or by interfering with the water molecule required for nucleophilic attack on the γ-phosphate of GTP (codon 61 mutations) [36]. This causes RAS to remain in the active GTP-bound state for extended periods of time, promoting its oncogenic effects [36]. About 30% of human cancers have a mutated RAS protein [39,42]. RAS can also be functionally activated through deregulation of upstream signal transduction components such as activation of EGFR [46], or by loss of a GAP, such as NF1 [47]. As such, there exist at least three distinct ways that lead to continued activation of RAS in cancer: 1) acquisition of an activating mutation, 2) RAS activation through deregulation of upstream signaling leading to increased RAS GEF activity, and 3) loss of RAS GAP function necessary to terminate activity of RAS [39]. Once RAS is activated, an interaction is possible with more than 20 effectors that leads to the regulation of numerous cell responses, such as proliferation, survival and differentiation [36,45,48,49].

Among these effectors, RAS is capable of activating the three closely related RAF proteins (RAF1, BRAF and ARAF), leading to the activation of the MAPK pathway and G1-S cell cycle progression. This pathway activation also

promotes the induction of angiogenesis through ERK-mediated transcriptional upregulation of angiogenic factors. Furthermore, ERK promote increased tumor invasiveness by elevating expression of matrix metalloproteinases. A second effector RAS can interact directly with is PI3K. This results in the activation of AKT and PDK1 pathways, promoting cell survival. RAS also activates the RALGDS pathway to overcome factors inducing cell cycle arrest and apoptosis. The ability of activated RAS to interact with numerous downstream effectors enforces its role as a promoter of various characteristics of malignant transformation. Therefore, targeting the RAS pathway is crucial for tumors expressing aberrant activation of this pathway [38].

1.3.2 Targeting the RAS Pathway

Among the RAS genes, KRAS mutations encompass 86% of all RAS mutations. Indeed, 21.6% of all human cancers harbor KRAS mutations. The need for KRAS inhibitors is especially pronounced in pancreatic, colon and lung cancers which frequently harbor K-RAS mutations, the predominantly mutated RAS gene in three of the top four mortality-associated neoplasms in the United States [35,36,42]. Currently, there are no available drugs that can shut down KRAS directly [42,50]. Finding KRAS inhibitors has been previously regarded as the Holy Grail of cancer research [51]. Unfortunately, targeting KRAS directly has proven to be vexing and quite difficult [35,36,45,48,51]. Historically, the most studied RAS gene has been HRAS, which ironically is the least frequently mutated [38,42]. This paved the way for RAS inhibitor studies on HRAS, leading to the discovery of farnesyltransferase inhibitors (FTIs) which successfully inhibit the transportation of HRAS onto the plasma membrane [38]. However, these inhibitors failed to function effectively on K-RAS due to the protein’s increased affinity towards farnsesyltransferases and its ability to receive a geranylgeranyl isoprenoid, which can substitute for the farnesyl

group and support membrane association of the protein and transforming activity [35,38,42-44,52]. After the failure of FTIs in the clinic, researchers have attempted to use farnesylthiosalicylic acid (FTS), which functions to dislodge RAS from the plasma membrane and making it susceptible to protein degradation [42]. However, a clinical trial conducted on NSCLC has shown FTS fails to elicit tumor regression [53].

Since RAS is required to be bound to GTP for activation, a possible approach to inhibit RAS would be to design a small molecule capable of displacing the GTP from the RAS protein [39]. This approach was encouraged in the light of the success observed with small molecules competing against ATP for the active site of protein kinases [54]. Unfortunately, competing for the nucleotide binding site in RAS is not a promising approach for targeting activated RAS. This is due to the inherent kinetic properties of Ras:GTP binding, which is marked by a very high affinity (picomolar range) in the context of millimolar cytosolic GTP levels [39,55]. Conversely, the affinity of protein kinases for ATP is usually in the micromolar range in the context of millimolar cytosolic ATP. Therefore, the nanomolar affinity that can be accomplished with small molecule inhibitors is sufficient for successful competition and kinase inhibition [39,56]. However, there has been recent progress in targeting RAS protein-protein interactions necessary for RAS to acquire a GTP molecule. Indeed, in vitro experiments using peptides such as hydrogen bond surrogate (HBS) helices to block the interaction of wild-type RAS with one of its GEFs, SOS, have produced promising results [44]. Furthermore, a similar approach was adopted with the small molecules have been shown to block mutant KRAS interaction with SOS with equally promising results [43,57]. Lastly, efforts to target KRAS directly have witnessed a promising advancement with the development of small molecules that are capable of irreversibly binding and inhibiting a specific form of mutant KRAS. These compounds bind and inhibit

KRAS G12C by relying on the cysteine found in the mutant, thereby not affecting the wild-type protein. Indeed, this study has identified a new allosteric regulatory site on KRAS that is targetable in a mutant-specific manner [58].

The focus of RAS pharmacology inhibition strategy has shifted towards the development and utilization of selective inhibitors of the downstream pathways that are driven by RAS. Current strategies to shut down the RAS pathway have focused on inhibiting downstream effector pathways influenced by RAS, such as MAPK and PI3K and RalGEF [42,50]. Indeed, among these downstream pathways, inhibition of the MAPK pathway through MEK targeting has recorded promising results in cell lines with mutant RAS [59]. However, since the RAS pathway is complex, with various signaling branches driven by activated RAS, it is difficult to obtain effective overall inhibition by shutting down one effector pathway [39,42]. Consistent with this situation, preclinical studies have indicated increased antitumor effectiveness when the RAF-MEK-ERK and PI3K-AKT-mTOR arms of the RAS pathway are simultaneously targeted in RAS-active tumors. The formation of lung tumors driven by mutant KRAS in mice was inhibited only with concurrent treatment inhibition of MEK, PI3K and mTOR [60]. Similar results were observed in human melanoma cells when synergistic inhibition was recorded with co-targeting Raf-MEK-ERK and PI3K-AKT-mTOR pathways using RAF and AKT/mTOR inhibitors concurrently [61]. As a result, this project will aim to investigate potential combinations of clinically developed and available singular and combinatorial treatment of small molecules that can inhibit upstream or downstream components of the RAS pathway. This work is described in Chapter 2 of this dissertation. The next sections in the introduction will provide the background necessary for proper comprehension of the work described in Chapter 3.

1.4 Basal-like and Claudin-low Breast Cancer

Breast cancer affects more than 1.3 million women worldwide each year, making it the second most frequent type of cancer, immediately behind lung cancer. It is by far the most diagnosed cancer in women, making up 23-25% of all new cancer cases [25,62]. In the United States, an estimated 232,670 new cases of invasive breast cancer are expected to emerge among women and approximately 2,360 cases are expected in men for the year of 2014. An estimated 40,430 breast cancer deaths (40,000 women, 430 men) are expected to occur, ranking breast cancer second (lung cancer being first again) as a cause of cancer death in women. Death rates for breast cancer have steadily decreased in women since 1989, with larger decreases recorded in younger women. This decrease in breast cancer mortality rates can be attributed in part to the technological advancement in early detection methods, improved clinical treatment strategies, and possibly decreased incidence as a result of declining use of menopausal hormone therapy. The 5-year relative survival rate for female breast cancer patients has improved from 75% in the mid-1970s to 90% today [27].

Breast cancer is a heterogeneous disease, constituting multiple types associated with distinctive histological and biological features, as well as clinical presentations, behaviors and therapeutic response [63-65]. With the advancement of surgical procedures leading to breast-conserving therapy, a necessity emerged to accurately stratify patients based on relative risk of recurrence or progression. This led to the generation of a classification system that incorporated molecular histological markers such as the estrogen receptor (ER), progesterone receptor (PR), the human epidermal growth factor receptor 2 (HER2) to assess breast cancer subtype and risk [66]. Upon diagnosis, patient tumors are classified into one of four pathological subgroups based on whether the tumors express the estrogen receptor (ER positive) or the progesterone receptor (PR positive),

overexpress one of the members of the human epidermal-growth-factor receptor family (HER2 positive), or none of these (triple negative breast cancer) [67]. Among these, hormone receptor positive breast cancer has a better 5-year survival rate likely due to the effectiveness of endocrine therapy on the specific cancer, the decreased likelihood of recurrence and the less aggressive nature of the disease [68,69]. Meanwhile, targeted therapy for HER2 positive breast cancer exists through Herceptin, a monoclonal antibody capable of downregulating the activation of HER2, improving survival chances [15]. Triple-negative breast cancer (TNBC) on the other hand represents an important clinical challenge due to the lack of response to endocrine therapy or other available targeted agents. TNBCs exhibit similar metastatic potential to that of other breast cancer subtypes, but are associated with a shorter median time to relapse and death [70]. It is the subtype with the worst overall and disease free survival [69].

However, such a limited pathological classification system that incorporates only four receptors has been unable to account for the vast molecular heterogeneity inherent in breast cancer. For that purpose, global gene-expression analyses of breast cancer has been instrumental in providing additional insights into the heterogeneous nature of the disease and expanded on the understanding of breast cancer formation, progression, recurrence and treatment [65,71-75]. Landmark studies by Perou et al. and Sørlie et al. have identified a gene expression-based classification system of breast cancer that more accurately encompasses the genomic and prognostic diversity of breast tumors [65,74]. Gene-expression classification has characterized five molecular subtypes of breast cancer, identified as Luminal A, Luminal B, HER2-enriched, Claudin-low and Basal-like, with subtype variations in incidence, survival and treatment response [65,74-77]. Among these genomic classes, breast cancer patients diagnosed with Claudin-low and Basal-like breast tumors exhibit predominantly poor prognosis and suffer from limited

treatment options [78]. The next section covers the molecular characteristics and the clinical attributes of these Basal-like and Claudin-low breast cancers.

1.4.1 Molecular Characteristic of Basal-like and Claudin-low Breast Cancer

The Basal-like subtype is characterized by expressesing genes usually found transcribed in the normal breast myoepithelium such as high molecular weight cytokeratins (CK) such as CK5, 6, 14 and 17, P-cadherin, vimentin, fascin, caveolin 1/2, nestin, CD44 and EGFR [71,72]. In fact, it is primarily the expression of the cytokeratins that give rise to their description as Basal-like. These particular cytokeratins are also found expressed in the basal epithelial cells of the skin and airways [72]. Interestingly, Basal-like breast tumors also express luminal epithelium genes such as CK8/18 and Kit, but at levels significantly lower than those of found in luminal carcinomas [71]. Moreover, Basal-like subtype tumors cells frequently carry deficiencies in RB1, BRCA1 and TP53, promoting accelerated cell division [71,78]. Indeed, breast tumors carrying germ-line mutations in the BRCA1 are part of the Basal-like subgroup. This is the case since alterations that involve a decrease in the function of the BRCA1 gene prime development of basal-like tumors, lack of expression of ER and poor prognosis [71]. Moreover, a high rate of aneuploidy is observed in these tumors, potentially due to the loss of optimal function of these three proteins [78].

The Basal-like breast cancer subtype constitutes approximately 10-25% of all breast carcinomas and generally appears at an early age, predominantly in woman of African origin [71]. Pathologically, the tumors tend to be large in size at the time of diagnosis and of high histological grade and an elevated risk of lymph node infiltration. These tumors lack the expression of the three key receptors in breast cancer ER, PR and HER2, making them part of the triple negative breast

cancer phenotype. Thus in the clinic, the terms “Basal-like” and “triple negative” are often interchanged. However, it is important to note that these terms are not equivalent since a discordance of up to 30% between the two groups has been recorded [71,78]. This molecular subtype of breast cancer exhibits an aggressive pattern of metastatic relapse with predominant targeting of visceral organs, mainly lung, central nervous system and lymph nodes. Basal-like tumors generally exhibit a worse prognosis than luminals, as well as a high cancer relapse rate in the first 3 years, in spite of their high response to chemotherapy [71,74]. Therefore, it is crucial to identify new therapeutic targets to improve treatment options.

Interestingly, the Claudin-low group of breast tumors shares some genomic similarities with the Basal-like subtype such as the minimal expression of the HER2 and the luminal gene clusters [79]. Claudin-low breast tumors occur in approximately 12–14% of all breast cancer cases, clinically corresponding to high grade infiltrating ductal carcinomas, with metaplastic or medullary differentiation, and treatment resistance. Similar to Basal-like tumors, Claudin-low tumors are mostly triple negative (about 20% are hormone-positive) and exhibit a poor long-term prognosis. Furthermore, although BRCA1 mutations are most common in Basal-like tumors, they also tend to occur within the Claudin-low subtype. However, Claudin-low breast cancers remain a unique subgroup of breast tumors on their own, characterized by lacking cell–cell junction proteins, and having a concentrated immune cell infiltrate, stem cell properties, and features of epithelial–mesenchymal transition (EMT). Indeed, Claudin-low tumors have a low expression of tight junctions and cell–cell adhesion genes such as claudin 3, 4, 7, occludin, and E-cadherin. These tumors also highly express many mesenchymal genes such as vimentin, Snail 1 and 2, and Twist 1. This downregulation of epithelial cell traits and upregulation of mesenchymal features is reminiscent of the characteristics associated with stem cells [71,72,75,76,80]. Indeed, Creighton et al. observed

statistically significant enrichment for tumor-initiating cells or cancer stem cells in Claudin-low primary mammary tumors [81].

Due to the nonluminal nature of these two subtypes, and the lack of known protein targets on these cancers, limited treatment options are available. As such, there exists an urgent need to identify potential targets, biomarkers and therapeutics that can improve patient prognosis. One of the promising therapies being investigated are inhibitors of PARP1, a key player in the repair of DNA single-stand breaks [75]. As described earlier, both Basal-like and Claudin-low tumors commonly carry BRCA1 mutations [75,82]. Defects in the proper function of BRCA1 pathway results in deficient homologous recombination repair of the DNA. This leads to the accumulation of genetic aberrations that drive carcinogenesis [75]. The inhibition of PARP1 in tumors with dysfunctional BRCA1 leads to the accrual of collapsed replication forks, DNA double-strand breaks, and cell death [83]. Indeed, the addition of iniparib, a PARP1 inhibitor, to combination chemotherapy improved the clinical benefit and survival of patients with metastatic triple-negative breast cancer (a breast cancer subtype frequently found with BRCA1/2 mutations) without significantly increased toxic effects [84]. Furthermore, other DNA-repair pathway-related genes such as CHK1 are usually found highly expressed in Basal-like breast cancers, suggesting that these tumors may be under a continuous state of DNA-repair, which may not be the case in Claudin-low tumors [75]. Interestingly, however, this dissertation describes the increased sensitivity of both Basal-like and Claudin-low breast cancers to targeted CHK1 inhibition in Chapter 3. Another critical pathway in both these breast cancer subgroups identified in Chapter 3 is AMPK (AMP-activated protein kinase). As such, the next section will provide a proper background on both of these pathways, and their documented role in cancer.

1.4.2 The AMPK and CHK1 pathways

AMPK is a heterotrimeric serine/threonine kinase complex (comprising α, β, and γ subunits) that is a key regulator of cellular metabolism and energy homeostasis in mammalian tissues. AMPK is regulated by AMP/ATP ratios in the cell and functions as part of an evolutionarily conserved energy-sensing pathway [85,86]. Upon the exposure of a cell to nutrient deprivation or hypoxic stress, the catalytic α subunit of AMPK is phosphorylated at threonine 172 by upstream kinases such as LKB1, CAMKKβ, and TAK1. This leads to an allosteric activation through AMP binding to the regulatory γ subunit [87]. The activation of AMPK signaling restores metabolic homeostasis by 1) reducing energy consumption by decreasing the synthesis of protein, lipid, and fatty acids; 2) increasing energy production by upregulating glucose and fatty acid uptake, glycolysis, fatty acid oxidation; and 3) promotion of angiogenic regulators such as VEGF [88]. AMPK is also capable of directing cell fate by promoting apoptosis through the direct phosphorylation of p53 or by promoting cell survival through activating the ULK1-autophagy axis [89,90]. The collective effects of AMPK signaling activation lead to the protection of cellular integrity by blocking the advancement of the cell cycle progression when insufficient resources are available for the cell [88]. The activation of AMPK results in ATP conservation via the activation of catabolic metabolism pathways and inhibition of anabolic processes that consume ATP. The end result of AMPK activation is escape from bioenergetic catastrophe and cell death through the conservation of cellular energy [86].

Interestingly, the role of AMPK in cancer is dichotomous; AMPK can exert pro- or antitumor effects based on cellular context. AMPK is central to a tumor suppressor network, the LKB1-AMPK-TSC-mTOR signaling cascade, known to regulate cell growth and proliferation in response to stress [91]. Loss of AMPK can cooperate with oncogenes such as BRAF and MYC to reprogram tumor cell

metabolism and promote rapid cell growth and proliferation [92,93]. Conversely, the activation of AMPK can also provide a growth advantage to cancer cells. Activation of AMPK in response to hypoxia and nutrient deprivation stresses provides cancers cells with the metabolic flexibility necessary for survival. AMPK promotes this metabolic plasticity through several mechanisms such as inducing autophagy, fatty acid oxidation, and maintenance of intracellular NADPH [86]. These opposing roles of AMPK highlight the complexity of the kinase's role in the cancer cell.

Pharmacologically, interest in the tumor suppressive role of AMPK has gained ground as evidence has emerged to show the antitumor effects of AMPK activation. AMPK agonists, such as the biguanides metformin and phenformin used to treat type II diabetes, have been investigated as potential cancer therapies. Metformin treatment has been observed to be associated with a significantly lower cancer incidence in patients relative to those using other medications to manage their diabetes [94]. However, recent work has indicated that the antitumoregenic effects of metformin and another known AMPK agonist, AICAR, are due to AMPK-independent effects [95]. Conversely, other studies have implicated AMPK as a mediator of cellular proliferation and survival, showing the promising effect of AMPK inhibition as a cancer therapy. Indeed, studies have shown that treating prostate cancer and glioblastoma cells with dorsomorphin c, an inhibitor of AMPK, leads to a reduction in cell growth [96,97].

The second pathway discussed in Chapter 3 as a potential target of Basal-like/Claudin-low breast cancer is the CHK1 pathway. CHK1 is a serine/threonine kinase activated in response to a diverse array of genotoxic insults. CHK1 assumes the role of the major cell-cycle checkpoint kinase mediating S- and G2-arrest [98]. CHK1 is also important for the stabilization of stalled replication forks, the control of replication origin firing and replication fork progression, and homologous recombination [99]. The key role of CHK1 is to relay the checkpoint signals from

the proximal checkpoint kinases ATM, ATR and ATX. CHK1 is primarily activated by ATR-mediated phosphorylation following the formation of double strand or single-strand DNA breaks, the latter being its main activator. This leads to the phosphorylation of downstream components such as TP53, CDC25 and TLK1/2 that promote apoptosis, cell cycle arrest and chromatin remodeling [100,101].

The rationale behind targeting CHK1 in cancer hinges upon the goal of inducing toxic levels of replication stress (RS) that leads to cell death [101]. RS is defined as the delaying or stalling of DNA synthesis and/or replication fork progression [102]. A certain degree of RS occurs during regular cell division, where it is normally detected and dealt with by the ATR and CHK1. Inhibiting these proteins leads to an increase in the occurrence of RS, which can ultimately lead to cell death by p53-independent means. As such, targeting CHK1 could be particularly toxic in cells carrying high endogenous levels of RS. Importantly, although tumors in general might normally carry certain degree of RS, inhibiting CHK1 then would only be toxic for those tumors harboring distinctly high levels of RS [101]. Therefore, it is important to identify the subpopulation of tumors sensitive to CHK1 inhibition. Indeed, studies have identified the effectiveness of single-agent CHK1 inhibition against neuroblastomas and MYC-driven lymphomas [103-105]. In breast cancer, the rationale of CHK1 targeted therapy use is supported by the well-documented evidence of alteration in the DNA damage repair machinery through either the high rate of BRCA or P53 mutations in the Basal-like/Claudin-low and triple negative subtypes [71,72,78]. Therefore, targeting CHK1, a DNA damage repair component may lead to the cell's inability to properly fix chromosomal damage, leading to accumulation of RS and cell death. Indeed, Albiges et al. have shown CHK1 as a potential target in TNBC using genomic analyses. Furthermore, the group described the induction of mitotic cell death upon treatment with CHK1 inhibition, and the effectiveness of the treatment on two TNBC cell lines [98].

1.5 Dissertation Overview

Overall, the goal of this dissertation is to incorporate personalized medicine approaches for treating cancer subtypes driven by complex or uncharacterized signaling pathways. To this extent, two different complex cancer phenotypes were targeted: RAS-driven NSCLC and Basal-like and Claudin-low breast cancer (BL-CL). Genomic analyses were used to characterize these phenotypes on a molecular level, and this information incorporated into high-throughput drug screening to identify novel therapeutic leads. Once a candidate treatment was identified, it was evaluated biochemically for the identification and description of the mechanism of action. Chapter 2 is a published manuscript that discusses the work performed to identify a personalized treatment strategy against RAS-driven NSCLC. Chapter 3 is a manuscript submitted to the AACR Journal of Molecular Cancer Therapeutics that focuses on the identification of a novel sterol sulfate that is personalized against BL-CL. This dissertation is concluded by Chapter 4, which provides a summary of the major points presented, and a discussion of how the work described here has impacted the field of personalized medicine and targeted therapy, with a view on future directions and outlook.

1.6 References

1. Schleidgen S, Klingler C, Bertram T, Rogowski WH, Marckmann G (2013) What is personalized medicine: sharpening a vague term based on a systematic literature review. BMC Med Ethics 14: 55.

2. Cho SH, Jeon J, Kim SI (2012) Personalized medicine in breast cancer: a systematic review. J Breast Cancer 15: 265-272.

3. Katsnelson A (2013) Momentum grows to make ‘personalized’ medicine more ‘precise’. Nat Med 19: 249.

4. Roden DM, Tyndale RF (2013) Genomic medicine, precision medicine, personalized medicine: what’s in a name? Clin Pharmacol Ther 94: 169-172.

5. Peppercorn J, Perou CM, Carey LA (2008) Molecular subtypes in breast cancer evaluation and management: divide and conquer. Cancer Invest 26: 1-10.

6. van de Vijver MJ, He YD, van't Veer LJ, Dai H, Hart AA, et al. (2002) A gene-expression signature as a predictor of survival in breast cancer. N Engl J Med 347: 1999-2009.

7. Rosenwald A, Wright G, Chan WC, Connors JM, Campo E, et al. (2002) The use of molecular profiling to predict survival after chemotherapy for diffuse large-B-cell lymphoma. N Engl J Med 346: 1937-1947.

8. Schilsky RL (2010) Personalized medicine in oncology: the future is now. Nat Rev Drug Discov 9: 363-366.

9. The Cancer Genome Atlas Research Network, Weinstein JN, Collisson EA, Mills GB, Shaw KR, et al. (2013) The Cancer Genome Atlas Pan-Cancer analysis project. Nat Genet 45: 1113-1120.

10. Chin L, Andersen JN, Futreal PA (2011) Cancer genomics: from discovery science to personalized medicine. Nat Med 17: 297-303.

11. Stratton MR, Campbell PJ, Futreal PA (2009) The cancer genome. Nature 458: 719-724.

12. Garraway LA, Lander ES (2013) Lessons from the cancer genome. Cell 153: 17-37.

13. La Thangue NB, Kerr DJ (2011) Predictive biomarkers: a paradigm shift towards personalized cancer medicine. Nat Rev Clin Oncol 8: 587-596.

14. Rosell R, Carcereny E, Gervais R, Vergnenegre A, Massuti B, et al. (2012) Erlotinib versus standard chemotherapy as first-line treatment for European patients with advanced EGFR mutation-positive non-small-cell lung cancer (EURTAC): a multicentre, open-label, randomised phase 3 trial. Lancet Oncol 13: 239-246.

15. Romond EH, Perez EA, Bryant J, Suman VJ, Geyer CE, Jr., et al. (2005) Trastuzumab plus adjuvant chemotherapy for operable HER2-positive breast cancer. N Engl J Med 353: 1673-1684.

16. Amado RG, Wolf M, Peeters M, Van Cutsem E, Siena S, et al. (2008) Wild-type KRAS is required for panitumumab efficacy in patients with metastatic colorectal cancer. J Clin Oncol 26: 1626-1634.

17. DeVita VT, Jr., Chu E (2008) A history of cancer chemotherapy. Cancer Res 68: 8643-8653.

18. Struewing JP, Hartge P, Wacholder S, Baker SM, Berlin M, et al. (1997) The

risk of cancer associated with specific mutations of BRCA1 and BRCA2 among Ashkenazi Jews. N Engl J Med 336: 1401-1408.

19. Roy R, Chun J, Powell SN (2012) BRCA1 and BRCA2: different roles in a common pathway of genome protection. Nat Rev Cancer 12: 68-78.

20. Meijers-Heijboer H, van Geel B, van Putten WL, Henzen-Logmans SC, Seynaeve C, et al. (2001) Breast cancer after prophylactic bilateral mastectomy in women with a BRCA1 or BRCA2 mutation. N Engl J Med 345: 159-164.

21. Nicoletto MO, Donach M, De Nicolo A, Artioli G, Banna G, et al. (2001) BRCA-1 and BRCA-2 mutations as prognostic factors in clinical practice and genetic counselling. Cancer Treat Rev 27: 295-304.

22. van ‘t Veer LJ, Dai H, van de Vijver MJ, He YD, Hart AA, et al. (2002) Gene expression profiling predicts clinical outcome of breast cancer. Nature 415: 530-536.

23. Paik S, Tang G, Shak S, Kim C, Baker J, et al. (2006) Gene expression and benefit of chemotherapy in women with node-negative, estrogen receptor-positive breast cancer. J Clin Oncol 24: 3726-3734.

24. Kittaneh M, Montero AJ, Gluck S (2013) Molecular profiling for breast cancer: a comprehensive review. Biomark Cancer 5: 61-70.

25. International Agency for Research on Cancer and Cancer Research UK (2014) World Cancer Factsheet. Cancer Research, UK, London: World Health Organization.

26. Minna JD, Larsen JE (2011) Molecular biology of lung cancer: clinical implications. Clinics in Chest Medicine 32: 703–740.

27. American Cancer Society (2014) Cancer Fact and Figures 2014. Atlanta: American Cancer Society.

28. Herbst RS, Heymach JV, Lippman SM (2008) Molecular origins of cancer: lung cancer. N Engl J Med 359: 1367-1380.

29. Speicher MR, Petersen S, Uhrig S, Jentsch I, Fauth C, et al. (2000) Analysis of chromosomal alterations in non-small cell lung cancer by multiplex-FISH, comparative genomic hybridization, and multicolor bar coding. Lab Invest 80: 1031-1041.

30. Sun S, Schiller JH, Gazdar AF (2007) Lung cancer in never smokers--a different disease. Nat Rev Cancer 7: 778-790.

31. Khuder SA (2001) Effect of cigarette smoking on major histological types of

lung cancer: a meta-analysis. Lung Cancer 31: 139-148.

32. Chen Z, Fillmore CM, Hammerman PS, Kim CF, Wong KK (2014) Non-small-cell lung cancers: a heterogeneous set of diseases. Nat Rev Cancer 14: 535-546.

33. Davidson MR, Gazdar AF, Clarke BE (2013) The pivotal role of pathology in the management of lung cancer. J Thorac Dis 5: S463-478.

34. Riely GJ, Marks J, Pao W (2009) KRAS mutations in non-small cell lung cancer. Proc Am Thorac Soc 6: 201-205.

35. Karnoub AE, Weinberg RA (2008) Ras oncogenes: split personalities. Nat Rev Mol Cell Biol 9: 517-531.

36. Pylayeva-Gupta Y, Grabocka E, Bar-Sagi D (2011) RAS oncogenes: weaving a tumorigenic web. Nat Rev Cancer 11: 761-774.

37. Johnson ML, Sima CS, Chaft J, Paik PK, Pao W, et al. (2012) Association of KRAS and EGFR mutations with survival in patients with advanced lung adenocarcinomas. Cancer.

38. Downward J (2003) Targeting RAS signalling pathways in cancer therapy. Nat Rev Cancer 3: 11-22.

39. Mattingly RR (2013) Activated RAS as a therapeutic target: constraints on directly targeting RAS isoforms and wild-type versus mutated proteins. ISRN Oncol 2013: 536529.

40. Rodenhuis S (1992) RAS and human tumors. Semin Cancer Biol 3: 241-247.

41. Johnson L, Greenbaum D, Cichowski K, Mercer K, Murphy E, et al. (1997) K-ras is an essential gene in the mouse with partial functional overlap with N-RAS. Genes Dev 11: 2468-2481.

42. Baines AT, Xu D, Der CJ (2011) Inhibition of RAS for cancer treatment: the search continues. Future Med Chem 3: 1787-1808.

43. Maurer T, Garrenton LS, Oh A, Pitts K, Anderson DJ, et al. (2012) Small-molecule ligands bind to a distinct pocket in RAS and inhibit SOS-mediated nucleotide exchange activity. Proc Natl Acad Sci U S A 109: 5299-5304.

44. Patgiri A, Yadav KK, Arora PS, Bar-Sagi D (2011) An orthosteric inhibitor of the RAS-Sos interaction. Nat Chem Biol 7: 585-587.

45. Cox AD, Der CJ (2010) RAS history: the saga continues. Small GTPases 1: 2-27.

46. Kamata T, Feramisco JR (1984) Epidermal growth factor stimulates guanine nucleotide binding activity and phosphorylation of ras oncogene proteins. Nature 310: 147-150.

47. Martin GA, Viskochil D, Bollag G, McCabe PC, Crosier WJ, et al. (1990) The GAP-related domain of the neurofibromatosis type 1 gene product interacts with ras p21. Cell 63: 843-849.

48. Der CJ (2012) Targeting KRAS for the treatment of gastrointestinal cancers: mission impossible? 2012 Gastrointestinal Cancers Symposium.

49. Schubbert S, Shannon K, Bollag G (2007) Hyperactive RAS in developmental disorders and cancer. Nat Rev Cancer 7: 295-308.

50. Gysin S, Salt M, Young A, McCormick F (2011) Therapeutic strategies for targeting RAS proteins. Genes Cancer 2: 359-372.

51. Helwick C (2012) Targeting KRAS in GI cancers: the hunt for the Holy Grail in cancer research. ASCO Post 3:6. http://www.ascopost.com/issues/april-15-2012/targeting-kras-in-gi-cancers-the-hunt-for-the-holy-grail-in-cancer-research.aspx

52. Fiordalisi JJ, Johnson RL, 2nd, Weinbaum CA, Sakabe K, Chen Z, et al. (2003) High affinity for farnesyltransferase and alternative prenylation contribute individually to K-RAS4B resistance to farnesyltransferase inhibitors. J Biol Chem 278: 41718-41727.

53. Riely GJ, Johnson ML, Medina C, Rizvi NA, Miller VA, et al. (2011) A phase II trial of Salirasib in patients with lung adenocarcinomas with KRAS mutations. J Thorac Oncol 6: 1435-1437.

54. Cohen P (2002) Protein kinases--the major drug targets of the twenty-first century? Nat Rev Drug Discov 1: 309-315.

55. John J, Rensland H, Schlichting I, Vetter I, Borasio GD, et al. (1993) Kinetic and structural analysis of the Mg(2+)-binding site of the guanine nucleotide-binding protein p21H-ras. J Biol Chem 268: 923-929.

56. Goekjian PG, Jirousek MR (1999) Protein kinase C in the treatment of disease: signal transduction pathways, inhibitors, and agents in development. Curr Med Chem 6: 877-903.

57. Sun Q, Burke JP, Phan J, Burns MC, Olejniczak ET, et al. (2012) Discovery of small molecules that bind to K-RAS and inhibit Sos-mediated activation. Angew Chem Int Ed Engl 51: 6140-6143.

58. Ostrem JM, Peters U, Sos ML, Wells JA, Shokat KM (2013) K-RAS(G12C) inhibitors allosterically control GTP affinity and effector interactions. Nature 503:

548-551.

59. Gilmartin AG, Bleam MR, Groy A, Moss KG, Minthorn EA, et al. (2011) GSK1120212 (JTP-74057) is an inhibitor of MEK activity and activation with favorable pharmacokinetic properties for sustained in vivo pathway inhibition. Clin Cancer Res 17: 989-1000.

60. Engelman JA, Chen L, Tan X, Crosby K, Guimaraes AR, et al. (2008) Effective use of PI3K and MEK inhibitors to treat mutant KRAS G12D and PIK3CA H1047R murine lung cancers. Nat Med 14: 1351-1356.

61. Molhoek KR, Brautigan DL, Slingluff CL, Jr. (2005) Synergistic inhibition of human melanoma proliferation by combination treatment with B-RAF inhibitor BAY43-9006 and mTOR inhibitor Rapamycin. J Transl Med 3: 39.

62. Grayson M (2012) Breast cancer. Nature 485: S49.

63. Weigelt B, Mackay A, A'Hern R, Natrajan R, Tan DS, et al. (2010) Breast cancer molecular profiling with single sample predictors: a retrospective analysis. Lancet Oncol 11: 339-349.

64. Vargo-Gogola T, Rosen JM (2007) Modelling breast cancer: one size does not fit all. Nat Rev Cancer 7: 659-672.

65. Perou CM, Sorlie T, Eisen MB, van de Rijn M, Jeffrey SS, et al. (2000) Molecular portraits of human breast tumours. Nature 406: 747-752.

66. Malhotra GK, Zhao X, Band H, Band V (2010) Histological, molecular and functional subtypes of breast cancers. Cancer Biol Ther 10: 955-960.

67. Powell K (2012) Molecular oncology: the positive in the negative. Nature 485: S52-53.

68. Maxmen A (2012) The hard facts. Nature 485: S50-51.

69. Onitilo AA, Engel JM, Greenlee RT, Mukesh BN (2009) Breast cancer subtypes based on ER/PR and HER2 expression: comparison of clinicopathologic features and survival. Clin Med Res 7: 4-13.

70. Hudis CA, Gianni L (2011) Triple-negative breast cancer: an unmet medical need. Oncologist 16 Suppl 1: 1-11.

71. Eroles P, Bosch A, Perez-Fidalgo JA, Lluch A (2012) Molecular biology in breast cancer: intrinsic subtypes and signaling pathways. Cancer Treat Rev 38: 698-707.

72. Perou CM, Borresen-Dale AL (2011) Systems biology and genomics of breast cancer. Cold Spring Harb Perspect Biol 3.

73. Goldhirsch A, Wood WC, Coates AS, Gelber RD, Thurlimann B, et al. (2011) Strategies for subtypes--dealing with the diversity of breast cancer: highlights of the St. Gallen International Expert Consensus on the primary therapy of early breast cancer 2011. Ann Oncol 22: 1736-1747.

74. Sorlie T, Perou CM, Tibshirani R, Aas T, Geisler S, et al. (2001) Gene expression patterns of breast carcinomas distinguish tumor subclasses with clinical implications. Proc Natl Acad Sci U S A 98: 10869-10874.

75. Prat A, Perou CM (2011) Deconstructing the molecular portraits of breast cancer. Mol Oncol 5: 5-23.

76. Prat A, Parker JS, Karginova O, Fan C, Livasy C, et al. (2010) Phenotypic and molecular characterization of the claudin-low intrinsic subtype of breast cancer. Breast Cancer Res 12: R68.

77. Rouzier R, Perou CM, Symmans WF, Ibrahim N, Cristofanilli M, et al. (2005) Breast cancer molecular subtypes respond differently to preoperative chemotherapy. Clin Cancer Res 11: 5678-5685.

78. Perou CM (2010) Molecular stratification of triple-negative breast cancers. Oncologist 15 Suppl 5: 39-48.

79. Parker JS, Mullins M, Cheang MC, Leung S, Voduc D, et al. (2009) Supervised risk predictor of breast cancer based on intrinsic subtypes. J Clin Oncol 27: 1160-1167.

80. Herschkowitz JI, Simin K, Weigman VJ, Mikaelian I, Usary J, et al. (2007) Identification of conserved gene expression features between murine mammary carcinoma models and human breast tumors. Genome Biol 8: R76.

81. Creighton CJ, Li X, Landis M, Dixon JM, Neumeister VM, et al. (2009) Residual breast cancers after conventional therapy display mesenchymal as well as tumor-initiating features. Proc Natl Acad Sci U S A 106: 13820-13825.

82. Foulkes WD, Stefansson IM, Chappuis PO, Begin LR, Goffin JR, et al. (2003) Germline BRCA1 mutations and a basal epithelial phenotype in breast cancer. J Natl Cancer Inst 95: 1482-1485.

83. Rottenberg S, Jaspers JE, Kersbergen A, van der Burg E, Nygren AO, et al. (2008) High sensitivity of BRCA1-deficient mammary tumors to the PARP inhibitor AZD2281 alone and in combination with platinum drugs. Proc Natl Acad Sci U S A 105: 17079-17084.

84. O'Shaughnessy J, Osborne C, Pippen JE, Yoffe M, Patt D, et al. (2011) Iniparib plus chemotherapy in metastatic triple-negative breast cancer. N Engl J Med 364: 205-214.

85. Hardie DG, Carling D, Gamblin SJ (2011) AMP-activated protein kinase: also regulated by ADP? Trends Biochem Sci 36: 470-477.

86. Faubert B, Vincent EE, Poffenberger MC, Jones RG (2014) The AMP-activated protein kinase (AMPK) and cancer: many faces of a metabolic regulator. Cancer Lett 356: 165-170.

87. Stein SC, Woods A, Jones NA, Davison MD, Carling D (2000) The regulation of AMP-activated protein kinase by phosphorylation. Biochem J 345 Pt 3: 437-443.

88. Fox MM, Phoenix KN, Kopsiaftis SG, Claffey KP (2013) AMP-Activated protein kinase alpha 2 Isoform suppression in primary breast cancer alters AMPK growth control and apoptotic signaling. Genes Cancer 4: 3-14.

89. Kim J, Kundu M, Viollet B, Guan KL (2011) AMPK and mTOR regulate autophagy through direct phosphorylation of Ulk1. Nat Cell Biol 13: 132-141.

90. Thoreen CC, Sabatini DM (2005) AMPK and p53 help cells through lean times. Cell Metab 1: 287-288.

91. Shackelford DB, Shaw RJ (2009) The LKB1-AMPK pathway: metabolism and growth control in tumour suppression. Nat Rev Cancer 9: 563-575.

92. Zheng B, Jeong JH, Asara JM, Yuan YY, Granter SR, et al. (2009) Oncogenic B-RAF negatively regulates the tumor suppressor LKB1 to promote melanoma cell proliferation. Mol Cell 33: 237-247.

93. Faubert B, Boily G, Izreig S, Griss T, Samborska B, et al. (2013) AMPK is a negative regulator of the Warburg effect and suppresses tumor growth in vivo. Cell Metab 17: 113-124.

94. Pierotti MA, Berrino F, Gariboldi M, Melani C, Mogavero A, et al. (2013) Targeting metabolism for cancer treatment and prevention: metformin, an old drug with multi-faceted effects. Oncogene 32: 1475-1487.

95. Liu X, Chhipa RR, Pooya S, Wortman M, Yachyshin S, et al. (2014) Discrete mechanisms of mTOR and cell cycle regulation by AMPK agonists independent of AMPK. Proc Natl Acad Sci U S A 111: E435-444.

96. Rios M, Foretz M, Viollet B, Prieto A, Fraga M, et al. (2013) AMPK activation by oncogenesis is required to maintain cancer cell proliferation in astrocytic tumors. Cancer Res 73: 2628-2638.

97. Park HU, Suy S, Danner M, Dailey V, Zhang Y, et al. (2009) AMP-activated protein kinase promotes human prostate cancer cell growth and survival. Mol Cancer Ther 8: 733-741.

98. Albiges L, Goubar A, Scott V, Vicier C, Lefebvre C, et al. (2014) CHK1 as a new therapeutic target in triple-negative breast cancer. Breast 23: 250-258.

99. Thompson R, Eastman A (2013) The cancer therapeutic potential of CHK1 inhibitors: how mechanistic studies impact on clinical trial design. Br J Clin Pharmacol 76: 358-369.

100. Bartek J, Lukas J (2003) CHK1 and CHK2 kinases in checkpoint control and cancer. Cancer Cell 3: 421-429.

101. Toledo LI, Murga M, Fernandez-Capetillo O (2011) Targeting ATR and CHK1 kinases for cancer treatment: a new model for new (and old) drugs. Mol Oncol 5: 368-373.

102. Zeman MK, Cimprich KA (2014) Causes and consequences of replication stress. Nat Cell Biol 16: 2-9.

103. Davies KD, Humphries MJ, Sullivan FX, von Carlowitz I, Le Huerou Y, et al. (2011) Single-agent inhibition of CHK1 is antiproliferative in human cancer cell lines in vitro and inhibits tumor xenograft growth in vivo. Oncol Res 19: 349-363.

104. Ferrao PT, Bukczynska EP, Johnstone RW, McArthur GA (2012) Efficacy of CHK inhibitors as single agents in MYC-driven lymphoma cells. Oncogene 31: 1661-1672.

105. Cole KA, Huggins J, Laquaglia M, Hulderman CE, Russell MR, et al. (2011) RNAi screen of the protein kinome identifies checkpoint kinase 1 (CHK1) as a therapeutic target in neuroblastoma. Proc Natl Acad Sci U S A 108: 3336-3341.

CHAPTER 2

GENOMIC CLASSIFICATION OF THE RAS NETWORK IDENTIFIES A PERSONALIZED TREATMENT STRATEGY FOR LUNG CANCER

Chapter 2 is a manuscript reprinted from the journal Molecular Oncology, volume 8, issue 7, October 2014, pages 1339-1354. The article is titled “Genomic classification of the RAS network identifies a personalized treatment strategy for lung cancer” and is authored by Nader N. El-Chaar, Stephen R. Piccolo, Kenneth M. Boucher, Adam L. Cohen, Jeffrey T. Chang, Philip J. Moos and Andrea H. Bild (2014).

This manuscript was written by Nader N. El-Chaar and Andrea H. Bild

ARTICLE IN PRESS

MOLECULAR ONCOLOGY XXX (2014) 1–16

available at www.sciencedirect.com

ScienceDirect

www.elsevier.com/locate/molonc

Genomic classification of the RAS network identifies a personalized treatment strategy for lung cancer

Nader N. El-Chaar[a], *Stephen R. Piccolo*[b,c], *Kenneth M. Boucher*[a], *Adam L. Cohen*[d], *Jeffrey T. Chang*[e], *Philip J. Moos*[b,1], *Andrea H. Bild*[a,b,*,1]

[a]*Department of Oncological Sciences, University of Utah, Salt Lake City, UT 84112, USA*
[b]*Department of Pharmacology and Toxicology, University of Utah, Salt Lake City, UT 84112, USA*
[c]*Division of Computational Biomedicine, Boston University School of Medicine, Boston, MA 02118, USA*
[d]*Department of Medicine, Division of Oncology, University of Utah, Salt Lake City, UT 84112, USA*
[e]*Department of Integrative Biology and Pharmacology, University of Texas Medical School, Houston 77030, USA*

ARTICLE INFO

Article history:
Received 18 April 2014
Accepted 9 May 2014
Available online ■

Keywords:
Cancer
Genomics
Networks
RAS
Signaling
Individualized medicine

ABSTRACT

Better approaches are needed to evaluate a single patient's drug response at the genomic level. Targeted therapy for signaling pathways in cancer has met limited success in part due to the exceedingly interwoven nature of the pathways. In particular, the highly complex RAS network has been challenging to target. Effectively targeting the pathway requires development of techniques that measure global network activity to account for pathway complexity. For this purpose, we used a gene-expression-based biomarker for RAS network activity in non-small cell lung cancer (NSCLC) cells, and screened for drugs whose efficacy was significantly highly correlated to RAS network activity. Results identified EGFR and MEK co-inhibition as the most effective treatment for RAS-active NSCLC amongst a panel of over 360 compounds and fractions. RAS activity was identified in both RAS-mutant and wild-type lines, indicating broad characterization of RAS signaling inclusive of multiple mechanisms of RAS activity, and not solely based on mutation status. Mechanistic studies demonstrated that co-inhibition of EGFR and MEK induced apoptosis and blocked both EGFR-RAS-RAF-MEK-ERK and EGFR-PI3K-AKT-RPS6 nodes simultaneously in RAS-active, but not RAS-inactive NSCLC. These results provide a comprehensive strategy to personalize treatment of NSCLC based on RAS network dysregulation and provide proof-of-concept of a genomic approach to classify and target complex signaling networks.

* *Corresponding author*. Department of Pharmacology and Toxicology, University of Utah, 20 South, 2030 East, Biomedical Polymers Research Building (BPRB), Room 410A, Salt Lake City, UT 84112, USA. Tel.: +1 801 581 6353.
E-mail addresses: n.elchaar@utah.edu (N.N. El-Chaar), stephen.piccolo@hsc.utah.edu (S.R. Piccolo), kenneth.boucher@hci.utah.edu (K.M. Boucher), adam.cohen@hci.utah.edu (A.L. Cohen), jeffrey.t.chang@uth.tmc.edu (J.T. Chang), philip.moos@pharm.utah.edu (P.J. Moos), andreab@genetics.utah.edu (A.H. Bild).
[1] These authors contributed equally.
http://dx.doi.org/10.1016/j.molonc.2014.05.005
1574-7891/

Please cite this article in press as: El-Chaar, N.N., et al., Genomic classification of the RAS network identifies a personalized treatment strategy for lung cancer, Molecular Oncology (2014), http://dx.doi.org/10.1016/j.molonc.2014.05.005

1. Introduction

Cancer is among the principal causes of disease in the world, with an approximated 12.7 million new cancer cases occurring in 2008 (International Agency for Research on Cancer and Cancer Research UK, 2012). The RAS proto-oncogenes are frequently mutated in human cancers, with constitutively active mutations observed in approximately one third of human tumors (Baines et al., 2011; Downward, 2003; Riely et al., 2009). In humans, three genes encode four different RAS proteins: HRAS, NRAS, KRAS-4A and KRAS-4B, the latter two being alternative splice variants of the KRAS gene (Pylayeva-Gupta et al., 2011). These highly homologous GTPase proteins, sharing 90% amino acid identity (Baines et al., 2011), localize to the cytosolic part of the plasma membrane, where they cycle through "on" (GTP-bound) and "off" (GDP-bound) states (Downward, 2003; Karnoub and Weinberg, 2008). RAS can be switched on through multiple mechanisms, such as via receptor tyrosine kinases like EGFR and other growth factor receptors like PDGFR and IGFR (Bazenet and Kazlauskas, 1993; Chan et al., 2001; Innocenti et al., 2002; Ono and Kuwano, 2006; Repasky et al., 2004), or by obtaining activating mutations in the gene (Downward, 2003). The most common RAS mutations occur in codons 12, 13 and 61 (COSMIC Database; Schubbert et al., 2007), all of which impair hydrolysis of GTP (Downward, 2003). These variants cause RAS to remain in an active GTP-bound state, promoting its oncogenic effects for extended periods of time (Pylayeva-Gupta et al., 2011). Activated RAS can interact with more than 20 effectors to regulate various cellular responses, including cellular proliferation, survival and differentiation (Cox and Der, 2010; Der, 2012; Pylayeva-Gupta et al., 2011; Schubbert et al., 2007). Despite extensive efforts, the RAS proteins have remained undruggable targets (Baines et al., 2011)—no therapies exist in the clinic to directly treat RAS-active tumors (Baines et al., 2011; Gysin et al., 2011).

Targeting the RAS pathway would be beneficial for lung cancer, the leading neoplasm in incidence and mortality in the world (International Agency for Research on Cancer and Cancer Research UK, 2012). KRAS mutations occur in 20–30% of non-small cell lung cancers (NSCLC), which make up 87% of all lung cancer cases; these mutations occur predominantly in the adenocarcinoma subtype of NSCLC (Aviel-Ronen et al., 2006; Graziano et al., 1999; Minna and Larsen, 2011; Roberts et al., 2010), and they represent the most common molecular change in NSCLC (Roberts and Stinchcombe, 2013). In the US, an estimated 228,190 new cases of lung cancer are predicted to have occured in 2013, with an approximate 70% fatality rate (American Cancer Society, 2013). The 5-year survival rate for lung cancer has only modestly improved since 1975, increasing from 12% in 1975 to 16% in 2007. Lung cancer today still accounts for more deaths than any other cancer in both men and women, killing almost three times as many men as prostate cancer, and almost twice as many women as breast cancer (American Cancer Society, 2013). The survival rate is even worse for KRAS positive lung cancer patients (Guan et al., 2013; Johnson et al., 2012; Meng et al., 2013; Roberts and Stinchcombe, 2013), highlighting the desperate need for novel therapeutics that can treat RAS-active tumors.

The RAS pathway is a large and complicated signaling cascade, comprising a network as opposed to a linear pathway. It is composed of numerous interacting proteins, upstream and downstream of RAS, providing feedback and crosstalk to the different components of the pathway (Stites et al., 2007). Together, these components establish and promote tumorigenic effects in the cell (Cox and Der, 2010; Pylayeva-Gupta et al., 2011). Numerous growth factor receptors, such as EGFR, PDGFR and IGFR are among the upstream proteins that can activate the RAS pathway (Bazenet and Kazlauskas, 1993; Chan et al., 2001; Innocenti et al., 2002; Ono and Kuwano, 2006; Repasky et al., 2004); downstream effector proteins include ERK, PI3K, and RPS6, which each have been shown to have primary roles in cell proliferation and survival (Fan et al., 2009; Schubbert et al., 2007). Thus, tumors cells can have an activated RAS pathway by dysregulation of up or downstream pathway components, even without harboring a RAS mutation. Relying on biochemical analysis of RAS through mutation testing and measuring the active form of RAS (GTP-bound form) as means to record RAS-pathway activation status is limited; the existence of mutated RAS does not necessarily predicate an oncogenic addiction to the RAS pathway, as it has been previously shown that KRAS dependency is widely variable in KRAS-mutant cancer cell lines. Therefore, cancer cells may harbor a mutation in RAS, but not necessarily be addicted and dependent on the continual signaling of the pathway (Singh et al., 2009). Furthermore, if RAS is not mutated, it cannot be assumed that the network is "off", as additional components of the network may still be activated. In addition to redundancy in the network, the relative importance of different RAS network components may be context dependent; thus, focusing on a single protein might limit the ability to accurately reflect activity (Downward, 2006). Therefore, it is critical to study RAS-pathway activation in a comprehensive manner; we use a genomics framework to accomplish this goal.

In order to effectively measure activity in the RAS network, we utilize a RAS gene-expression signature capable of providing a network-scale measurement of activation by measuring the acute transcriptional changes that occur after RAS activation (Bild et al., 2006). As RAS can be activated by many mechanisms, it is critical to measure the RAS network more comprehensively than just by analysis of mutation status in order to obtain a reliable predictor of pathway activation. The need for comprehensive pathway measurements is especially true for complex branching pathways such as RAS (Downward, 2006). To that extent, our RAS gene-expression signature has been previously validated to accurately predict RAS-pathway activity in a variety of diverse settings; including 1) prediction of activity in primary human NSCLC adenocarcinoma tumors (Bild et al., 2006), 2) predictions of RAS activity in a multitude of cancer subtypes represented in Oncomine (Rhodes et al., 2007), 3) measurement of RAS-pathway activity in gastric cancer and ER + breast cancer bone metastasis (Ooi et al., 2009; Zhang et al., 2009) 4) and analysis of K-RAS dependency signature genes and "RAS addiction" in primary lung tumors (Singh et al., 2009). Together, these studies provide support to the robustness

Please cite this article in press as: El-Chaar, N.N., et al., Genomic classification of the RAS network identifies a personalized treatment strategy for lung cancer, Molecular Oncology (2014), http://dx.doi.org/10.1016/j.molonc.2014.05.005

and accuracy of the RAS signature to analyze RAS network activation in multiple settings.

In this study, we develop a network-based genomics framework for drug discovery. Specifically, we use a RAS gene-expression signature to discover therapeutic regimens that target the RAS network in lung cancer. We used this signature to determine RAS activity in a panel of NSCLC cell lines – these RAS-pathway activity measurements for each cancer sample are on a continuous scale, and can be correlated with drug response across the panel of cancer cell lines activity (West et al., 2001). Therefore, we identify compounds whose efficacy correlates to the genomics-based measurement of RAS activity in a drug screen that included 366 known and novel drug compounds. The results from the genomics-based drug screen identified that combined inhibition of EGFR and MEK pathway components most effectively inhibited RAS-active tumor cells. Indeed, there was a highly significant and reproducible correlation between treatment response and RAS-pathway activity in a large panel of lung cancer cell lines, highlighting the ability of this drug combination to selectively block tumor cells with RAS activation independent of the manner in which the RAS pathway is turned on. Additional novel compounds or drug regimens that target other components of the RAS network were not as effective at inhibiting RAS-active tumor cells. We show that in combination, these treatments block both the EGFR-RAS-RAF-ERK and EGFR-PI3K-AKT-RPS6 nodes of the RAS-pathway network and induce apoptosis, while either drug alone did not effectively inhibit both nodes. These results indicate that EGFR-RAS-RAF-ERK and EGFR-PI3K-AKT-RPS6 are key nodes important for RAS-activated lung cancer tumor cell survival. Our study combines genomic profiling with a high-throughput drug screen to guide the discovery of treatments that can be used to target certain cancer phenotypes. This approach can individualize drug therapies to target signaling pathways more efficiently through gene-expression profiling of network activation (Ascierto et al., 2013; Bentley et al., 2013; Favata et al., 1998; Janne et al., 2013; To et al., 2012).

2. Materials and methods

2.1. Small molecules

Gefitinib, AEW541, *erlotinib*, *trametinib*, *U0126*, *sorafenib*, and *temsirolimus* were purchased from Selleckchem and dissolved in 100% DMSO to generate 100 mM stock solutions of each, stored at −80 °C. For *erlotinib*, the 100 mM stock solution was further diluted to 30 mM in 100% DMSO for complete solubility. Novel compounds were provided by Dr. Chris Ireland and Dr. Sunil Sharma at the University of Utah.

2.2. Genomic data acquisition and normalization

We used gene-expression microarray data that had previously been used to profile the transcriptomic effects of RAS-pathway activation (Barbie et al., 2009; Bild et al., 2006; Boutros et al., 2009; Chang et al., 2009; Kim et al., 2009; Watanabe et al., 2011). We downloaded gene-expression microarray data for lung cancer cell lines from the Cancer Cell Line Encyclopedia (CCLE) (Barretina et al., 2012). Collaborators at Duke University also provided gene-expression data for 56 lung cancer cell lines. This dataset was uploaded to the Gene-Expression Omnibus (GEO) under accession identifier GSE47206. We MAS5 normalized (Hubbell et al., 2002) these datasets using the *affy* Bioconductor package (Gautier et al., 2004) for our analysis.

2.3. RAS-pathway activation predictions

Using the RAS gene-expression signature (Barbie et al., 2009; Bild et al., 2006; Boutros et al., 2009; Chang et al., 2009; Kim et al., 2009; Watanabe et al., 2011), we predicted RAS-pathway activation for each cell line using the Bayesian binary regression algorithm version 2.0 (BinReg2.0) used as a MATLAB plug-in (West et al., 2001). Prior to making the predictions, the data were log2 transformed and DWD normalized (Benito et al., 2004) to reduce biases that can result from differences in batch processing and microarray platforms. In making the predictions, we used default parameters, except that our signature used 350 genes and 1 metagene (as determined previously to be optimal for the RAS pathway) (Bild et al., 2006). The CCLE dataset was used for the expanded lung and breast cancer cell line predictions, while GSE47206 was used for the 14 lung cancer pilot experiments. For the pilot screen, the SK-MES-1 RAS-pathway activation value was obtained from the CCLE dataset run, as that cell line was not available in the GSE47206 dataset.

2.4. Preliminary genomics-based drug screen assay

Drugs were serially diluted 1:3 in 8 doses of each drug, starting from 30 μM and ending with 13.7 nM. To make the highest doses soluble in aqueous 5% FBS RPMI media solution, the drugs were sonicated twice on ice, and then used for serial dilution. For combinatorial treatments, doses had equal molar concentrations for each compound. All treatment doses were performed in four replicates. Cell viability and growth was measured using CellTiter-Glo (Promega, Madison, Wisconsin) 72 h post-treatment. EC50 values were calculated from dose response data by plotting on GraphPad Prism 4 and using the equation $Y = 1/(1 + 10((\log EC50 - X)*\text{HillSlope}))$ with a variable slope ($Y_{min} = 0$ and $Y_{max} = 1$). Plots were forced to start from the *x*-axis by plotting for an *x*-intercept point. Predictions were then correlated against EC50 values of the treatments, and an unbiased approach was used to identify candidate therapies by selecting drugs based on Pearson correlation values of less than or equal to −0.5, significant two-tailed unpaired *t*-test *p*-values ($p < 0.05$) and a 95% confidence interval calculated in GraphPad Prism 6.01.

2.5. Novel compounds and fractions drug screen and expanded dose response assays

Cell lines were plated at 1500 cells/well. Detailed information on the cell lines used and their growth conditions is provided in the Supplementary Information sheet. Cell lines were obtained from ATCC. For the dose response assays, known targeted therapeutics were serially diluted 1:3 from 90 μM to the lowest dose of 41.15 nM in media containing 5% FBS

Please cite this article in press as: El-Chaar, N.N., et al., Genomic classification of the RAS network identifies a personalized treatment strategy for lung cancer, Molecular Oncology (2014), http://dx.doi.org/10.1016/j.molonc.2014.05.005

(Gibco/Life technologies, Carlsbad, CA) and 1× Anti–Anti (Gibco/Life technologies, Carlsbad, CA). To make the highest dose soluble in aqueous media, drugs were sonicated twice on ice. For combination treatments, doses had equal molar concentrations for each compound. Cell viability was measured as described before. Every dose was done at least in duplicate. Dose response curves were generated using the same methodology described above. For novel fractions and compounds used in the screen, two or three doses of each were used respectively. For the novel compounds, the dose most negatively correlated to predicted probability of RAS-pathway activation was represented on the histogram. For the known targeted therapeutics, drug EC50 correlation to RAS-pathway activation was plotted.

2.6. Statistical and multivariate analysis

Linear correlation graphs and box plots were created using Graphpad Prism 6.01, and their corresponding statistical significance tests performed using the software. For correlation plots, a built-in two-tailed significance test calculated by Graphpad Prism 6.01 was used. Graphpad computes a t ratio from the Pearson r and the sample size using the Student's t-distribution method, and computes p from t values using a standard algorithm. For box plots, a standard two-tailed Mann–Whitney U-test was used when two samples were being compared, with the exception of the box plot diagrams for *erlotinib + trametinib*, where an unpaired t-test with Welch's correction was used due to the normality of the data and the unequal standard deviations. When testing for significance across more than 2 samples, we adjusted for multiple comparisons using GraphPad's built-in Dunn's multiple comparisons test, which compares the mean rank difference among samples against an $\alpha = 0.05$. For the Annexin V Apoptosis assay, Dunn's multiple comparison significance test was used to compare the Annexin V positive cell means of the different drug treatments against the DMSO control, for RAS-active and RAS-inactive cell lines separately. We sought to model the multivariate relationship between *gefitinib + U0126* EC50 and the predictor variables: RAS-pathway activity prediction, tumor subtype (adenocarcinoma, large cell carcinoma, or squamous cell carcinoma), KRAS mutation, TP53 mutation, MEK1 mutation, and EGFR mutation. The mutations were coded as (Y/N) based on observations from the CCLE hybrid capture sequencing dataset; we used mutations listed as non-neutral variant SNPs. We then used a two-step approach to construct a parsimonious model. First, a univariate analysis was used to determine the set of predictor variables that were individually associated with *gefitinib + U0126* log10 EC50. t-tests were used for binary predictors (mutations), and linear models were used for the continuous predictor (RAS-pathway activation) and for the ternary predictor (tumor subtype). Only those variables that were individually significant ($p < 0.05$, unadjusted) were included in the multivariate analysis. The multivariate analysis was a linear model. The log10 EC50 values were used in the analysis as they were much less skewed than the μM EC50 values and more closely agreed with the normality assumptions. The multivariate analysis was performed using the "R" statistical computing software, version 2.15.0 (R Development Core Team, 2011).

2.7. Immunostaining and KRAS-GTP pull down

9 NSCLC cell lines with a range of RAS-pathway activation profiles were used for the protein analysis (H1373, LCLC-97TMI, SK-MES-1, H441, H1944, H1563, H661, H520, H522). Cells were treated with 5 μM of *gefitinib*, *U0126*, *gefitinib + U0126* and DMSO control in 5% FBS media and 1× Anti–Anti for 6 h. Cells were washed, lysates extracted and western blots run (Supplementary Methods). Primary antibodies for GAPDH (#5174S), EGFR (#4267S), pEGFR-Y1068 (#2234S), pRAF1-S289/296/301 (#9431S), pRAF1-S338 (#9427S), MEK1/2 (#8727S), pMEK1/2-S217/221 (#9154S), pERK1/2-T202/Y204 (#4370S), pAKT-S473 (#4060S), RPS6 (#2217S), pRPS6-S240/244 (#5364S) and pRPS6-S235/236 (#4858S) were obtained from Cell Signaling Technology (Beverly, MA). RAF1 (sc-373722), AKT1/2/3 (sc-8312), ERK1/2 (sc-292838) and KRAS (sc-30) antibodies were purchased from Santa Cruz Biotechnology (Santa Cruz, CA). The KRAS Activation Assay (Cellbiolabs, San Diego, CA) was used to pull down RAS GTP, according to manufacturer's protocol and run on a western blot. KRAS-GTP was then blotted for using the described KRAS antibody.

2.8. Annexin V apoptosis assay

RAS-active cell lines H358, Calu-3, H2122 and RAS-inactive cell lines H520, H522 and H661 were plated overnight with 400,000 cells per plate in 60 mm plates and grown in their corresponding media (Supplementary Methods). The selected cell lines exhibited high or low probability of RAS-pathway activation, and the highest or lowest response to the combined therapy regimen. All cell lines selected were lines that were part of the drug screens. Cell lines were treated with 1 μM *of gefitinib*, *U0126*, *gefitinib + U0126* or *DMSO control*, which was prepared in 5% FBS media and 1× Anti–anti, for 72 h, then washed and collected for Annexin V staining. For the stain, the Dead Cell Apoptosis Kit with Annexin V Alexa Fluor® 488 & Propidium Iodide for flow cytometry (Life Technologies, Carlsbad, CA) was utilized according to manufacturer's protocol. Using flow cytometry analysis, the percentage of Annexin V positive cells was recorded, and the means of the positive Annexin V cells (early-stage apoptosis) calculated for the different treatments, separately for the 3 RAS-active cell lines and the 3 RAS-inactive cell lines.

2.9. Erlotinib *and* trametinib *combination dose response assay*

The highest drug combination dose was serially diluted 1:3 in 8 doses, starting from 90 μM and ending with 41.15 nM. To make the highest dose soluble in aqueous 5% FBS RPMI media solution, it was sonicated twice on ice, and then used for serial dilution. Doses had equal molar concentrations for each compound. All treatment doses were performed in four replicates. Cell viability was measured and EC50 obtained as described before in the methods. Predictions were then correlated against EC50 values of the combination treatment using Pearson correlation and the built-in GraphPad p-value test for correlation significance and a 95% confidence interval.

Please cite this article in press as: El-Chaar, N.N., et al., Genomic classification of the RAS network identifies a personalized treatment strategy for lung cancer, Molecular Oncology (2014), http://dx.doi.org/10.1016/j.molonc.2014.05.005

3. Results

3.1. *Genomics-based drug screen identifies an effective regimen for RAS-pathway inhibition*

The goal of this research is to develop a pathway-based genomics framework that can be used to discover drugs to effectively inhibit difficult-to-target oncogenic pathways such as RAS. Complex signaling pathways underlie many diseases, and it remains difficult to align individual patients with therapies that target these pathways effectively. To address this need, we developed a genomic approach to identify inhibitors that target specific pathways (Figure 1). Briefly, we used our validated genomic signature to estimate the RAS-pathway's activity in NSCLC cells (Bild et al., 2006). This activity is represented by a continuous scale of probability from low to high (0–1 respectively), and produces a quantitative estimate of the pathway's activity in cells. We correlated these genomic-based pathway activity measurements with cell line response to *in vitro* treatment of a large catalog of compounds. We then identified the compounds whose efficacy correlated best with genomics-based pathway activity.

The advantages of our drug screening approach are the following: 1) knowledge of the direct drug target is not necessary and instead focuses on the drug's effect on overall pathway activity rather than on any single pathway component's activity; 2) measurement of network activity is more comprehensive than just mutation status, thereby capturing all pathway-active cells, and 3) it is relatively high-throughput in the sense that an unlimited number of genomic pathway profiles can be applied to all compounds tested in the drug screen, facilitating the characterization of drug mechanism.

We carried out an initial drug screen on a panel of 14 NSCLC cell lines, and validated our findings in a two larger drug screens that included over 35 NSCLC cell lines each. For our initial screen, we tested several well-characterized small molecule inhibitors that target different components of the growth factor receptor network; these inhibitors include the EGFR inhibitor *gefitinib* (Mok et al., 2009; Ono and Kuwano, 2006), IGFR inhibitor *AEW541* (Garcia-Echeverria et al., 2004), MEK1/2 inhibitor *U0126* (Favata et al., 1998) and a mTOR inhibitor *temsirolimus* (Hudes et al., 2007), which were administered alone and in paired combinations. The drug response data were then correlated to predicted probabilities of RAS-

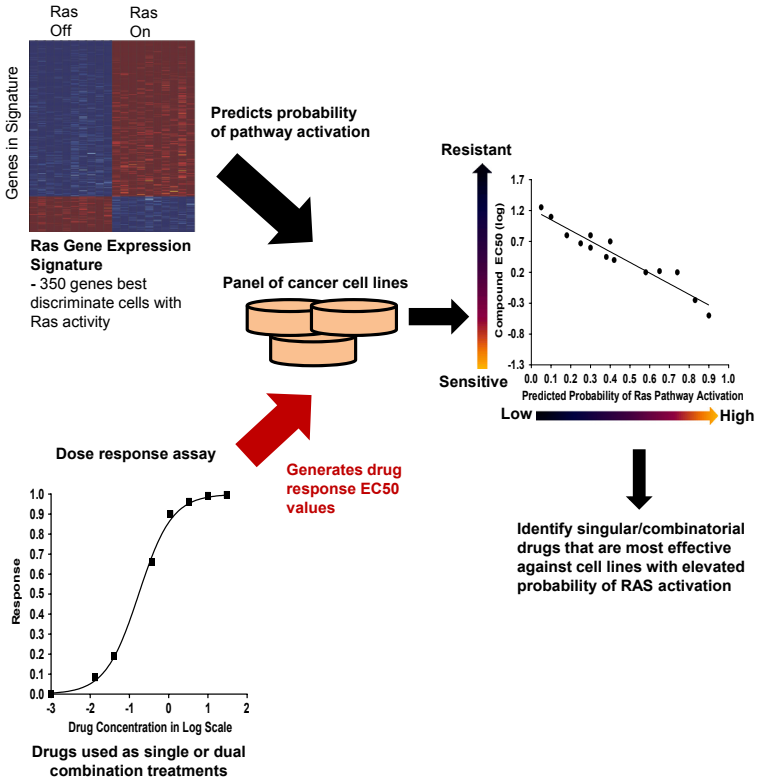

Figure 1 – The overall design of the Screenome approach to find RAS-driven tumor treatments. The RAS gene-expression signature is used to predict the probability of pathway activation in a panel of cancer cell lines. These same cell lines undergo dose response assays. The EC50 values are calculated and correlated against the predicted probability of RAS-pathway activation. The treatments whose effectiveness correlated negatively to RAS activity (the higher the probability of RAS being on, the more sensitive to the drug) are picked out as potential treatments for tumors with an activated RAS pathway.

Please cite this article in press as: El-Chaar, N.N., et al., Genomic classification of the RAS network identifies a personalized treatment strategy for lung cancer, Molecular Oncology (2014), http://dx.doi.org/10.1016/j.molonc.2014.05.005

pathway activation in our panel of NSCLC cell lines, obtained through the use of our RAS gene-expression signature (Bild et al., 2006) (Figure 1). Our preliminary screen showed a significant correlation between predicted RAS-pathway activation and co-inhibition of EGFR and MEK1/2 through the use of *gefitinib* and *U0126*, respectively ($R = -0.69$, p-value $= 0.0066$) (Supplementary Figure 1A). A significant correlation between RAS activity, as defined by the genomic signature, and drug efficacy did not exist for either of these inhibitors alone (*gefitinib*: $p = 0.0866$, *U0126*: $p = 0.2676$), suggesting that the drugs must be combined to effectively block RAS activity in NSCLC cells (Supplementary Figure 1B and C). We also investigated the effects of directly targeting the mTOR component of the growth factor receptor and RAS pathway, but mTOR inhibition through *temsirolimus* did not lead to growth inhibition of RAS-active cells, even with coupled inhibition of EGFR and MEK inhibition (Supplementary Figure 2A–C), and was therefore not pursued further.

3.2. Validation of the genomics-based drug screen results

Next, to validate and further interrogate the relationship between RAS-pathway activity and response to single and combined drug treatments, we performed multiple larger genomics-based screens on an expanded panel of 39 NSCLC cell lines (Figure 2A and Supplementary Figure 3A). In addition to a panel of well-characterized inhibitors, this larger screen also included over 360 novel drug-like compounds. As with the initial genomics-based screen, these experiments validated that the efficacy of EGFR and MEK1/2 co-inhibition through *gefitinib* and *U0126* was most correlated to RAS activity than any other single or combination drug treatments, resulting in a Pearson R score of -0.57 and $p = 0.0002$ (Figure 2A and C). Specifically, NSCLC cells with high genomics-predicted RAS activity (predicted probability of RAS-pathway activation > 0.5) had significantly lower EC50 scores (drug dose leading to 50% cell survival relative to untreated cells) than cancer cells with low RAS activity (predicted probability of RAS-pathway activation < 0.5), indicating higher drug sensitivity ($p < 0.0001$, Figure 2B). Cell lines with high RAS averaged an EC50 $= 0.436$ (log10) $= 2.7$ μM, while low RAS cell lines averaged an EC50 $= 1.07$ (log10) $= 11.76$ μM. As shown in Figure 2C, no other single drug/drug combination showed stronger correlation to RAS-pathway activity. This finding includes other drugs that target the growth factor receptor pathway such as single agent EGFR or MEK inhibitors, as well as single agent or combination therapies such as the RAF inhibitor *sorafenib*, and novel drug-like compounds (Figure 2C) (Liu et al., 2006). We compared this result against findings from a recently published study that demonstrated efficacy for IGFR and MEK co-inhibition in RAS-mutant cancers (Molina-Arcas et al., 2013). In our data, cell responses for MEK and EGFR co-inhibition correlated more strongly ($R = -0.57$) to RAS-pathway activity than MEK and IGFR co-inhibition ($R = -0.35$).

We also investigated the efficacy of the EGFR or MEK inhibitors in isolation. EGFR and MEK inhibition alone had average EC50 values of 11.87 μM and 10.02 μM respectively in the top 50% of responsive cell lines (Supplementary Figure 3B). In comparison, the combined treatment with MEK and EGFR inhibitors had an average EC50 of 1.83 μM (Supplementary Figure 3B). Additionally, as shown in Figure 2C and Supplementary Figure 3C and D, EGFR but not MEK1/2 inhibition showed an individual correlation to RAS-pathway activity, albeit not as strongly as the combined therapy (EGFR inhibition: $R = -0.47$, $p = 0.0027$. MEK inhibition: $R = -0.26$, $p = 0.1068$). This result is consistent with observations that KRAS dependent NSCLC cells exhibit some sensitivity to EGFR inhibitors (Singh et al., 2009), yet the combination therapy required one-tenth as much drug as *gefitinib* monotherapy. Furthermore, the BRAF/CRAF inhibitor *sorafenib* did not show a significant correlation to RAS activity, both alone ($p = 0.1247$) or in combination with EGFR ($p = 0.455$) and MEK1/2 ($p = 0.5356$) inhibitors (Supplementary Figure 4A–C). In support of this finding, *sorafenib* also failed to show efficacy in patients with KRAS mutated NSCLC in the phase III MISSION trial (Goodman, 2012).

The effectiveness of the EGFR/MEK inhibition as a treatment for NSCLC in general is further highlighted by the overall synergy of these agents in NSCLC cancer cell lines (Supplementary Figures 5A and 6A) and the significantly lower total EC50 scores for combination therapies in comparison with monotherapies observed across all the NSCLC cell lines (Supplementary Figure 5B and C). The EGFR + MEK combination exhibited a synergistic response relationship for 29 out of 39 cell lines (74%), signified by a synergy score greater than one (Figure 6A). Synergy was not as prevalent for RAF + EGFR and RAF + MEK inhibitor combinations (Supplementary Figure 6B–D).

Finally, the correlation between EGFR and MEK1/2 inhibitors combined efficacy and RAS-pathway activation was unskewed by the 8 most correlative cell lines (Supplementary Figure 7A) and potentially NSCLC specific, as the relationship between RAS-pathway activity and drug response was not observed in a panel of 35 breast cancer cell lines (Supplementary Figure 7B), possibly due to the dependency of breast cancer on alternate pathways such as PI3K, HER2 and the estrogen receptor pathway (Burstein, 2005; Campbell et al., 2004; Rosen et al., 2010; Sommer and Fuqua, 2001).

3.3. Genomics-based RAS activity predictions, and not RAS mutation status, significantly correlates to EGFR + MEK1/2 inhibitor therapy response

RAS can be aberrantly activated by different mechanisms, including via activating mutations or through dysregulation of other growth factor receptor pathway components (Downward, 2003; Karnoub and Weinberg, 2008; Pylayeva-Gupta et al., 2011). We investigated the relative treatment responsiveness for KRAS mutated cells compared to cells without KRAS mutations. Our studies show that KRAS mutations alone did not account for the responsiveness to combined EGFR/MEK inhibition ($p = 0.577$, Figure 3A); however, when RAS activity was considered more broadly by measuring pathway activity via our genomic profiling approach, there was a significant correlation between EGFR/MEK drug sensitivity and RAS activity ($p = 0.0004$, Figure 3B). No significant relationship existed between RAS mutation and drug

Please cite this article in press as: El-Chaar, N.N., et al., Genomic classification of the RAS network identifies a personalized treatment strategy for lung cancer, Molecular Oncology (2014), http://dx.doi.org/10.1016/j.molonc.2014.05.005

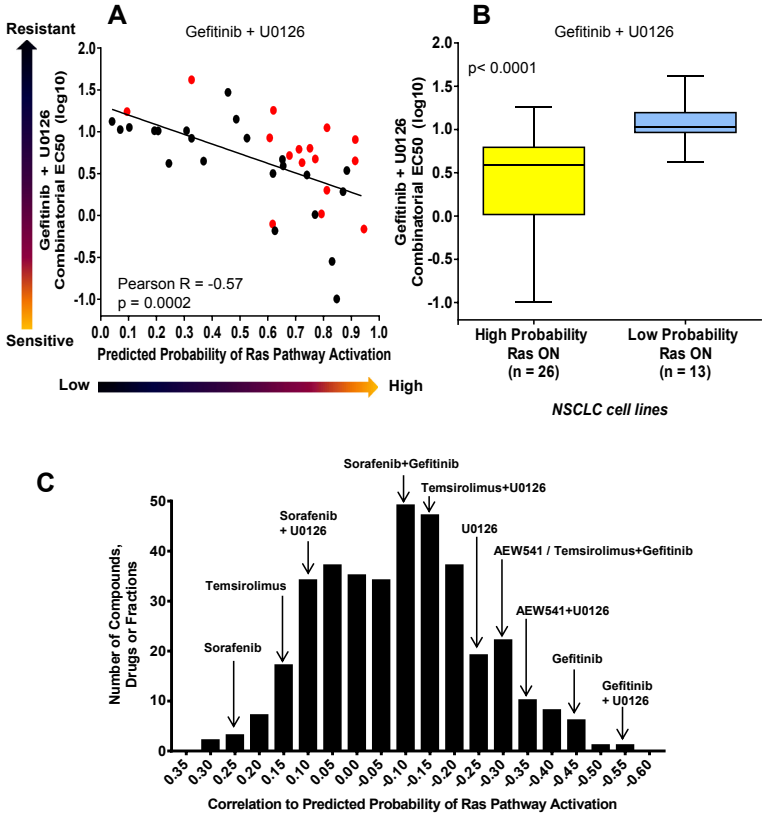

Figure 2 – Combinatorial inhibition of EGFR + MEK is correlated to RAS-pathway activity in NSCLC. (A) Linear correlation of *Gefitinib + U0126* EC50 values with the predicted probability of RAS-pathway activation across 39 NSCLC cell lines. Every dot represents a cell line, with a *y* value representing the cell line's *Gefitinib + U0126* EC50, and an *x* value representing the cell line's predicted probability of RAS-pathway activation. Response to *Gefitinib + U0126* is significantly negatively correlated to RAS. Legend = Red: K-RAS-mutant cell lines, Black: K-RAS wild-type cell lines. (B) Cell lines of the 39 NSCLC panel were divided accordingly and box plot diagrams of *Gefitinib + U0126* EC50 values were plotted. Box boundaries denote the 25–75th percentiles, while the error bars indicate maximum and minimum values. The line inside the box indicates the median value. Response to *Gefitinib + U0126* as measured by EC50 values is shown. Cell lines with elevated probability of RAS activation (predicted probability of RAS-pathway activation > 0.5) were significantly more sensitive to *Gefitinib + U0126* treatment than cell lines with low probability of RAS activation (predicted probability of RAS-pathway activation < 0.5). (C) Frequency Distribution of the Correlation of Compounds, Drugs and Fractions with the probability of RAS-pathway activation. A panel of 366 novel small molecules was tested against 39 NSCLC cell lines, and their effects on cell viability correlated to the predicted probability of RAS-pathway activation. These correlation values were plotted on a histogram. Correlation values of *temsirolimus*, *temsirolimus + U0126* and *temsirolimus + gefitinib* were obtained from the 14 NSCLC cell line preliminary screen and plotted onto the histogram. *Gefitinib + U0126* was the treatment most negatively correlated to RAS-pathway activation.

response for any other inhibitor we tested (Supplementary Figures 8 and 9). These results highlight the importance of comprehensively characterizing pathway activity via gene-expression profiles to link pathway activation with drug response.

Next, we performed a single and multivariate analysis to investigate whether the relationship between RAS-pathway activity and EGFR and MEK co-inhibition might be confounded by factors unrelated to RAS-pathway activity or by mutations in EGFR and MEK, the protein targets of *gefitinib* and *U0126* respectively. Potential variables that we evaluated were tumor subtype (adenocarcinoma, large cell carcinoma, or squamous cell carcinoma), KRAS mutation, TP53 mutation, MEK1 mutation, and EGFR mutation, using the adenocarcinoma subtype as the reference sample (Supplementary Table 1). This was especially important since as expected, predicted probability of RAS-pathway activation was the highest in the adenocarcinoma subtype, in comparison to squamous and large cell carcinoma subtypes (Bild et al., 2006) (Supplementary Figure 10). Univariate analysis highlighted the large cell carcinoma

Please cite this article in press as: El-Chaar, N.N., et al., Genomic classification of the RAS network identifies a personalized treatment strategy for lung cancer, Molecular Oncology (2014), http://dx.doi.org/10.1016/j.molonc.2014.05.005

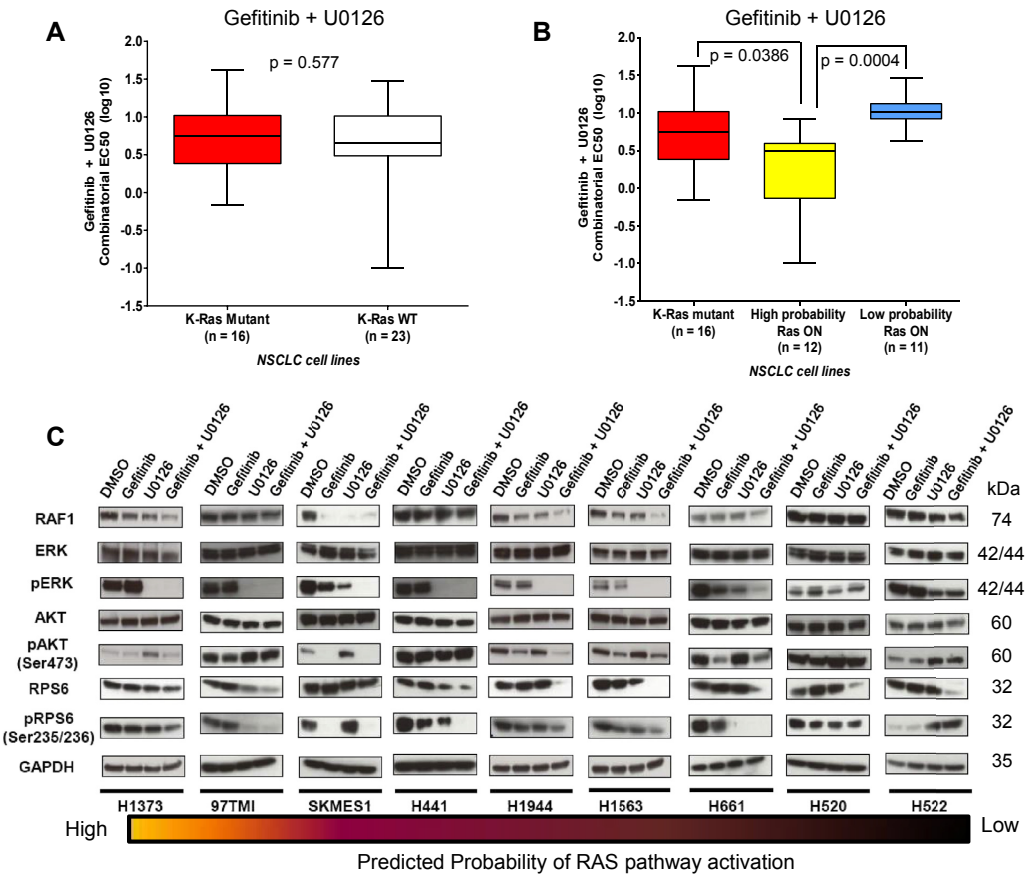

Figure 3 – Ras gene-expression signature predicts response to combined EGFR + MEK inhibition efficacy which inhibits ERK and RPS6 simultaneously. The cell lines of the 39 NSCLC panel were divided accordingly and box plot diagrams of *Gefitinib + U0126* EC50 values plotted. (A) Response to *Gefitinib + U0126* with respect to the mutation status of KRAS, as measured by EC50 values. KRAS mutation does not predict response to *gefitinib + U0126*. (B) Response to *Gefitinib + U0126* with respect to mutation status of KRAS and predicted probability of RAS-pathway activation, were RAS-active cell lines signified cell lines with a predicted probability of RAS-pathway activation > 0.5, and RAS-inactive cell lines < 0.5. Gene-expression signature prediction of probability of RAS-pathway activation predicts response to *Gefitinib + U0126*. (C) A panel of 9 NSCLC cell lines, ranging from high to low predicted probability of RAS-pathway activation was treated with *Gefitinib*, *U0126* and *Gefitinib + U0126* at a 5 μM dose for 6 h, and compared to DMSO control in a western blot. Combinatorial treatment inhibits the ERK and RPS6 nodes of the EGFR pathway in cell lines with high probability of RAS-pathway activation.

subtype and our RAS-pathway activation predictions as the primary potential predictors of EGFR and MEK1/2 co-inhibition response (Table 1). NSCLC subtype was considered as a single variable with two levels (large cell carcinoma and squamous cell carcinoma), and since one level was significant at $p = 0.05$, all levels were included in the multivariate analysis.

Based on the multivariate analysis (Table 2), response to EGFR/MEK inhibition was significantly higher in the NSCLC cell lines with high genomics-based RAS-pathway activity, after adjusting for subtype ($p = 0.00139$). This analysis provides further support to the validity and potential use of our RAS-pathway predictions as a biomarker of response to EGFR + MEK inhibition in NSCLC. Moreover, these results show that the ability of RAS-pathway activity to predict response to combination therapy is not confounded by EGFR nor MEK1 mutations.

3.4. *Combined inhibition of EGFR and MEK1/2 blocks key downstream components of the RAS pathway and induces apoptosis in RAS-active, but not RAS-inactive NSCLC cells*

Since a variability of response to EGFR and MEK dual inhibition was observed between tumor cells exhibiting an active and inactive RAS pathway, we investigated the potential differences in signaling effects of this drug regimen in NSCLC RAS-active and RAS-inactive tumor cells. We examined the

Please cite this article in press as: El-Chaar, N.N., et al., Genomic classification of the RAS network identifies a personalized treatment strategy for lung cancer, Molecular Oncology (2014), http://dx.doi.org/10.1016/j.molonc.2014.05.005

Table 1 – Univariate predictors of *Gefitinib + U0126* response (log10 EC50). Univariate analysis was first used to determine the set of predictor variables that were individually significantly related to *Gefitinib + U0126* response (log10 EC50). *t*-tests were used for the binary predictors (the mutations) and linear models were used for the continuous predictor (RAS-Pathway activation) and the ternary predictor (Tumor Subtype). The statistical tests used and the *p*-values are described. The large cell carcinoma subtype variable level and the RAS-pathway activity prediction variable were significant univariate predictors of response.

Predictor	Statistical test	*p*-value
KRAS mutation	Two sample *t*-test	0.56
TP53 mutation	Two sample *t*-test	0.55
MEK1 mutation	Two sample *t*-test	0.36
EGFR mutation	Two sample *t*-test	0.56
Subtype: Large cell carcinoma	Wald test from Linear model	0.044
Subtype: Squamous cell carcinoma	Two sample *t*-test	0.16
RAS-pathway Activity Prediction	Two sample *t*-test	0.00017

effects of EGFR and/or MEK inhibition on components of the EGFR and RAS pathways in a representative panel of 9 NSCLC cell lines, ranging from high to low predicted probability of RAS-pathway activation. In general, combined inhibition of EGFR + MEK led to concurrent inhibition of ERK and RPS6 phosphorylation, with variable effects on AKT activation in cells with higher levels of predicted RAS-pathway activation (Figure 3C). These cell lines also exhibited a general trend towards RAF1 protein loss, while a decrease in RPS6 protein was observed regardless of RAS-pathway activation status (Figure 3C). Conversely, cells with the lowest predicted probability of RAS-pathway activation (H520, H522) maintained RAF1 protein expression and activated ERK, AKT and RPS6 regardless of the treatment, with cell line H522 even upregulating the activation of AKT and RPS6, even with significant RPS6 protein loss (Figure 3C).

While combined inhibition of EGFR and MEK blocked both ERK and RPS6 activation in cells with higher RAS activation probability, EGFR monotherapy on the other hand only inhibited the activation of AKT and RPS6 with little effect on ERK, while MEK monotherapy only inhibited activation of ERK with a small effect on RPS6. Furthermore, EGFR monotherapy did not inhibit ERK, RPS6 or AKT in cells with the lowest probability of RAS-pathway activation, while MEK monotherapy had minimal effects on ERK activation, and even leading to the activation of AKT in cell line H522, highlighting the dual-node effect of the combination therapy.

Interestingly, we observe that the activation pattern of RPS6 did not correlate to probability of RAS-pathway activation. In cell lines H1373, 97TMI, H441 and H661, activation of RPS6 correlated to the phosphorylation of ERK, while in cell lines SK-MES-1, H1944, H1563, H520 and H522 it correlated to phosphorylation of AKT (Figure 3C). This is potentially due to the fact that RPS6 can be phosphorylated by the ERK and AKT arms of the pathway (Roux et al., 2007). Moreover, MEK inhibition decreased the ERK-mediated phosphorylation-dependent feedback inhibition of RAF1 (Ser289/296/301 phosphorylation) as expected (Fritsche-Guenther et al., 2011) (Supplementary Figure 11A). This pattern was more prominent when MEK inhibition was coupled with EGFR inhibition. Furthermore, a mild decrease in the Ser240/244 phosphorylation mark of RPS6 was observed, as well as a substantial decrease in the activating phosphorylation mark of RAF1 (Ser338) (Supplementary Figure 11A). Lastly, we did not observe the downregulation of ERK activation through MEK inhibition leading to an activation of EGFR upon MEK inhibition (Supplementary Figure 11A), as has been observed in colon cancer, marking a difference between the response of NSCLC and colon cancer to ERK inhibition (Klinger et al., 2013; Prahallad et al., 2012).

Among the two monotherapies and the dual therapy tested, *gefitinib* was the only treatment to produce RAS inhibition (Supplementary Figure 11B). One explanation for the failure of the combined therapy to inhibit RAS is that the combination of EGFR + MEK inhibition abrogates the effects of RAS inhibition by shutting down EGFR due to the removal of the ERK-mediated negative feedback loop on SOS caused by the complete inhibition of ERK (Shin et al., 2009) (Figure 5). In conclusion, dual inhibition of EGFR + MEK with *gefitinib* and *U0126*, respectively, is capable of shutting down both RPS6 and ERK in RAS-active tumors, while single agent treatment only suppresses a single component of the pathway. This is not the case for RAS-inactive tumors, where neither monotherapy nor dual therapy using an EGFR and a MEK inhibitor was able to inhibit activation of ERK, AKT and RPS6.

Next, we studied the ability of combinatorial therapy to induce apoptosis in RAS-active or RAS-inactive NSCLC tumor cells. Interestingly, we observed that upon treating 3 RAS-active and 3 RAS-inactive cell lines with a dose of 1 μM, apoptosis is only induced at significant levels in RAS-active tumor cells via combined inhibition of EGFR and MEK (Figure 4A–C). None of our treatments were capable of inducing apoptosis in RAS-inactive tumor cells (Figure 4B and D). These results were in line with the above observations whereby RAS-inactive cell lines recorded a marked resistance to EGFR + MEK inhibition, and retained activation of ERK, RPS6 and AKT (Figure 3C). These data highlight the importance of identifying the most beneficial cancer phenotypes prior to therapy administration.

In summary, combined inhibition of EGFR and MEK blocks growth of RAS-active NSCLC tumor cells by concurrent inhibition of ERK and RPS6. Combinatorial therapy performed significantly better at targeting RAS-active cells and blocking ERK and RPS6 than single agent therapy, or with therapies that target other nodes of the RAS-pathway network (Figure 5). These observations did not hold true for only RAS- or EGFR-mutant NSCLC tumor cells, providing evidence to the importance of utilizing characterization of pathway activity that allows for multiple mechanisms of pathway activation.

3.5. *Determining RAS-pathway activity is crucial to identify tumors that are most responsive to EGFR + MEK dual inhibition*

As *gefitinib* and *U0126* are not FDA-approved small molecule inhibitors of EGFR and MEK1/2 respectively, we sought to

Please cite this article in press as: El-Chaar, N.N., et al., Genomic classification of the RAS network identifies a personalized treatment strategy for lung cancer, Molecular Oncology (2014), http://dx.doi.org/10.1016/j.molonc.2014.05.005

Table 2 – Multivariate predictors of *Gefitinib + U0126* response (log10 EC50). Given that the dataset consisted of 39 cell lines, the univariate analysis done previously was used to determine the set of predictor variables that were individually significantly related to *Gefitinib + U0126* response (log10 EC50). These variables were included in the multivariate analysis. The multivariate analysis was a linear model. Multivariate analysis determined the RAS-pathway activity predictions as the sole predictor of EGFR + MEK inhibition response.

Predictor	Estimate	Std error	*t*-value	Wald *p*-value (two-sided)
(Intercept)	1.1743	0.2027	5.793	0.0000014
RAS-Pathway Activity Prediction	−1.0184	0.2933	−3.472	0.00139
Subtype: Large cell carcinoma	0.2626	0.2321	1.130	0.27
Subtype: Squamous cell carcinoma	0.2263	0.2230	1.015	0.32

validate the observation of a correlation between RAS-pathway activation and response to EGFR + MEK dual inhibition by using clinically-relevant inhibitors of EGFR and MEK1/2. We tested a combination of *erlotinib* and *trametinib*, two FDA-approved inhibitors of EGFR and MEK1/2 respectively (United States Food and Drug Administration, 2013a,b) on a panel of 16 NSCLC cell lines with a varying range of RAS-pathway activation. In support of our previous findings, we recorded a similar strong and significant correlation between RAS-pathway activation and response to the combination therapy (Figure 6A). Moreover, we observe that NSCLC cells with high genomics-predicted RAS activity had significantly lower EC50 scores than NSCLC cells with low RAS activity, indicating higher drug sensitivity ($p = 0.025$, Figure 6B). Cell lines with predicted high RAS averaged an EC50 = −0.6934 (log10) = 0.20 μM, while low RAS cell lines averaged an EC50 = 0.9545 (log10) = 9.01 μM, a 45-fold difference in sensitivity. As previously observed, there was no difference in response when the cell lines were divided based on KRAS mutation status ($p = 0.553$, Figure 6C). These results support the clinical relevancy of our previous observations with *gefitinib* and *U0126*, and highlight the immediate clinical relevance of this combinatorial regimen to treat RAS-active tumors in the clinic.

In summary, we show that determining RAS-pathway activation status is pivotal to tailor EGFR + MEK dual inhibition therapy to the most responsive NSCLC tumors. In Figures 2A and 6A a strong and highly significant correlation between RAS-pathway activity and response to EGFR + MEK combination therapy is evident. Cell lines with higher probability of RAS-pathway activation responded significantly better to the combination therapy (Figures 2B and 6B). The predictive power of RAS-pathway activity is not confounded by other tested variables, providing further support to the importance of RAS-pathway activation status as a determiner of response to EGFR + MEK inhibition (Tables 1 and 2). This is important to note as KRAS mutation status fails to predict response to EGFR + MEK inhibition (Figures 3A, B and 6C). The strength of this correlation lies in its reproducibility, which is observed in either a small or large sample size, using *gefitinib* and *U0126* (Supplementary Figures 1A, 2A and B) or FDA-approved and clinically used EGFR and MEK inhibitors in the form of *erlotinib* and *trametinib* (Figure 6). The identification of RAS-active tumor cells as being most vulnerable to a specific type of combinatorial therapy—in this case EGFR + MEK inhibition—emphasizes a need to reassess the design of clinical studies, with a focus on identifying the potential patient populations that could benefit the most from treatments prior to clinical trial design.

4. Discussion

RAS is a critical target for many solid tumors such as NSCLC; however, targeting the RAS protein directly has proven elusive. Furthermore, RAS can be activated by many mechanisms, making it challenging to identify RAS-active tumors. To discover therapeutics that can target RAS-active tumors, we performed a genomics-based drug screen in which cancer cells are characterized for RAS-pathway activity using a gene-expression signature and then screened against a panel of compounds to identify those drugs whose efficacy correlates to pathway activity. By measuring RAS-pathway activity by a genomics-based biomarker, we are able to more broadly define RAS activity and are not limited to examining mutation status alone. Furthermore, as the pathway predictions generate a continuous scale of RAS activity, we can identify drugs and/or drug combinations whose efficacy correlates to RAS-pathway activity. The genomics-based drug screen has various advantages compared to alternative drug screens such as conventional or siRNA screens as it provides a comprehensive characterization of a pathway's activity in cells that is not dependent on biochemical testing, and does not require knowledge of the direct drug target.

By using this approach, we have identified two targeted therapies that when combined effectively inhibit growth of RAS-active cancer cells: *gefitinib*, which inhibits EGFR and *U0126*, which inhibits MEK1/2. The use of *U0126* has been at the forefront of MEK inhibitor research with more than 2500 citations of its parent discovery publication. *U0126* is highly selective, with a nanomolar specificity for MEK1/2, and recorded off-target effects when concentrations greater than 10 μM are used (Favata et al., 1998), which is greater than the dose used in our biochemical analyses. Moreover, *U0126* shares similar inhibitory characteristics and functions as the recently FDA-approved MEK inhibitor, *trametinib* (United States Food and Drug Administration, 2013b; Yoshida et al., 2012), potentially extending our observation to the clinic. Indeed, we observe that using the FDA-approved EGFR and MEK1/2 inhibitors *erlotinib* and *trametinib* in combination led to similar results, lending support to the clinical relevancy and feasibility of this treatment against RAS-active NSCLC (Figure 6).

EGFR + MEK dual inhibition blocks two arms of the growth factor receptor network in RAS-active NSCLC tumor cells: EGFR-RAS-RAF-ERK and EGFR-PI3K-AKT-RPS6, whereas either agent alone failed to achieve this multi-pathway inhibition effect. Of note, KRAS mutation status alone did not predict response to this drug regimen; our analysis provides evidence

Please cite this article in press as: El-Chaar, N.N., et al., Genomic classification of the RAS network identifies a personalized treatment strategy for lung cancer, Molecular Oncology (2014), http://dx.doi.org/10.1016/j.molonc.2014.05.005

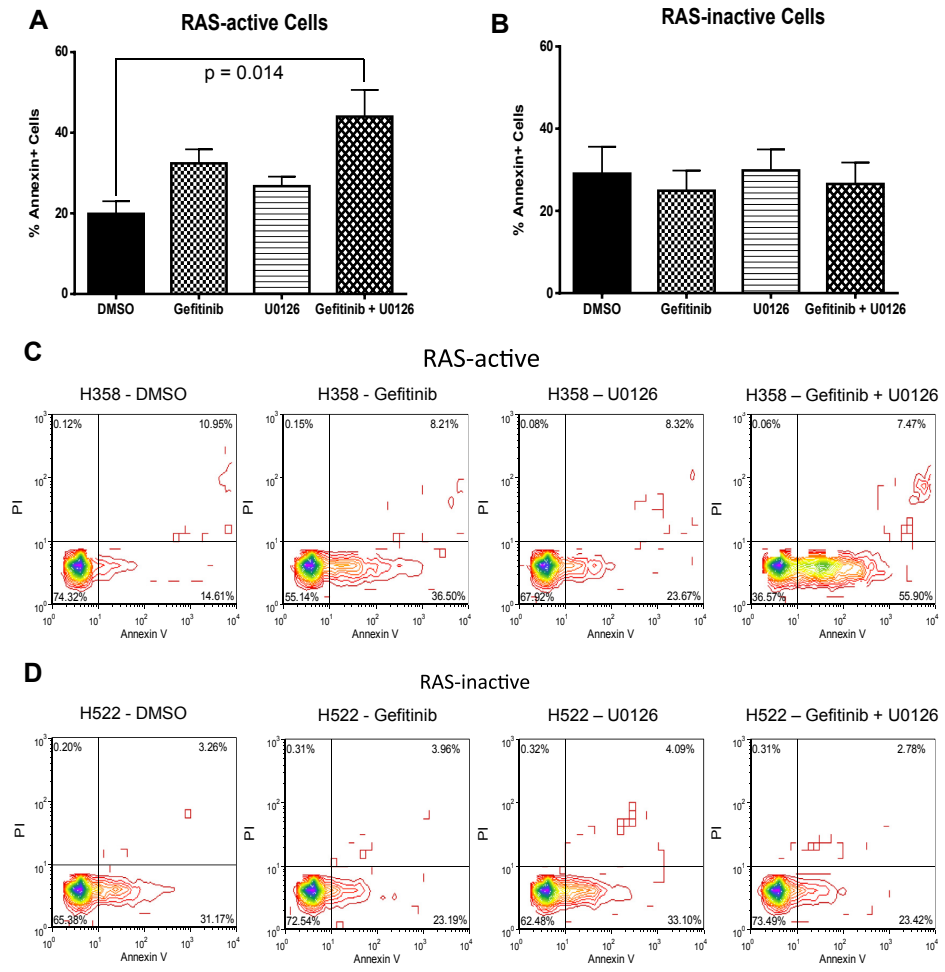

Figure 4 – EGFR + MEK combinatorial inhibition induces apoptosis in RAS-active, but not RAS-inactive tumor cells. (A) 3 RAS-active cell lines, H358, Calu-3 and H2122 were treated with 1 μM of *gefitinib*, *U0126* and *gefitinib + U0126* as well as DMSO control for 72 h, and stained for Annexin V. The percentage of Annexin V positive cells was calculated, averaged, and plotted, with the error bars indicating SEM. Only the combined treatment of *gefitinib + U0126* significantly induces apoptosis. (B) 3 RAS-inactive cell lines, H661, H520 and H522 were treated with 1 μM of *gefitinib*, *U0126* and *Gefitinib + U0126* as well as DMSO control for 72 h, and stained for Annexin V. The percentage of Annexin V positive cells was calculated, averaged, and plotted, with the error bars indicating SEM. Neither treatment induces apoptosis. (C) Contour plots of Annexin V/Propidium Iodide (PI) staining for RAS-active H358 cell line and (D) RAS-inactive cell line H522. The *x*-axis indicates Annexin V staining, while the *y*-axis indicated PI staining. The lower right part of the graph shows the percentage of cells in early-stage apoptosis (Annexin V positive cells), the top right the percentage of cells in late-stage apoptosis (Annexin V + PI double positive cells). The top left shows necrotic cells (PI positive cells), while the bottom right shows live cells. Apoptosis is only induced in the RAS-active cell line.

that some lung cancer cell lines with wild-type KRAS exhibit high RAS-pathway activity. This is in line with observations published by Molina-Arcas et al. (2013) that highlighted the IGFR-centric nature of mutant KRAS—but not wild-type KRAS—lung cancer, in activating the PI3K-AKT-RPS6 node of the pathway, with a strong implication of significant input from EGFR in the wild-type KRAS cells. We observed that best responders to EGFR + MEK inhibition were wild-type KRAS lung cancer cell lines with an activated RAS pathway. This result may explain why the response to EGFR + MEK inhibition correlates better to RAS-pathway activity than IGFR and MEK inhibition (Figure 2C).

By studying RAS network activation through the genomics-based biomarker, we have observed the requirement of EGFR + MEK signaling in maintaining activation of the PI3K-AKT-RPS6 and EGFR-RAS-RAF-ERK nodes in RAS-active

Please cite this article in press as: El-Chaar, N.N., et al., Genomic classification of the RAS network identifies a personalized treatment strategy for lung cancer, Molecular Oncology (2014), http://dx.doi.org/10.1016/j.molonc.2014.05.005

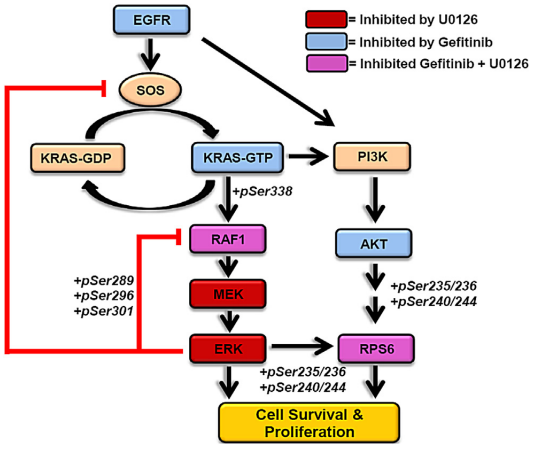

Figure 5 – The EGFR pathway and the model of the effect of EGFR/MEK/EGFR + MEK inhibition on the pathway in RAS-active NSCLC cell lines. EGFR monotherapy inhibits activation of EGFR, KRAS and AKT (blue), while U0126 inhibits the activity of MEK, preventing the activation of ERK (red). Combined therapy leads to the inhibition of all the aforementioned proteins (blue and red) plus RPS6 and RAF1 (purple), which are also degraded.

NSCLC. Interestingly, combinatorial inhibition of EGFR with other components of the growth factor receptor network, such as RAF or mTOR, does not correlate to RAS activity in lung cancer cells. One reason the RAF inhibitor sorafenib is not equivalent to MEK inhibition could be due to *sorafenib*'s inability to block ERK signaling in KRAS-mutant cells (Takezawa et al., 2009; Wilhelm et al., 2004). Together, these studies highlight the complexity of RAS-centric signaling in cancer, and the need to identify an appropriate target population prior to initiation of clinical trials, as data suggests that the different growth factor receptor network combinatorial treatments will be effective only in discrete patient populations.

Although clinical trials, such as the IPASS trial (Mok et al., 2009) have shown efficacy of anti-EGFR tyrosine kinase inhibitors in EGFR-mutant NSCLC, inhibition of growth factor receptors has also been effective in unselected second-line patients. For example, inhibition by anti-EGFR antibody *cetuximab* was beneficial in EGFR-positive patients in the FLEX and IPASS trials (Mok et al., 2009; Pirker et al., 2009). Indeed, in contrast to colon cancer, KRAS mutations do not predict resistance to EGFR inhibition in lung cancer (Guan et al., 2013; Krejci et al., 2011; Mazzoni et al., 2011; O'Byrne et al., 2011). While not nearly as effective as the *gefitinib/U0126* combination, we do see some efficacy of *gefitinib* alone in our panel of lung cancer cell lines. However, upon investigation of the mechanisms by which these drugs function, we find that EGFR antagonism alone does not significantly block downstream growth factor receptor network components such as RAF, ERK and RPS6. Alternatively, MEK1/2 inhibition does effectively inhibit ERK activity, but often fails to inhibit alternative upstream EGFR signaling components such as RAS and AKT. Only by combined treatment of both EGFR + MEK1/2 do we see effective inhibition of both up and downstream growth factor receptor network components. As ERK inhibition is a key regulator of proliferation and survival of cancer cells (Wortzel and Seger, 2011), and RPS6 also plays vital roles important in cell survival as well as translation initiation (Ruvinsky and Meyuhas, 2006), we expect that effectively blocking these two pathways in cancer cells contributes to their synergistic function and decreased cancer cell growth.

Interestingly, although RAS-inactive cell line H520 displays synergy between *gefitinib* and *U0126* (Supplementary Figure 6A), the cell line still remains significantly recalcitrant to the treatment, requiring a combinatorial EC50 dose of 11.27 μM, more than 4-fold less responsive than the average response in RAS-active cell lines (EC50 = 2.7 μM) (Supplementary Figure 2B and Table 1). This is also the case for the RAS-inactive cell line H661. Although it displays similar overall pharmacodynamic pattern of pathway component inhibition as RAS-active cell lines when treated with *gefitinib* and *U0126*, this cell line is also not comparatively sensitive to the treatment (EC50 = 10.28 μM). The observed synergy for these lines is an interesting area for future mechanistic studies. However, our conclusion that RAS-active cell lines are sensitive to combined EGFR/MEK inhibition remains accurate. Indeed, the RAS-inactive cell lines H520 and H661 are not sensitive to this combined treatment (Supplementary Table 1), independent of their synergy profiles (Figure 3C, Supplementary Figure 6A).

It will be critical in future clinical trials to identify those tumors that are RAS-active independent of the mechanism of RAS activation in order to best treat those patients with a drug regimen that effectively blocks these key nodes in the RAS pathway. By using mutation analysis alone, one overlooks a large population of tumors that do not carry particular mutations yet harbor activated oncogenic pathways. There are currently clinical trials such as recruiting patients for EGFR + MEK inhibitor combinations based on mutation status alone. Our results suggest that mutation status alone cannot always provide optimal selection of responsive patients. By more comprehensively characterizing patients with dysregulated pathway independent of the mechanism of activation, it may be possible to better select patients for clinical trial inclusion.

Gene-expression signatures have recently made their way to the clinical and commercial sectors, laying the foundation for the feasibility of bringing any future gene-expression signatures to the clinic (Arpino et al., 2013). One example is the FDA-approved microarray-based gene-expression profiling signature Mammaprint® which uses tissue core sampled on fresh specimens preserved in RNA later or frozen archived tissue as source material, to output and score low/high risk of tumor metastasis (Arpino et al., 2013; van 't Veer et al., 2002; van de Vijver et al., 2002). Therefore, the application of a gene-expression signature as a genomic biomarker of RAS-pathway activation is both promising and feasible.

Overall, our data shows the significant correlation between RAS-pathway activity and response to EGFR + MEK inhibition (Figure 2A and B), and the predictive power of our signature

Please cite this article in press as: El-Chaar, N.N., et al., Genomic classification of the RAS network identifies a personalized treatment strategy for lung cancer, Molecular Oncology (2014), http://dx.doi.org/10.1016/j.molonc.2014.05.005

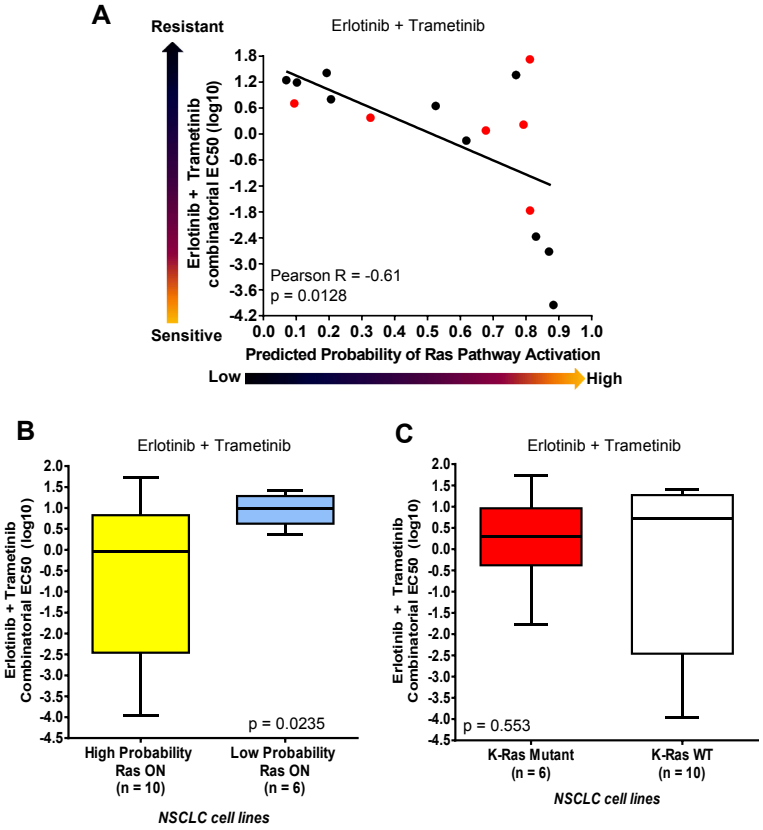

Figure 6 – Combinatorial inhibition of EGFR + MEK using FDA-approved inhibitors is correlated to RAS-pathway activity in NSCLC. (A) Linear correlation of *erlotinib* + *trametinib* EC50 values with the predicted probability of RAS-pathway activation across 16 NSCLC cell lines. Response to *erlotinib* + *trametinib* is significantly negatively correlated to RAS. Legend = Red: KRAS-mutant cell lines, Black: KRAS wild-type cell lines. (B) Cell lines of the 16 NSCLC panel were divided accordingly and box plot diagrams of *erlotinib* + *trametinib* EC50 values were plotted. Response to *erlotinib* + *trametinib* as measured by EC50 values is shown. Cell lines with elevated probability of RAS activation (predicted probability of RAS-pathway activation > 0.5) were significantly more sensitive to *erlotinib* + *trametinib* treatment than cell lines with low probability of RAS activation (predicted probability of RAS-pathway activation < 0.5). (C) Response to *erlotinib* + *trametinib* with respect to the mutation status of KRAS, as measured by EC50 values. K-RAS mutation does not predict response to *erlotinib* + *trametinib*.

which is independent of other factors such as cancer subtype of mutations in key pathway components (Tables 1 and 2). In the clinic, the RAS gene-expression signature could be used to assess RAS-pathway activation status in a patient's tumor. If the tumor has high pathway activity, that patient may be a candidate to receive EGFR + MEK dual inhibition. Indeed, the clinical potential of our study is supported by the validation of our observed correlation of RAS-pathway activation and EGFR + MEK dual inhibition using FDA-approved inhibitors (Figure 6).

Lastly, it is important to note that while tumor heterogeneity will ultimately be important in identifying and treating refractory subclones within a tumor, our current approach is to analyze the overall RAS activity within a tumor. Thus, higher levels of RAS activity within a tumor will predict greater overall response. Arguably, our approach measures RAS activity within the bulk tumor, where there may be subclones that are a minority population but still have varied RAS activity. Current and future studies are dedicated to addressing this ongoing issue in tumor characterization and treatment.

In summary, we described a genomic-based screen that characterizes RAS-pathway activation and identifies drugs that effectively target the pathway, inducing an apoptotic tumor cell response. By using a genomic approach to characterize oncogenic pathway activity in tumor cells, the ability to find drugs that target and inhibit a specific pathway is increased. Given the complexity and crosstalk of signaling pathways that is unique to individual tumor phenotypes, it is essential to identify and block the relevant pathway components for optimal drug response. By applying a genomic

Please cite this article in press as: El-Chaar, N.N., et al., Genomic classification of the RAS network identifies a personalized treatment strategy for lung cancer, Molecular Oncology (2014), http://dx.doi.org/10.1016/j.molonc.2014.05.005

approach to discovery of pathway-specific drug regimens, we can identify the patients who may best benefit from those treatment regimens prior to initiation of a clinical trial.

Author contributions

NNE, AHB and PJM conceived the study. NNE and SRP performed the bioinformatic analysis. NNE and KMB performed the experimental work and data analysis. ALC and JTC provided critical input on the concept design. NNE and AHB wrote the manuscript. PJM, SRP, JTC and ALC provided crucial manuscript feedback and suggestions.

Conflict of interests

Authors declare no conflicts of interest.

Acknowledgments

This study was supported by the National Institute of Health and Medical Research (R01GM085601 and U01CA164720, AHB) and by the Cancer Center Support Grant Program (CCSG): in Imaging, Diagnostics and Therapeutics (IDT) through the Huntsman Cancer Institute at the University of Utah. We are thankful for Drs. Chris Ireland, Sunil Sharma and Mary Kay Harper who supplied us with the novel compound libraries used in our screen. All authors involved in the study declare no competing interests. Gene-expression microarray data used for the 39 lung cancer cell lines can be found on the Cancer Cell Line Encyclopedia (CCLE) website. Gene-expression microarray data used for the pilot screen with 14 lung cancer cell lines was uploaded to the Gene-Expression Omnibus (GEO) under accession identifier GSE47206.

Appendix A. Supplementary data

Supplementary data related to this article can be found at http://dx.doi.org/10.1016/j.molonc.2014.05.005.

REFERENCES

American Cancer Society, 2013. Cancer Fact and Figures 2013. American Cancer Society, Atlanta.

Arpino, G., Generali, D., Sapino, A., Del Matro, L., Frassoldati, A., de Laurentis, M., Paolo, P., Mustacchi, G., Cazzaniga, M., De Placido, S., Conte, P., Cappelletti, M., Zanoni, V., Antonelli, A., Martinotti, M., Puglisi, F., Berruti, A., Bottini, A., Dogliotti, L., 2013. Gene expression profiling in breast cancer: a clinical perspective. Breast 22, 109–120.

Ascierto, P.A., Schadendorf, D., Berking, C., Agarwala, S.S., van Herpen, C.M., Queirolo, P., Blank, C.U., Hauschild, A., Beck, J.T., St-Pierre, A., Niazi, F., Wandel, S., Peters, M., Zubel, A., Dummer, R., 2013. MEK162 for patients with advanced melanoma harbouring NRAS or Val600 BRAF mutations: a non-randomised, open-label phase 2 study. Lancet Oncol. 14, 249–256.

Aviel-Ronen, S., Blackhall, F.H., Shepherd, F.A., Tsao, M.S., 2006. K-ras mutations in non-small-cell lung carcinoma: a review. Clin. Lung Cancer 8, 30–38.

Baines, A.T., Xu, D., Der, C.J., 2011. Inhibition of Ras for cancer treatment: the search continues. Future Med. Chem. 3, 1787–1808.

Barbie, D.A., Tamayo, P., Boehm, J.S., Kim, S.Y., Moody, S.E., Dunn, I.F., Schinzel, A.C., Sandy, P., Meylan, E., Scholl, C., Frohling, S., Chan, E.M., Sos, M.L., Michel, K., Mermel, C., Silver, S.J., Weir, B.A., Reiling, J.H., Sheng, Q., Gupta, P.B., Wadlow, R.C., Le, H., Hoersch, S., Wittner, B.S., Ramaswamy, S., Livingston, D.M., Sabatini, D.M., Meyerson, M., Thomas, R.K., Lander, E.S., Mesirov, J.P., Root, D.E., Gilliland, D.G., Jacks, T., Hahn, W.C., 2009. Systematic RNA interference reveals that oncogenic KRAS-driven cancers require TBK1. Nature 462, 108–112.

Barretina, J., Caponigro, G., Stransky, N., Venkatesan, K., Margolin, A.A., Kim, S., Wilson, C.J., Lehar, J., Kryukov, G.V., Sonkin, D., Reddy, A., Liu, M., Murray, L., Berger, M.F., Monahan, J.E., Morais, P., Meltzer, J., Korejwa, A., Jane-Valbuena, J., Mapa, F.A., Thibault, J., Bric-Furlong, E., Raman, P., Shipway, A., Engels, I.H., Cheng, J., Yu, G.K., Yu, J., Aspesi Jr., P., de Silva, M., Jagtap, K., Jones, M.D., Wang, L., Hatton, C., Palescandolo, E., Gupta, S., Mahan, S., Sougnez, C., Onofrio, R.C., Liefeld, T., MacConaill, L., Winckler, W., Reich, M., Li, N., Mesirov, J.P., Gabriel, S.B., Getz, G., Ardlie, K., Chan, V., Myer, V.E., Weber, B.L., Porter, J., Warmuth, M., Finan, P., Harris, J.L., Meyerson, M., Golub, T.R., Morrissey, M.P., Sellers, W.R., Schlegel, R., Garraway, L.A., 2012. The Cancer Cell Line Encyclopedia enables predictive modelling of anticancer drug sensitivity. Nature 483, 603–607.

Bazenet, C., Kazlauskas, A., 1993. The PDGF receptor a subunit activates p21r- and triggers DNA synthesis without interacting with rasGAP. Oncogene 9, 517–525.

Benito, M., Parker, J., Du, Q., Wu, J., Xiang, D., Perou, C.M., Marron, J.S., 2004. Adjustment of systematic microarray data biases. Bioinformatics 20, 105–114.

Bentley, C., Jurinka, S.S., Kljavin, N.M., Vartanian, S., Ramani, S.R., Gonzalez, L.C., Yu, K., Modrusan, Z., Du, P., Bourgon, R., Neve, R.M., Stokoe, D., 2013. A requirement for wild-type Ras isoforms in mutant KRas-driven signalling and transformation. Biochem. J. 452, 313–320.

Bild, A.H., Yao, G., Chang, J.T., Wang, Q., Potti, A., Chasse, D., Joshi, M.B., Harpole, D., Lancaster, J.M., Berchuck, A., Olson Jr., J.A., Marks, J.R., Dressman, H.K., West, M., Nevins, J.R., 2006. Oncogenic pathway signatures in human cancers as a guide to targeted therapies. Nature 439, 353–357.

Boutros, P.C., Lau, S.K., Pintilie, M., Liu, N., Shepherd, F.A., Der, S.D., Tsao, M.S., Penn, L.Z., Jurisica, I., 2009. Prognostic gene signatures for non-small-cell lung cancer. Proc. Natl. Acad. Sci. U.S.A. 106, 2824–2828.

Burstein, H.J., 2005. The distinctive nature of HER2-positive breast cancers. N. Engl. J. Med. 353, 1652–1654.

Campbell, I.G., Russell, S.E., Choong, D.Y., Montgomery, K.G., Ciavarella, M.L., Hooi, C.S., Cristiano, B.E., Pearson, R.B., Phillips, W.A., 2004. Mutation of the PIK3CA gene in ovarian and breast cancer. Cancer Res. 64, 7678–7681.

Chan, T.W., Pollak, M., Huynh, H., 2001. Inhibition of insulin-like growth factor signaling pathways in mammary gland by pure antiestrogen ICI 182,780. Clin. Cancer Res. 7, 2545–2554.

Chang, J.T., Carvalho, C., Mori, S., Bild, A.H., Gatza, M.L., Wang, Q., Lucas, J.E., Potti, A., Febbo, P.G., West, M., Nevins, J.R., 2009. A genomic strategy to elucidate modules of oncogenic pathway signaling networks. Mol. Cell 34, 104–114.

COSMIC Database. Distribution of somatic mutations in HRAS. Sanger Institute.

Please cite this article in press as: El-Chaar, N.N., et al., Genomic classification of the RAS network identifies a personalized treatment strategy for lung cancer, Molecular Oncology (2014), http://dx.doi.org/10.1016/j.molonc.2014.05.005

COSMIC Database. Distribution of somatic mutations in KRAS. Sanger Institute.

COSMIC Database. Distribution of somatic mutations in NRAS. Sanger Institute.

Cox, A.D., Der, C.J., 2010. Ras history: the saga continues. Small GTPases 1, 2–27.

Der, C.J., 2012. Targeting KRAS for the treatment of gastrointestinal cancers: mission impossible? In: 2012 Gastrointestinal Cancers Symposium.

Downward, J., 2003. Targeting RAS signalling pathways in cancer therapy. Nature reviews. Cancer 3, 11–22.

Downward, J., 2006. Cancer biology: signatures guide drug choice. Nature 439, 274–275.

Fan, Q.W., Cheng, C., Knight, Z.A., Haas-Kogan, D., Stokoe, D., James, C.D., McCormick, F., Shokat, K.M., Weiss, W.A., 2009. EGFR signals to mTOR through PKC and independently of Akt in glioma. Sci. Signal. 2, ra4.

Favata, M.F., Horiuchi, K.Y., Manos, E.J., Daulerio, A.J., Stradley, D.A., Feeser, W.S., Van Dyk, D.E., Pitts, W.J., Earl, R.A., Hobbs, F., Copeland, R.A., Magolda, R.L., Scherle, P.A., Trzaskos, J.M., 1998. Identification of a novel inhibitor of mitogen-activated protein kinase. J. Biol. Chem. 273, 18623–18632.

Fritsche-Guenther, R., Witzel, F., Sieber, A., Herr, R., Schmidt, N., Braun, S., Brummer, T., Sers, C., Bluthgen, N., 2011. Strong negative feedback from Erk to Raf confers robustness to MAPK signalling. Mol. Syst. Biol. 7, 489.

Garcia-Echeverria, C., Pearson, M.A., Marti, A., Meyer, T., Mestan, J., Zimmermann, J., Gao, J., Brueggen, J., Capraro, H.G., Cozens, R., Evans, D.B., Fabbro, D., Furet, P., Porta, D.G., Liebetanz, J., Martiny-Baron, G., Ruetz, S., Hofmann, F., 2004. In vivo antitumor activity of NVP-AEW541-A novel, potent, and selective inhibitor of the IGF-IR kinase. Cancer Cell 5, 231–239.

Gautier, L., Cope, L., Bolstad, B.M., Irizarry, R.A., 2004. affy–analysis of Affymetrix GeneChip data at the probe level. Bioinformatics 20, 307–315.

Goodman, A., 2012. Sorafenib Fails to Improve Survival as Third- or Fourth-line Treatment of Advanced Non-small Cell Lung Cancer. ASCO Post.

Graziano, S.L., Gamble, G.P., Newman, N.B., Abbott, L.Z., Rooney, M., Mookherjee, S., Lamb, M.L., Kohman, L.J., Poiesz, B.J., 1999. Prognostic significance of K-ras codon 12 mutations in patients with resected stage I and II non-small-cell lung cancer. J. Clin. Oncol. 17, 668–675.

Guan, J.L., Zhong, W.Z., An, S.J., Yang, J.J., Su, J., Chen, Z.H., Yan, H.H., Chen, Z.Y., Huang, Z.M., Zhang, X.C., Nie, Q., Wu, Y.L., 2013. KRAS mutation in patients with lung cancer: a predictor for poor prognosis but not for EGFR-TKIs or chemotherapy. Ann. Surg. Oncol. 20, 1381–1388.

Gysin, S., Salt, M., Young, A., McCormick, F., 2011. Therapeutic strategies for targeting ras proteins. Genes Cancer 2, 359–372.

Hubbell, E., Liu, W.M., Mei, R., 2002. Robust estimators for expression analysis. Bioinformatics 18, 1585–1592.

Hudes, G., Carducci, M., Tomczak, P., Dutcher, J., Figlin, R., Kapoor, A., Staroslawska, E., Sosman, J., McDermott, D., Bodrogi, I., Kovacevic, Z., Lesovoy, V., Schmidt-Wolf, I.G., Barbarash, O., Gokmen, E., O'Toole, T., Lustgarten, S., Moore, L., Motzer, R.J., Global, A.T., 2007. Temsirolimus, interferon alfa, or both for advanced renal-cell carcinoma. N. Engl. J. Med. 356, 2271–2281.

Innocenti, M., Tenca, P., Frittoli, E., Faretta, M., Tocchetti, A., Di Fiore, P.P., Scita, G., 2002. Mechanisms through which Sos-1 coordinates the activation of Ras and Rac. J. Cell Biol. 156, 125–136.

International Agency for Research on Cancer and Cancer Research UK, 2012. World Cancer Factsheet. World Health Organization, Cancer Research, UK, London.

Janne, P.A., Shaw, A.T., Pereira, J.R., Jeannin, G., Vansteenkiste, J., Barrios, C., Franke, F.A., Grinsted, L., Zazulina, V., Smith, P., Smith, I., Crino, L., 2013. Selumetinib plus docetaxel for KRAS-mutant advanced non-small-cell lung cancer: a randomised, multicentre, placebo-controlled, phase 2 study. Lancet Oncol. 14, 38–47.

Johnson, M.L., Sima, C.S., Chaft, J., Paik, P.K., Pao, W., Kris, M.G., Ladanyi, M., Riely, G.J., 2012. Association of KRAS and EGFR mutations with survival in patients with advanced lung adenocarcinomas. Cancer 119, 356–362.

Karnoub, A.E., Weinberg, R.A., 2008. Ras oncogenes: split personalities. Nature reviews. Mol. Cell Biol. 9, 517–531.

Kim, W.Y., Perera, S., Zhou, B., Carretero, J., Yeh, J.J., Heathcote, S.A., Jackson, A.L., Nikolinakos, P., Ospina, B., Naumov, G., Brandstetter, K.A., Weigman, V.J., Zaghlul, S., Hayes, D.N., Padera, R.F., Heymach, J.V., Kung, A.L., Sharpless, N.E., Kaelin Jr., W.G., Wong, K.K., 2009. HIF2alpha cooperates with RAS to promote lung tumorigenesis in mice. J. Clin. Invest. 119, 2160–2170.

Klinger, B., Sieber, A., Fritsche-Guenther, R., Witzel, F., Berry, L., Schumacher, D., Yan, Y., Durek, P., Merchant, M., Schafer, R., Sers, C., Bluthgen, N., 2013. Network quantification of EGFR signaling unveils potential for targeted combination therapy. Mol. Syst. Biol. 9, 673.

Krejci, J., Pesek, M., Grossmann, P., Krejci, M., Ricar, J., Benesova, L., Minarik, M., 2011. Extraordinary response to erlotinib therapy in a patient with lung adenocarcinoma exhibiting KRAS mutation and EGFR amplification. Cancer Genom Proteomics 8, 135–138.

Liu, L., Cao, Y., Chen, C., Zhang, X., McNabola, A., Wilkie, D., Wilhelm, S., Lynch, M., Carter, C., 2006. Sorafenib blocks the RAF/MEK/ERK pathway, inhibits tumor angiogenesis, and induces tumor cell apoptosis in hepatocellular carcinoma model PLC/PRF/5. Cancer Res. 66, 11851–11858.

Mazzoni, F., Rotella, V., Pratesi, N., Boni, L., Simi, L., Orlando, C., Comin, C.E., Maddau, C., Di Costanzo, F., 2011. From clinical trials to clinical practice: predictors of response to erlotinib in advanced non-small cell lung cancer patients pretreated with chemotherapy. Tumori 97, 160–165.

Meng, D., Yuan, M., Li, X., Chen, L., Yang, J., Zhao, X., Ma, W., Xin, J., 2013. Prognostic value of K-RAS mutations in patients with non-small cell lung cancer: a systematic review with meta-analysis. Lung Cancer 81, 1–10.

Minna, J.D., Larsen, J.E., 2011. Molecular biology of lung cancer: clinical implications. Clin. Chest Med. 32, 703–740.

Mok, T.S., Wu, Y.L., Thongprasert, S., Yang, C.H., Chu, D.T., Saijo, N., Sunpaweravong, P., Han, B., Margono, B., Ichinose, Y., Nishiwaki, Y., Ohe, Y., Yang, J.J., Chewaskulyong, B., Jiang, H., Duffield, E.L., Watkins, C.L., Armour, A.A., Fukuoka, M., 2009. Gefitinib or carboplatin-paclitaxel in pulmonary adenocarcinoma. N. Engl. J. Med. 361, 947–957.

Molina-Arcas, M., Hancock, D.C., Sheridan, C., Kumar, M.S., Downward, J., 2013. Coordinate direct input of both KRAS and IGF1 receptor to activation of PI3 kinase in KRAS-mutant lung cancer. Cancer Discov. 3, 548–563.

O'Byrne, K.J., Gatzemeier, U., Bondarenko, I., Barrios, C., Eschbach, C., Martens, U.M., Hotko, Y., Kortsik, C., Paz-Ares, L., Pereira, J.R., von Pawel, J., Ramlau, R., Roh, J.K., Yu, C.T., Stroh, C., Celik, I., Schueler, A., Pirker, R., 2011. Molecular biomarkers in non-small-cell lung cancer: a retrospective analysis of data from the phase 3 FLEX study. Lancet Oncol. 12, 795–805.

Ono, M., Kuwano, M., 2006. Molecular mechanisms of epidermal growth factor receptor (EGFR) activation and response to gefitinib and other EGFR-targeting drugs. Clin. Cancer Res. 12, 7242–7251.

Ooi, C.H., Ivanova, T., Wu, J., Lee, M., Tan, I.B., Tao, J., Ward, L., Koo, J.H., Gopalakrishnan, V., Zhu, Y., Cheng, L.L., Lee, J.,

Please cite this article in press as: El-Chaar, N.N., et al., Genomic classification of the RAS network identifies a personalized treatment strategy for lung cancer, Molecular Oncology (2014), http://dx.doi.org/10.1016/j.molonc.2014.05.005

Rha, S.Y., Chung, H.C., Ganesan, K., So, J., Soo, K.C., Lim, D., Chan, W.H., Wong, W.K., Bowtell, D., Yeoh, K.G., Grabsch, H., Boussioutas, A., Tan, P., 2009. Oncogenic pathway combinations predict clinical prognosis in gastric cancer. PLoS Genet. 5, e1000676.

Pirker, R., Pereira, J.R., Szczesna, A., von Pawel, J., Krzakowski, M., Ramlau, R., Vynnychenko, I., Park, K., Yu, C.T., Ganul, V., Roh, J.K., Bajetta, E., O'Byrne, K., de Marinis, F., Eberhardt, W., Goddemeier, T., Emig, M., Gatzemeier, U., Team, F.S., 2009. Cetuximab plus chemotherapy in patients with advanced non-small-cell lung cancer (FLEX): an open-label randomised phase III trial. Lancet 373, 1525–1531.

Prahallad, A., Sun, C., Huang, S., Di Nicolantonio, F., Salazar, R., Zecchin, D., Beijersbergen, R.L., Bardelli, A., Bernards, R., 2012. Unresponsiveness of colon cancer to BRAF(V600E) inhibition through feedback activation of EGFR. Nature 483, 100–103.

Pylayeva-Gupta, Y., Grabocka, E., Bar-Sagi, D., 2011. RAS oncogenes: weaving a tumorigenic web. Nature Reviews. Cancer 11, 761–774.

R Development Core Team, 2011. R: A Language and Environment for Statistical Computing. R Foundation for Statistical Computing, Vienna, Austria.

Repasky, G.A., Chenette, E.J., Der, C.J., 2004. Renewing the conspiracy theory debate: does Raf function alone to mediate Ras oncogenesis? Trends Cell Biol. 14, 639–647.

Rhodes, D.R., Kalyana-Sundaram, S., Mahavisno, V., Varambally, R., Yu, J., Briggs, B.B., Barrette, T.R., Anstet, M.J., Kincead-Beal, C., Kulkarni, P., Varambally, S., Ghosh, D., Chinnaiyan, A.M., 2007. Oncomine 3.0: genes, pathways, and networks in a collection of 18,000 cancer gene expression profiles. Neoplasia 9, 166–180.

Riely, G.J., Marks, J., Pao, W., 2009. KRAS mutations in non-small cell lung cancer. Proc. Am. Thoracic Soc. 6, 201–205.

Roberts, P.J., Stinchcombe, T.E., 2013. KRAS mutation: should we test for it, and does it matter? J. Clin. Oncol. 31, 1112–1121.

Roberts, P.J., Stinchcombe, T.E., Der, C.J., Socinski, M.A., 2010. Personalized medicine in non-small-cell lung cancer: is KRAS a useful marker in selecting patients for epidermal growth factor receptor-targeted therapy? J. Clin. Oncol. 28, 4769–4777.

Rosen, L.S., Ashurst, H.L., Chap, L., 2010. Targeting signal transduction pathways in metastatic breast cancer: a comprehensive review. Oncologist 15, 216–235.

Roux, P.P., Shahbazian, D., Vu, H., Holz, M.K., Cohen, M.S., Taunton, J., Sonenberg, N., Blenis, J., 2007. RAS/ERK signaling promotes site-specific ribosomal protein S6 phosphorylation via RSK and stimulates cap-dependent translation. J. Biol. Chem. 282, 14056–14064.

Ruvinsky, I., Meyuhas, O., 2006. Ribosomal protein S6 phosphorylation: from protein synthesis to cell size. Trends Biochem. Sci. 31, 342–348.

Schubbert, S., Shannon, K., Bollag, G., 2007. Hyperactive Ras in developmental disorders and cancer. Nature reviews. Cancer 7, 295–308.

Shin, S.Y., Rath, O., Choo, S.M., Fee, F., McFerran, B., Kolch, W., Cho, K.H., 2009. Positive- and negative-feedback regulations coordinate the dynamic behavior of the Ras-Raf-MEK-ERK signal transduction pathway. J. Cell Sci. 122, 425–435.

Singh, A., Greninger, P., Rhodes, D., Koopman, L., Violette, S., Bardeesy, N., Settleman, J., 2009. A gene expression signature associated with "K-Ras addiction" reveals regulators of EMT and tumor cell survival. Cancer Cell 15, 489–500.

Sommer, S., Fuqua, S.A., 2001. Estrogen receptor and breast cancer. Semin. Cancer Biol. 11, 339–352.

Stites, E.C., Trampont, P.C., Ma, Z., Ravichandran, K.S., 2007. Network analysis of oncogenic Ras activation in cancer. Science 318, 463–467.

Takezawa, K., Okamoto, I., Yonesaka, K., Hatashita, E., Yamada, Y., Fukuoka, M., Nakagawa, K., 2009. Sorafenib inhibits non-small cell lung cancer cell growth by targeting B-RAF in KRAS wild-type cells and C-RAF in KRAS mutant cells. Cancer Res. 69, 6515–6521.

To, M.D., Rosario, R.D., Westcott, P.M., Banta, K.L., Balmain, A., 2012. Interactions between wild-type and mutant Ras genes in lung and skin carcinogenesis. Oncogene 32, 4028–4033.

United States Food and Drug Administration, 2013a. Erlotinib.

United States Food and Drug Administration, 2013b. Trametinib.

van 't Veer, L.J., Dai, H., van de Vijver, M.J., He, Y.D., Hart, A.A., Mao, M., Peterse, H.L., van der Kooy, K., Marton, M.J., Witteveen, A.T., Schreiber, G.J., Kerkhoven, R.M., Roberts, C., Linsley, P.S., Bernards, R., Friend, S.H., 2002. Gene expression profiling predicts clinical outcome of breast cancer. Nature 415, 530–536.

van de Vijver, M.J., He, Y.D., van't Veer, L.J., Dai, H., Hart, A.A., Voskuil, D.W., Schreiber, G.J., Peterse, J.L., Roberts, C., Marton, M.J., Parrish, M., Atsma, D., Witteveen, A., Glas, A., Delahaye, L., van der Velde, T., Bartelink, H., Rodenhuis, S., Rutgers, E.T., Friend, S.H., Bernards, R., 2002. A gene-expression signature as a predictor of survival in breast cancer. N. Engl. J. Med. 347, 1999–2009.

Watanabe, T., Kobunai, T., Yamamoto, Y., Matsuda, K., Ishihara, S., Nozawa, K., Iinuma, H., Ikeuchi, H., Eshima, K., 2011. Differential gene expression signatures between colorectal cancers with and without KRAS mutations: crosstalk between the KRAS pathway and other signalling pathways. Eur. J. Cancer 47, 1946–1954.

West, M., Blanchette, C., Dressman, H., Huang, E., Ishida, S., Spang, R., Zuzan, H., Olson Jr., J.A., Marks, J.R., Nevins, J.R., 2001. Predicting the clinical status of human breast cancer by using gene expression profiles. Proc. Natl. Acad. Sci. U.S.A. 98, 11462–11467.

Wilhelm, S.M., Carter, C., Tang, L., Wilkie, D., McNabola, A., Rong, H., Chen, C., Zhang, X., Vincent, P., McHugh, M., Cao, Y., Shujath, J., Gawlak, S., Eveleigh, D., Rowley, B., Liu, L., Adnane, L., Lynch, M., Auclair, D., Taylor, I., Gedrich, R., Voznesensky, A., Riedl, B., Post, L.E., Bollag, G., Trail, P.A., 2004. BAY 43-9006 exhibits broad spectrum oral antitumor activity and targets the RAF/MEK/ERK pathway and receptor tyrosine kinases involved in tumor progression and angiogenesis. Cancer Res. 64, 7099–7109.

Wortzel, I., Seger, R., 2011. The ERK cascade: distinct functions within various subcellular organelles. Genes Cancer 2, 195–209.

Yoshida, T., Kakegawa, J., Yamaguchi, T., Hantani, Y., Okajima, N., Sakai, T., Watanabe, Y., Nakamura, M., 2012. Identification and characterization of a novel chemotype MEK inhibitor able to alter the phosphorylation state of MEK1/2. Oncotarget 3, 1533–1545.

Zhang, X.H., Wang, Q., Gerald, W., Hudis, C.A., Norton, L., Smid, M., Foekens, J.A., Massague, J., 2009. Latent bone metastasis in breast cancer tied to Src-dependent survival signals. Cancer Cell 16, 67–78.

Please cite this article in press as: El-Chaar, N.N., et al., Genomic classification of the RAS network identifies a personalized treatment strategy for lung cancer, Molecular Oncology (2014), http://dx.doi.org/10.1016/j.molonc.2014.05.005

Supplementary Material Table of Contents

Supplementary Figure 1

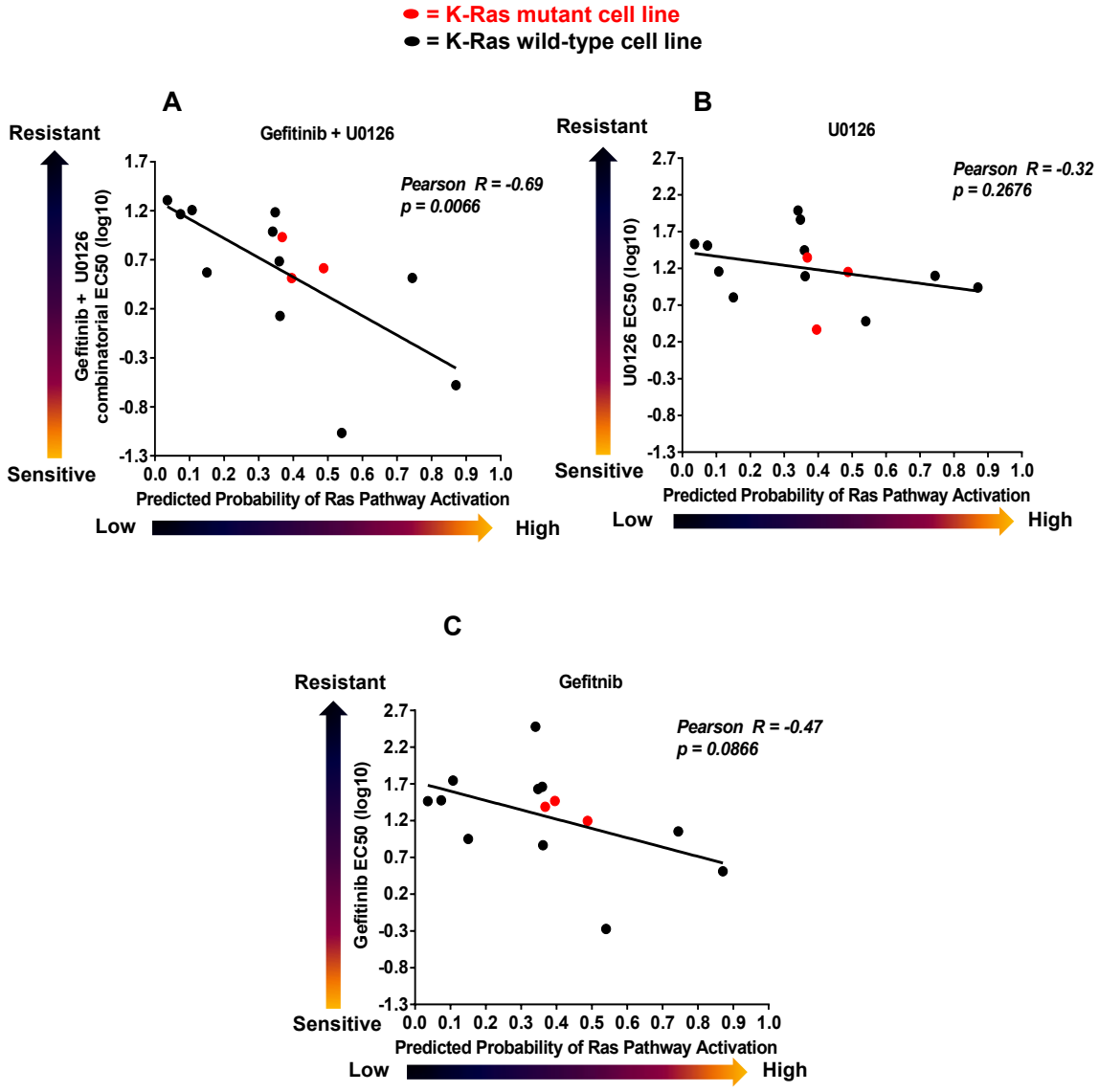

Supplementary Figure 2

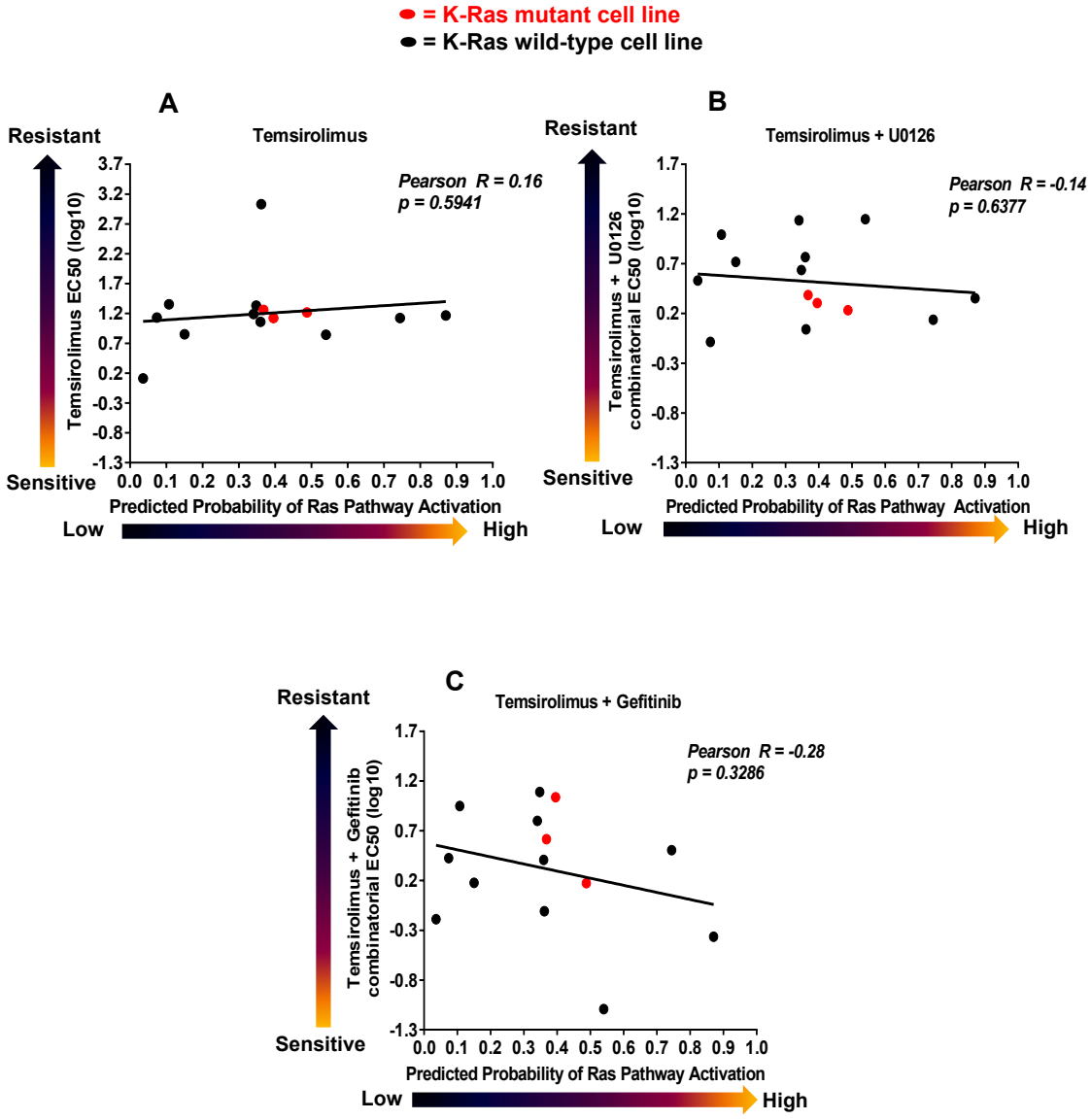

Supplementary Figure 3

● = K-Ras mutant cell line
● = K-Ras wild-type cell line

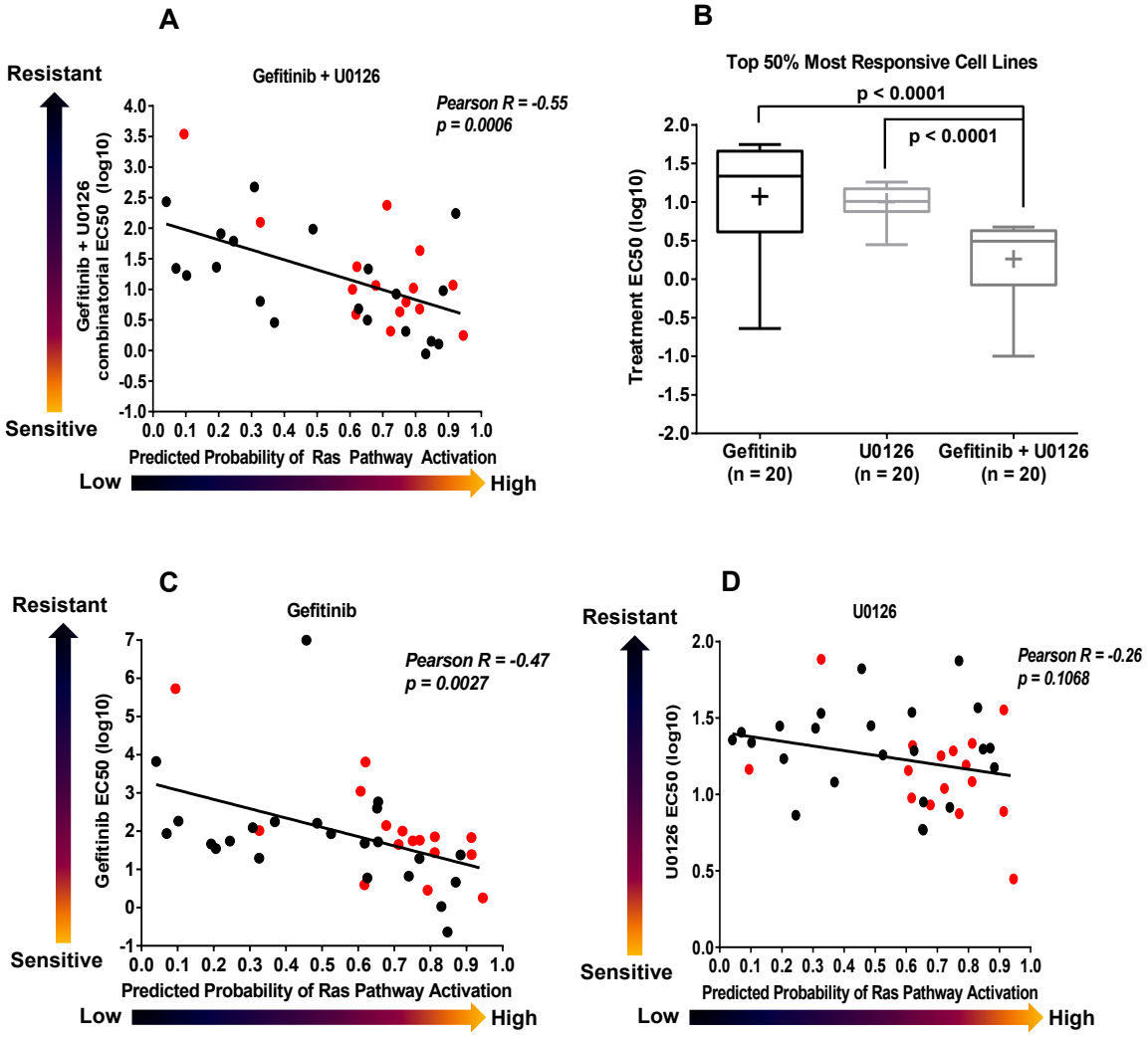

Supplementary Figure 4

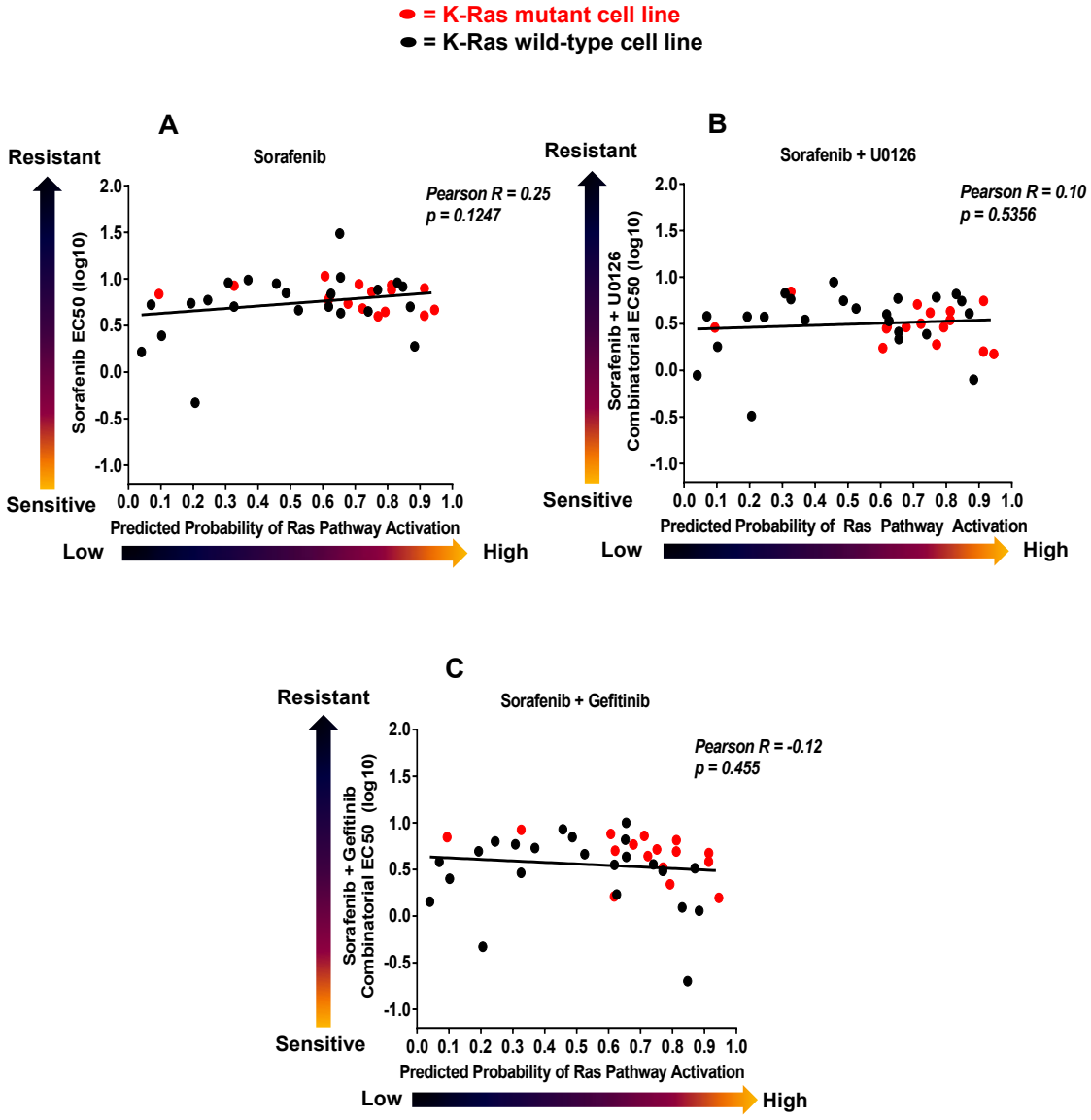

Supplementary Figure 5

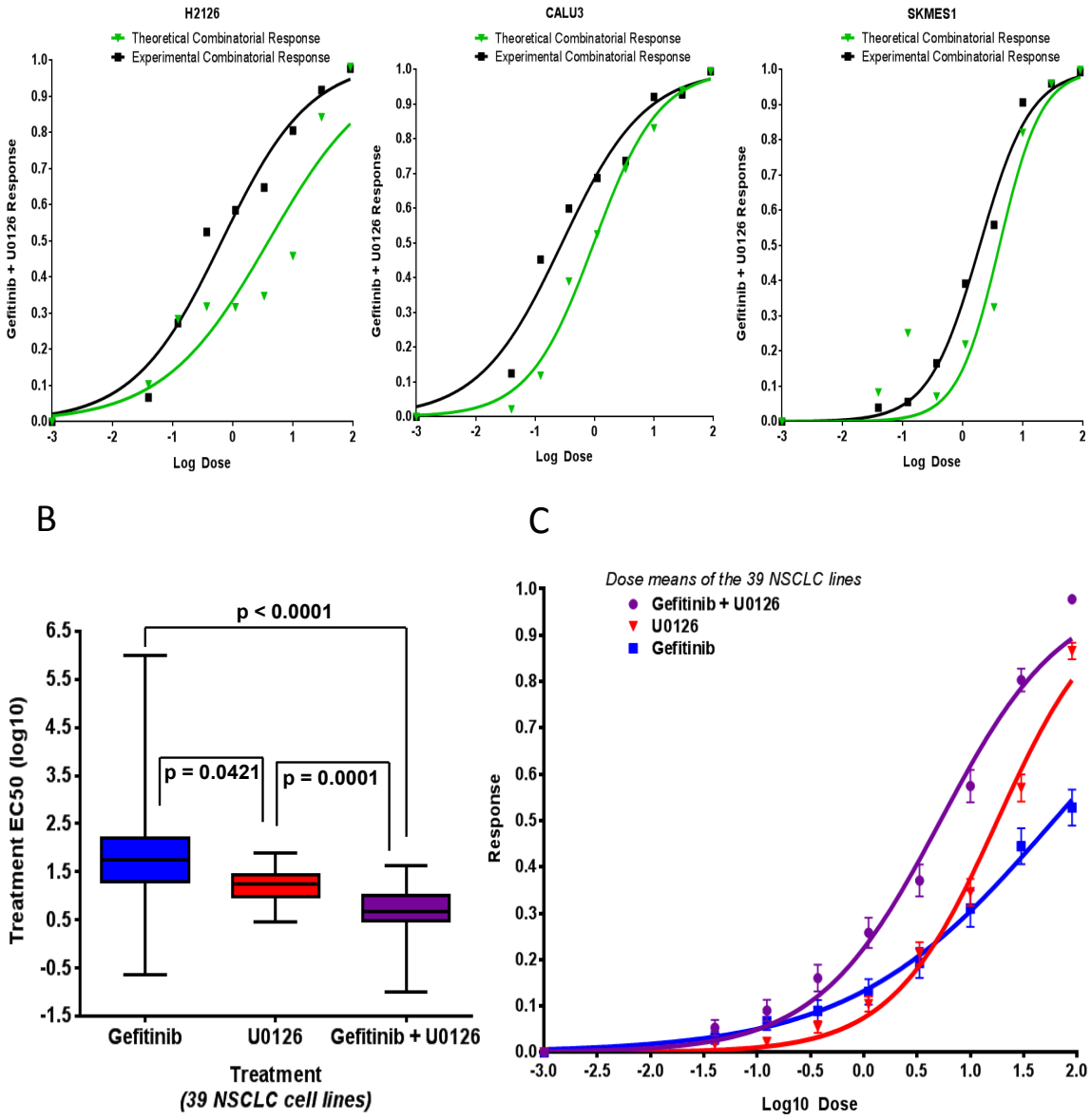

Supplementary Figure 6

A

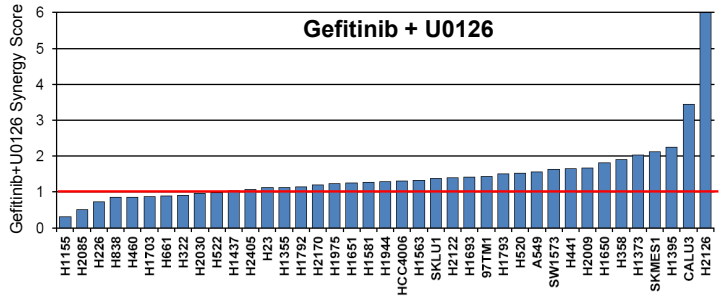

B

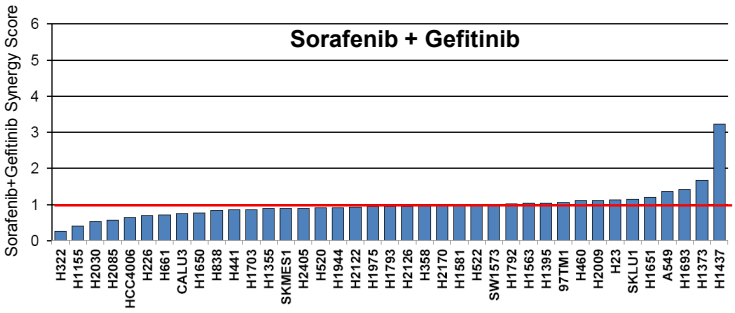

C

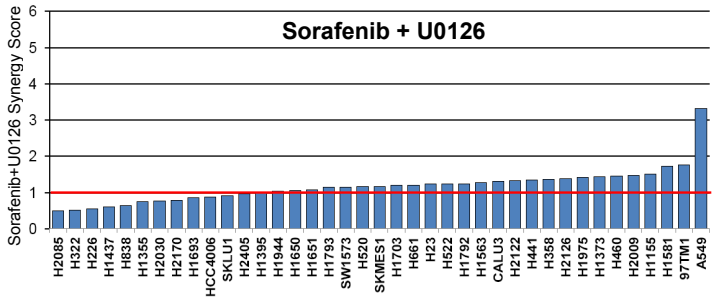

D

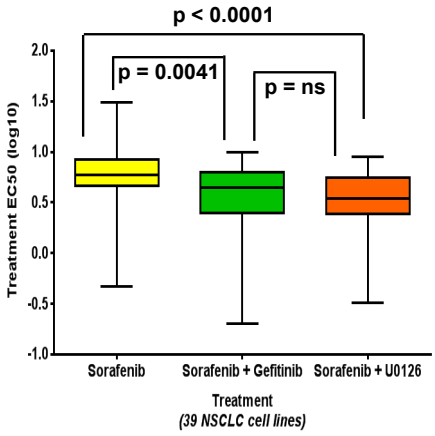

Supplementary Figure 7

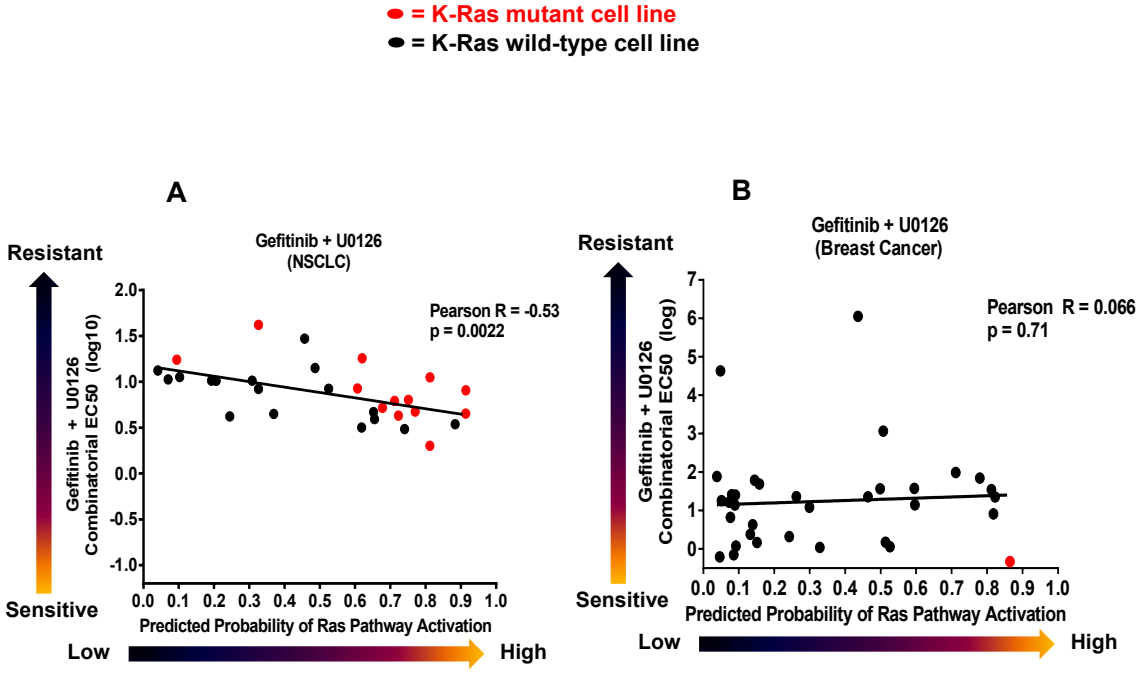

Supplementary Figure 8

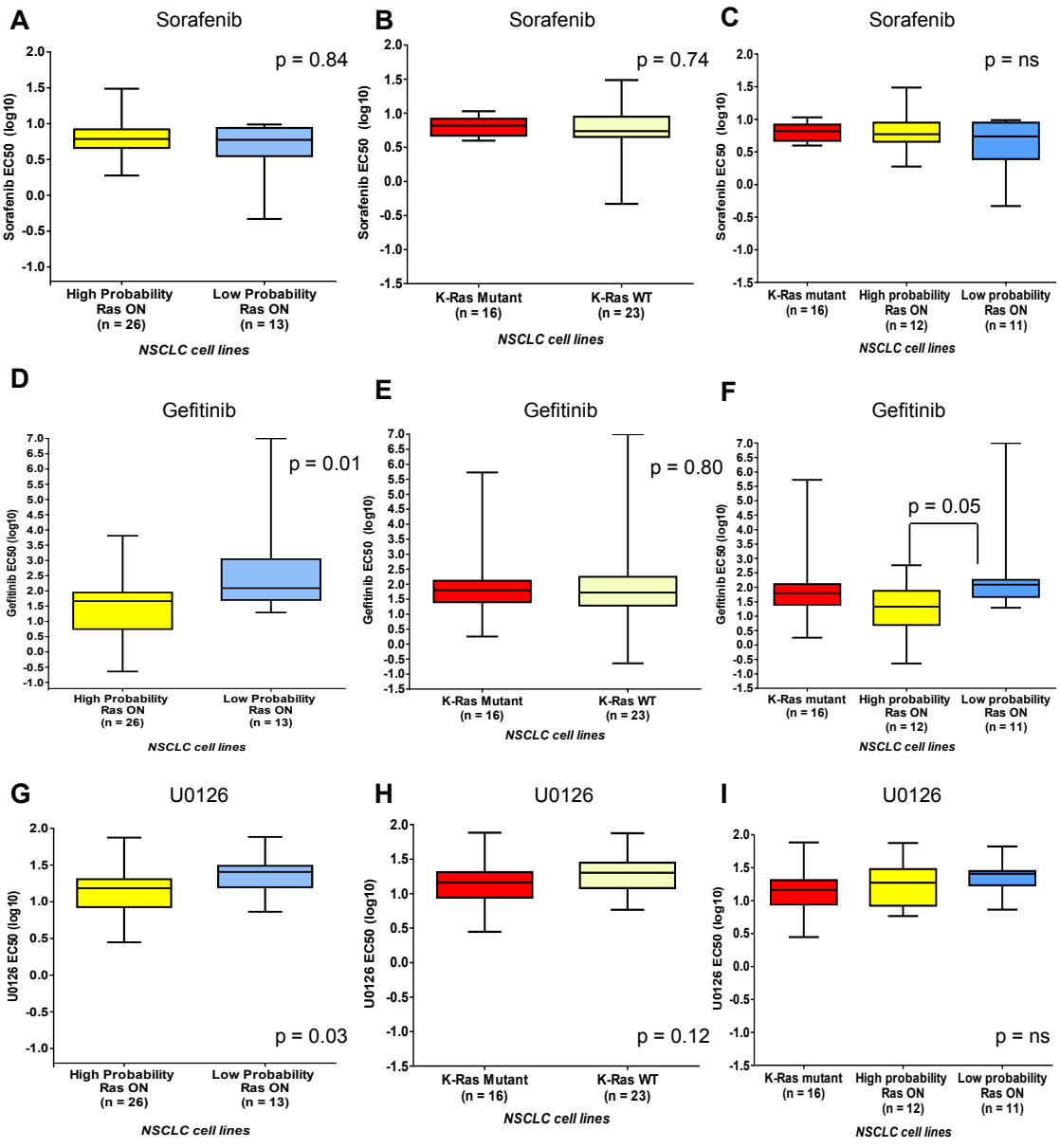

Supplementary Figure 9

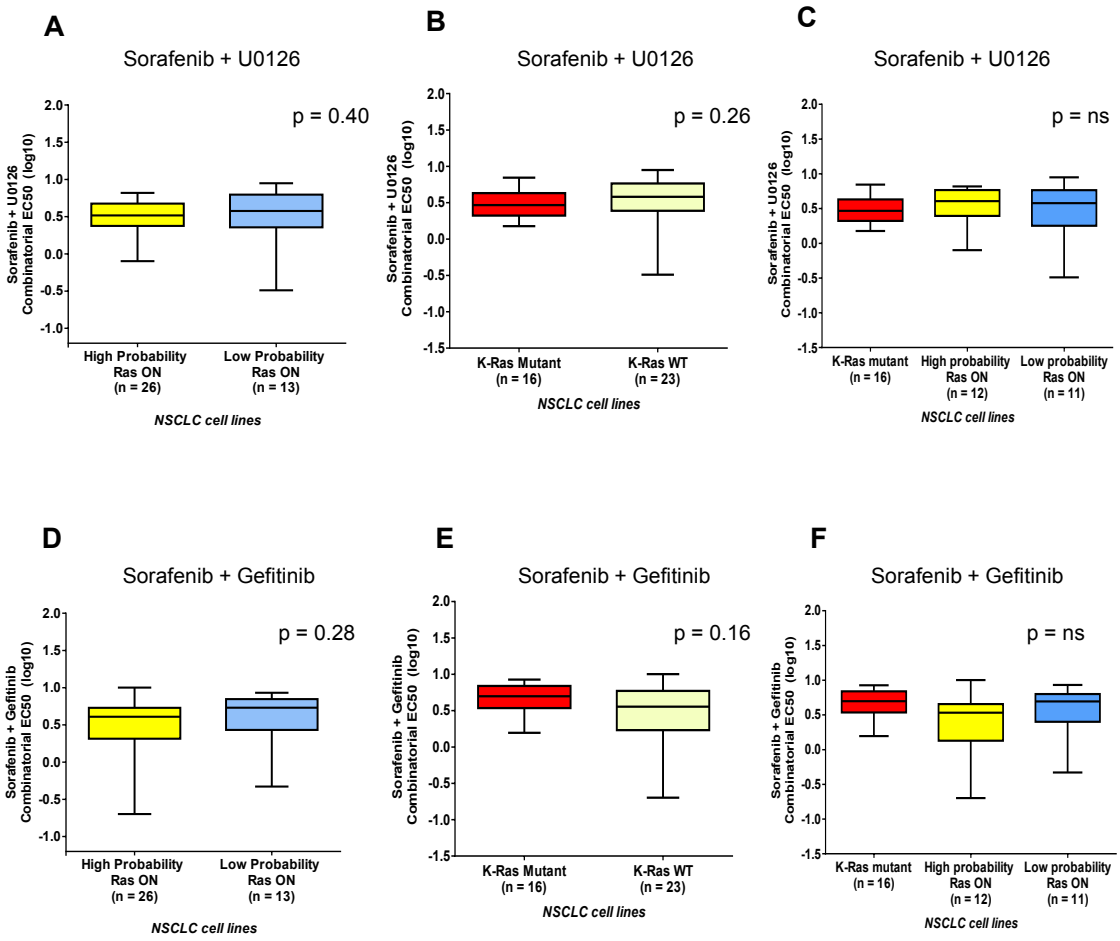

Supplementary Figure 10

A

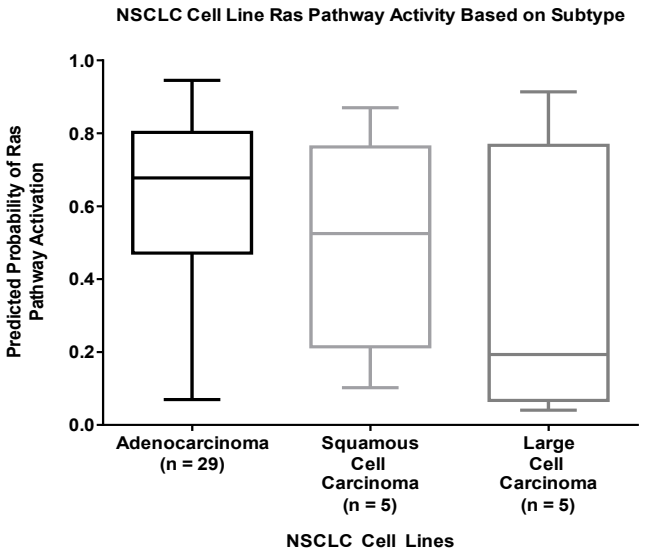

B

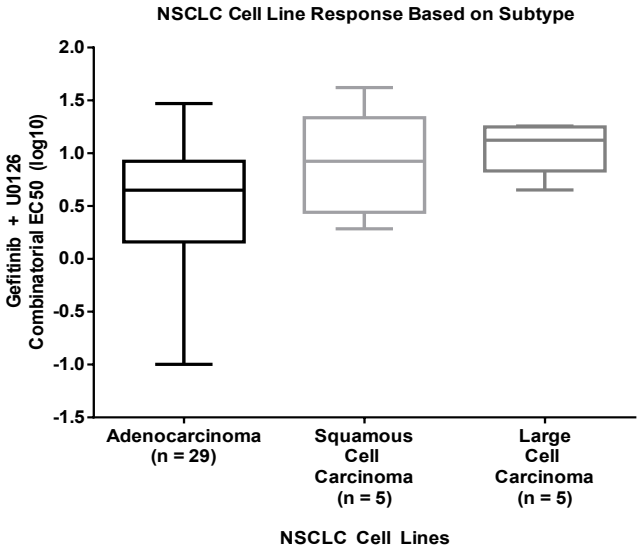

Supplementary Figure 11

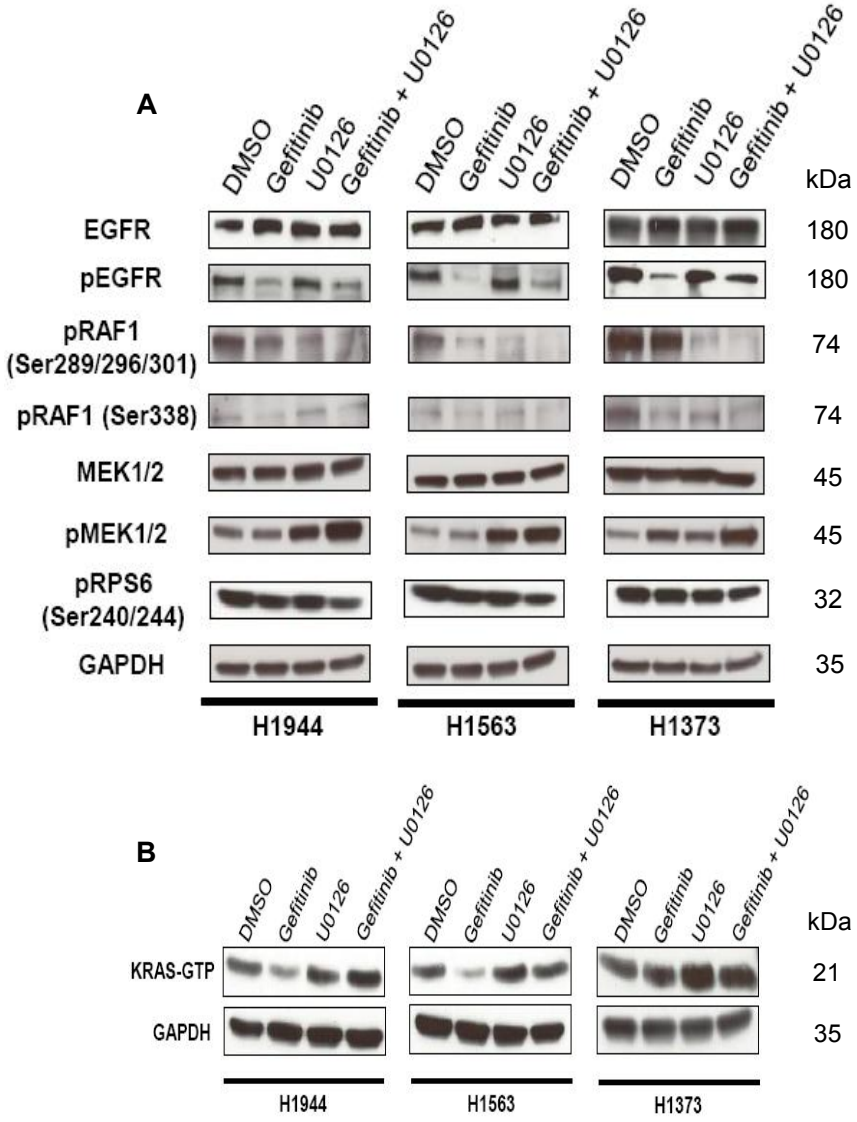

Supplementary Table 1: Characteristics of the 39 NSCLC cell lines used in the study

Cell Line	G+U EC50 (Log10)	RAS	Subtype	K-Ras Mut	P53 Mut	MEK1 Mut	EGFR Mut
97TM1	0.6524	0.9136026	L	G12V	P34fs FRAME SHIFT DEL	x	x
A549	0.9266	0.6067645	A	G12S	x	x	x
CALU3	-0.5487	0.8306487	A	x	M237I	x	x
H1155	1.241	0.0945059	L	Q61H	R273H	ND	x
H1355	0.7158	0.677792	A	G13C	E285K	x	Q1159H
H1373	0.9067	0.9139701	A	G12C	E339*	x	Intron
H1395	1.471	0.4569164	A	x	x	ND	x
H1437	0.6694	0.6525064	A	x	R267P	Q56P	x
H1563	0.6503	0.3695481	A	x	x	x	x
H1581	1.124	0.0405064	L	x	Q144*	x	x
H1650	0.5016	0.6184945	A	x	V225_splice	x	ELREA746del
H1651	1.012	0.3080696	A	x	C176Y	x	x
H1693	0.9227	0.3260345	A	x	Q331_splice	x	x
H1703	1.011	0.2062118	A	x	A307_splice	x	x
H1792	1.049	0.8125829	A	G12C	E224_splice	x	x
H1793	1.151	0.4864989	A	x	R209*	x	C311F
H1944	0.631	0.7229063	A	G13D	x	5'UTR INS	x
H1975	0.485	0.7404292	A	x	x	x	T790M, L858R
H2009	0.8024	0.751463	A	G12A	R273L	x	Intron
H2030	0.01976	0.7927377	A	G12C	G262V	x	x
H2085	0.5938	0.6550824	A	x	ND	ND	ND
H2122	-0.1607	0.9452425	A	G12C	C176F, Q16L	5'UTR INS	x
H2126	-0.1813	0.6254516	A	x	E62*	x	x
H2170	0.9238	0.5251964	S	x	R158G	x	x
H226	0.5961	0.6553798	S	x	x	x	x
H23	0.6753	0.7705322	A	G12C	M246I	x	x
H2405	0.5364	0.8837517	A	x	x	x	x
H322	0.009897	0.7698003	A	x	R248L	ND	x
H358	-0.1012	0.6174521	A	G12C	x	x	x
H441	0.3012	0.8120077	A	G12V	R158L	x	x
H460	1.257	0.6202589	L	Q61H	x	Y134C	x
H520	1.052	0.1024499	S	x	W146*	x	x

H522	1.026	0.0699702	A	x	P191fs FRAME SHIFT DEL	x	x
H661	1.012	0.1929882	L	x	R158L, S215I	x	x
H838	0.6219	0.2447621	A	x	x	x	x
HCC4006	-0.9972	0.847452	A	x	x	5'UTR INS	ELR746del INFRAME
SKLU1	0.7909	0.7119265	A	G12D	H193R	x	x
SKMES1	0.2849	0.870242	S	x	E298*	x	x
SW1573	1.621	0.3261704	S	G12C	Intron	x	x

SUPPLEMENTARY MATERIALS AND METHODS

Cell Lines and Media

The lung cancer cell lines used in this study and their characteristics are summarized in Supplementary Table 1. Cancer cell lines were grown and maintained in a humidified environment at 37°C and 5% CO_2 in their respective media (see below). For the preliminary genomics-based drug screen, 14 lung cancer cell lines were grown in 5% FBS (Gibco/Life technologies, Carlsbad, CA) and 1x Anti-Anti (Gibco/Life technologies, Carlsbad, CA) in their corresponding media, and plated 2000 cells/well onto 384-well plates. H838, H1563, A427, H1944, H2170, H520, HCC4006, H1650, H1975, H661 were grown in RPMI. H2126 was grown in HITES, A549 in F12K, SK-MES-1 in EMEM and H1581 in ACL-4. For the expanded drug screen, the following 39 NSCLC cell lines were used for the novel compound drug screen as well as to generate dose response curves for *gefitinib*, *sorafenib*, *U0126* and their dual combinations: H1155, H1355, H1581, H2085, H2405 and H1651 were grown in ACL-4; Calu-3, LCLC-97TM1, SK-LU-1 and SK-MES-1 were grown in EMEM; A549 in F12K; H1793, H2009 and H2126 were grown in HITES; SW1573 was grown in DMEM; H1373, H1437, H1395, H2170, H1650, H226, H1563, H1703, H1792, H1944, H1975, H2030, H2122, H23, H322, H358. H441, H460, H520, H522, H661, H838, HCC4006 and H1693 were grown in RPMI. The replicate screen was performed on 35 cell lines (adding H1648 grown in ACL-4, and excluding 97TM1, H226, H1395, H2170, H1650 due to an insufficient number of cells). For the 16 lung cancer cell line dose response assay for *erlotinib*+*trametinib*, the following cell lines were used in their media as described above: H1155, H1650, H1792, H2030, H441, SW1573, Calu-3, H1355, H1703, H2405, H322, H520, H522, H661, SK-MES-1, and H2170. For the breast cancer cell line screen, the following 35 cell lines were used: AU565, BT20, BT474, BT483, BT549,

CAMA-1, HCC1143, HCC1395, HCC1419, HCC1500, HCC1569, HCC1599, HCC1806, HCC1937, HCC1954, HCC2218, HCC38, HCC70, Hs343T, JMT-1, MCF-7, MDAMB134-VI, MDAMB157, MDAMB175-VII, MDAMB231, MDAMB361, MDAMB415, MDAMB436, MDAMB453, MDAMB468, SKBR3, T47D, UHCC812, ZR-75-1, ZR-75-30. Breast cancer cell lines were grown according to the media recommended by ATCC and in 5% FBS and 1x Anti-Anti (Gibco).

Breast Cancer Cell Line Dose Response Assay

For the breast cancer cell line screen, and the 35 NSCLC screen, cells were plated at 1500 cells/well. For the dose response assays, known targeted therapeutics were serially diluted 1:3 from 30μM to the lowest dose of 13.72nM in media containing 5% FBS (Gibco) and 1x Anti-Anti (Gibco). To make the highest dose soluble in aqueous media, drugs were sonicated twice on ice. For combination treatments, doses had equal molar concentrations for each compound. Dose response curves were generated using the same methodology described in the body of the paper, methods section.

Cell Lysis and Western Blotting

Cell lines were washed once in ice-cold PBS then lysed in buffer containing 1% Triton X-100, 50mM HEPES, pH 7.4, 150mM NaCl, 1.5mM MgCl2, 1mM EGTA, 100mM NaF, 10mM Na pyrophosphate, 1mM Na3VO4, 10% glycerol, and protease inhibitors (P8340) added fresh from Sigma-Aldrich (St Louis, Missouri). Lysates were incubated on ice for 15 minutes, then centrifuged at 14,000 RPMs in 4’C. Protein yield was analyzed using the Bradford reagent (Amresco, Solon, OH). Equivalent amounts of protein were resolved on 12% precast SDS-PAGE gels (Biorad, Hercules, CA) and transferred to Immobilon-P PVDF membranes (Millipore, Billerica, MA). IgG HRP-linked Secondary antibodies were used from GE Lifesciences

(Pittsburgh, PA). Western blots were developed using SuperSignal West Dura Substrate (Thermoscientific, Rockford, IL).

Synergy Calculation

The expected effects for each combinatorial therapy dose were calculated using the Bliss Independence method utilizing the following formula: Expected effect of dose A = (Drug1 dose A + Drug2 dose A) – (Drug1 dose A * Drug2 dose A) (Buck et al, 2006; Fitzgerald et al, 2006). Theoretical effect dose response curves were plotted for the 39 cell lines for *gefitinib+U0126, sorafenib+U0126* and *gefitinib+U0126* using these expected dose values, and the theoretical EC50 values computed using GraphPad Prism as described before. To determine synergy, the theoretical EC50 values were divided by the actual EC50 values; values greater than one signified synergy, values equal to one signified additivity, and values less than one indicated antagonism (Soldi et al, 2013).

SUPPLEMENTARY FIGURE AND TABLE LEGENDS

Supplementary Figure 1: Preliminary screen reveals a strong correlation between the response to dual suppression of EGFR and MEK and RAS pathway activation. EC50 values of *Gefitinib*, *U0126* and *Gefitinib+U0126* were calculated for a pilot panel of 14 NSCLC cell lines. The predicted probability of RAS pathway activation of these cell lines was also obtained using our RAS gene expression signature. These 2 values were plotted on a dot plot, and the linear correlation between the two investigated. Every dot represents a cell line, with a y value representing the line's treatment EC50 (log10), and an x value representing the cell lines predicted probability of RAS pathway activation score. **(A)** Linear correlation of

Gefitinib+U0126 EC50 values with the predicted probability scores of the 14 cell lines. **(B)** Linear correlation of U0126 with predicted probability of RAS pathway activation **(C)** Linear correlation of *Gefitinib* with predicted probability of RAS pathway activation. Legend: Red: KRAS mutant cell lines, Black: KRAS wild type cell lines

Supplementary Figure 2: Preliminary screen reveals the response to mTOR suppression, alone or in combination with EGFR and MEK inhibition does not correlate to RAS pathway activation. (A) Linear correlation of *Gefitinib+U0126* EC50 values with the predicted probability scores of the 14 cell lines. **(B)** Linear correlation of U0126 with predicted probability of RAS pathway activation **(C)** Linear correlation of *Gefitinib* with predicted probability of RAS pathway activation. Legend: Red: KRAS mutant cell lines, Black: KRAS wild type cell lines

Supplementary Figure 3: The response to combinatorial inhibition of EGFR and MEK, but not the monotherapy is correlated to RAS pathway activity in NSCLC. (A) Treatment of *Gefitinib+U0126* on an expanded panel of NSCLC cell lines was repeated in a second time, with nearly identical results. Linear correlation of *Gefitinib+U0126* EC50 values with the predicted probability of RAS pathway activation across 35 NSCLC cell lines. **(B)** The EC50 values of the top 50% most responsive cell lines for each treatment were averaged out and graphed into box plots. Box boundaries denote the 25^{th}-75^{th} percentiles, while the error bars indicate maximum and minimum values. The line inside the box indicates the median value, and the "+" indicates the mean value. **(C)** Linear correlation plot of *Gefitinib* across 39 NSCLC cell lines **(D)** Linear correlation plot of *U0126* across 39 NSCLC cell lines. Legend: Red: KRAS mutant cell lines, Black: KRAS wild type cell lines

Supplementary Figure 4: Response to RAF inhibition is not correlated to RAS pathway activation, regardless of combinatorial inhibition of MEK and EGFR. Linear correlation plot of Calculated EC50 values of response of the 39 cell lines and their predicted probability of RAS activation scores were plotted on for **(A)** *Sorafenib,* **(B)** *Sorafenib+U0126*, **(C)** *Sorafenib+Gefitinib*. Legend: Red: KRAS mutant cell lines, Black: KRAS wild type cell lines

Supplementary Figure 5: Combinatorial Inhibition of EGFR and MEK is an efficacious and synergistic therapy in NSCLC. (A) Dose response assay curves of 3 of the top 4 synergistic cell lines in our panel. Green shows the theoretical curve that would result from the additivity effect of combining *Gefitinib* and *U0126*, the black curve indicates the actual effect observed from the combinatorial therapy. **(B)** EC50 values of the single agent treatment of *Gefitinib* and *U0126* and the combinatorial therapy across all the 39 NSCLC cell lines are plotted as boxplots. **(C)** Dose response curves using the dose means of all the 39 cell lines of *Gefitinib*, *U0126*, and *Gefitinib+U0126*.

Supplementary Figure 6: Combinatorial Inhibition of RAF with EGFR or MEK is minimally synergistic, while EGFR and MEK dual inhibition is largely synergistic in NSCLC. (A) Synergy scores of *Gefitinib+U0126* Combinatorial treatment across the panel of 39 NSCLC cell lines. Synergy was investigated by calculating the theoretical EC50 of the combined treatment, and dividing it by the experimental EC50. Scores >1 (columns above the red line) indicate a synergistic relationship between *Gefitinib* and *U0126* in killing NSCLC tumor cells. Scores <1 indicated drug antagonism, and scores = 1 indicates drug additivity. A total of 29/39

cell lines (74%) of cell lines showed synergy for the combinatorial treatment. **(B)** A total of 13/39 cell lines (33%) of cell lines showed synergy for *Sorafenib+Gefitinib* combinatorial treatment. **(C)** Synergy scores of *Sorafenib+U0126* combinatorial treatment across the panel of 39 NSCLC cell lines. 26/39 cell lines (67%) showed synergy for the combinatorial treatment, although the synergy scores were much smaller than *Gefitinib+U0126*. **(D)** EC50 values of *Sorafenib*, *Sorafenib+Gefitinib* and *Sorafenib+U0126* across all the 39 NSCLC cell lines are plotted as boxplots

Supplementary Figure 7: EGFR+MEK inhibition is unskewed by the 8 most correlative cell lines and is not correlated to RAS pathway activation in Breast Cancer. (A) The graph shows the linear correlation of *Gefitinib+U0126* with the predicted probability of RAS pathway activation across the same panel of NSCLC cell lines in Figure 2A, with the 8 most correlative cell lines taken out. **(B)** The graph shows the linear correlation of *Gefitinib+U0126* with the predicted probability of RAS pathway activation across the 35 breast cancer cell lines. **Red**: KRAS mutant cell lines, **Black**: KRAS wild type cell lines.

Supplementary Figure 8: The RAS Gene expression signature and KRAS mutation do not predict response to Sorafenib, U0126 or Gefitinib in NSCLC. Cell lines of the 39 NSCLC panel were divided accordingly and Boxplot diagrams of *Gefitnib+U0126* and *Gefitinib+Sorafenib* and EC50 values plotted. **(A)** Response to *Sorafenib* with respect to the predicted probability of RAS pathway activation, as measured by EC50 values. **(B)** Response to *Sorafenib* with respect to the mutation status of KRAS, as measured by EC50 values. **(C)** Response to *Sorafenib* with respect to mutation status of KRAS, and predicted probability of

RAS pathway activation. **(D)** Response *to Gefitinib* with respect to the predicted probability of RAS pathway activation, as measured by EC50 values. **(E)** Response to *Gefitinib* with respect to the mutation status of KRAS, as measured by EC50 values. **(F)** Response to *Gefitinib* with respect to mutation status of KRAS, and predicted probability of RAS pathway activation. **(G)** Response to *U0126* with respect to the predicted probability of RAS pathway activation, as measured by EC50 values. **(H)** Response to *U0126* with respect to the mutation status of KRAS, as measured by EC50 values. **(I)** Response to *U0126* with respect to mutation status of KRAS and predicted probability of RAS pathway activation, as measured by EC50 values.

Supplementary Figure 9: The RAS Gene expression signature and KRAS mutation do not predict response to sorafenib+U0126 or sorafenib+gefitinib in NSCLC. Cell lines of the 39 NSCLC panel were divided accordingly and Box plot diagrams of *Gefitnib+U0126* and *Gefitinib+Sorafenib* and EC50 values plotted. **(A)** Response to *Sorafenib+U0126* with respect to the predicted probability of RAS pathway activation, as measured by EC50 values. **(B)** Response to *Sorafenib+U0126* with respect to the mutation status of KRAS, as measured by EC50 values. **(C)** Response to *Sorafenib+U0126* with respect to mutation status of KRAS, and predicted probability of RAS pathway activation. **(D)** Response to *Gefitinib+Sorafenib* with respect to the predicted probability of RAS pathway activation, as measured by EC50 values. **(E)** Response to *Gefitinib+Sorafenib* with respect to the mutation status of KRAS, as measured by EC50 values. **(F)** Response to *Gefitinib+Sorafenib* with respect to mutation status of KRAS, and predicted probability of RAS pathway activation.

Supplementary Figure 10: Box plots of the predicted probability of RAS pathway activation in the panel of 39 NSCLC cell lines and the overall EC50 response to EGFR and MEK inhibition based on subtype. Cell lines were divided according to their specified NSCLC subtype, and their (A) probability of RAS pathway activation scores (B) *Gefitinib+U0126* EC50 scores grouped together. Adenocarcinomas had the highest predicted probability of RAS pathway activation and sensitivity to *Gefitinib+U0126*.

Supplementary Figure 11: Further effects of gefitinib, U0126 and gefitinib+U0126 on the EGFR pathway and RAS protein activation. (A) The effects of the aforementioned treatments were further investigated on more components of the EGFR and RAS pathways through western blotting. **(B)** Activated KRAS (KRAS GTP) was pulled down and blotted for after cell line treatment of *gefitinib*, *U0126*, *gefitinib+U0126* at 5μM dose for 6hrs. GAPDH was blotted for on the same lysates to test for equal loading. Only *gefitinib* inhibits the activation of KRAS in 2/3 cell lines

Supplementary Table 1: Characteristics of the 39 NSCLC cell lines used in the study. "G+U EC50 (log10)" denotes the calculated EC50 dose of *Gefitinib+U0126* in log scale. "RAS" column denotes predicted probabilities of RAS pathway activation among the cell lines. ". "A" denotes the NSCLC Adenocarcinoma subtype, "S" denotes squamous cell carcinoma, and "L" denotes large cell carcinoma. The rest of the columns highlight the specific amino acid mutations and frameshift deletions observed in their respective proteins where "*" denotes a stop codon.

REFERENCES

Buck E, Eyzaguirre A, Brown E, Petti F, McCormack S, Haley JD, Iwata KK, Gibson NW, Griffin G (2006) Rapamycin synergizes with the epidermal growth factor receptor inhibitor erlotinib in non-small-cell lung, pancreatic, colon, and breast tumors. *Molecular cancer therapeutics* **5:** 2676-2684

Fitzgerald JB, Schoeberl B, Nielsen UB, Sorger PK (2006) Systems biology and combination therapy in the quest for clinical efficacy. *Nature chemical biology* **2:** 458-466

Soldi R, Cohen AL, Cheng L, Sun Y, Moos PJ, Bild AH (2013) A genomic approach to predict synergistic combinations for breast cancer treatment. *The pharmacogenomics journal* **13:** 94-104

CHAPTER 3

IDENTIFICATION OF A MARINE NATURAL PRODUCT THAT TARGETS BASAL-LIKE AND CLAUDIN-LOW BREAST CANCERS

Chapter 3 is a manuscript submitted to Molecular Cancer Therapeutics. The authors of this manuscript are Nader N. El-Chaar, Stephen R. Piccolo, Mary Kay Harper, Ryan M. Van Wagoner, Zhenyu Lu, Thomas E. Smith, Philip J. Moos, Chris M. Ireland and Andrea H. Bild

This manuscript was written by Nader N. El-Chaar and Andrea H. Bild

3.1 Abstract

Patients diagnosed with Basal-like or Claudin-low breast cancer (BL-CL) suffer from a poor prognosis and limited treatment options. To identify compounds with potential therapeutic efficacy, we used a step-wise screening approach personalized for the identification of a compound effective against BL-CL. We screened 2778 HP20 fractions from our marine invertebrate compound library (MICL) and identified a previously unreported trisulfated sterol, topsentinol L trisulfate (TLT) that exhibits increased efficacy against BL-CL relative to Luminal/HER2+ breast cancer. Biochemical investigation of the effects of TLT on BL-CL revealed its ability to inhibit activation of AMPK and CHK1. The importance of targeting these two proteins in BL-CL was validated by treating a panel of breast cancer cell lines with known small molecule inhibitors of AMPK and CHK1 and recording the increased effectiveness against BL-CL compared to Luminal/HER2+ breast cancer. Finally, we generated a TLT sensitivity gene-expression signature and projected it against a human tumor panel of 12 different cancer types and identified breast and bladder cancer as the cancers most sensitive to TLT. Conversely, glioblastoma multiforme was projected to be least sensitive to TLT. These results identify TLT, a previously uncharacterized trisulfated sterol, as a potential therapeutic selective against BL-CL. The mechanistic treatment effects of TLT are described, proposing the potential of AMPK and/or CHK1 inhibition as an effective therapy in BL-CL.

3.2 Introduction

Gene-expression profiling has identified five molecular subtypes of breast cancer, known as Luminal A, Luminal B, HER2-enriched, Claudin-low and Basal-like, with inter-subtype differences in incidence, survival and treatment response [1-5]. Among these, breast cancer patients diagnosed with the Claudin-low and

Basal-like molecular subtypes exhibit particularly poor prognosis and suffer from limited treatment options [6]. Basal-like breast cancers represent 10-25% of all breast carcinomas, generally occurring at an early age, with higher frequency in women of African origin [7]. Approximately 50%-70% of all basal-like cancers lack the expression of ER, PR and HER2 and are therefore clinically described as being triple negative. Basal-like breast cancer manifests as a highly aggressive tumor that is responsive to chemotherapy [6]. However, patient prognosis remains poor with Basal-like cancers exhibiting a high recurrence rate and low patient survival [2]. At the molecular level, Basal-like breast cancers exhibit expression patterns as also observed in the basal epithelial layer of the skin and airways; this includes expression of high molecular weight cytokeratins 5, 6 and 17 and deficiencies in RB1, BRCA1 and TP53. Moreover, a high rate of aneuploidy is observed in these tumors, reflective of increased genetic instability [6,7].

Interestingly, the Claudin-low group shares some similarities in gene-expression features with the Basal-like subtype such as low expression of HER2 and the luminal gene clusters, indicating genomic similarities between the two groups [8]. Moreover, like the Basal-like subtype, Claudin-low tumors are also triple negative and have a poor prognostic outcome. However, Claudin-low breast cancers remain an individual group on their own, characterized by the minimal expression of several claudin genes, such as claudin 3, 4 and 7, which are involved in epithelial cell tight-tight junctions. These tumors also lack cell–cell junction proteins, such as E-cadherin, and almost always are characterized by having an intense immune cell infiltrate, stem cell properties, and features of epithelial–mesenchymal transition (EMT) [3,4,7,9,10]. Due to the nonluminal molecular nature of these two subtypes, and the lack of known protein targets on these cancers, few effective treatment options are available. As such, there exists an urgent need to identify new therapeutic leads and potential targets that can

improve patient prognosis.

To identify a novel compound effective against Basal-like and Claudin-low breast cancer (BL-CL), we screened a subset of our unique library of marine invertebrate compounds against a large panel of cancer cell lines. The Marine Invertebrate Compound Library (MICL) is a unique resource that serves as a platform for discovery of novel small molecule-mediated biological activities in a variety of systems. MICL is derived from an extensive collection of over 1200 unique marine organisms (85% sponges from over 150 genera, 12% tunicates, 2% other phyla) collected from diverse locations around the world over the past 20 years [11,12]. Around 75% of all anticancer drugs developed between 1940 and 2010 were either derived from or inspired by natural products [13]. As of 2010, there were 13 marine natural products (MNPs) in clinical trials, ten of which target cancers [14]. Natural products tend to be more complementary in shape to their targets [15] due to their development in a competitive ecological selection process that favors the production of compounds with strong biological activity [16-18]. Several marine natural products in particular have been shown to exhibit anti-cancer properties, such as didemnin B, aplidine and ecteinascidin-743, the latter of which succeeded in passing clinical trials in Europe and is now approved by the European Commission for the treatment of refractory soft-tissue sarcomas [19]. In summary, MNPs have proven their potential for development into clinically-useful drugs [14,19].

In this study, we screened 2778 fractions from MICL with the goal of identifying a candidate fraction with anti-BL-CL activity and isolating the active compound responsible for such a property. To accomplish this goal, we first identified the fractions that exhibited anticancer activity by screening against a panel of cancer cell lines. These anticancer fractions were then used in a second screen to identify those with selectivity against BL-CL. The unique compounds in

each were isolated and validated for BL-CL activity, leading to the identification of a candidate compound. We identified a previously uncharacterized trisulfated sterol, topsentinol L trisulfate (TLT), purified from a marine sponge Topsentia sp. (PNG07-3-073) collected from Papua New Guinea. TLT, as well as its parent fraction and subfraction, exhibited increased effectiveness against BL-CL compared to Luminal and HER2+ subtypes. We showed that treating BL-CL cell lines with TLT leads to the inhibition of AMPK and CHK1 using biochemical and proteomic analyses. To validate the importance of inhibiting the activity of AMPK/CHK1 in BL-CL, we tested breast cancer cell lines with known small molecule inhibitors of AMPK and CHK1, and observed that they are significantly more effective against BL-CL than Luminal and HER2+ subtypes. This study was concluded by generating a genomic gene-expression signature of TLT sensitivity and projecting it against a panel of human patient tumors of 12 different cancer types, identifying breast and bladder cancer as the two cancers most sensitive to TLT. Overall, this study incorporates the genomic classification of breast cancer to high-throughput drug screening and identifies a novel small molecule, TLT, personalized against BL-CL. Furthermore, the work described here sheds light on the importance of targeting AMPK and/or CHK1 in this molecular subtype, and suggests the potential of these proteins as therapeutic targets in BL-CL.

3.3 Materials and Methods

3.3.1 Cell lines and Viability Measurement

Cell lines were obtained from ATCC and plated at 1500-2000 cells/well in 384-well plates in 5% FBS (Gibco/Life Technologies, Carlsbad, CA) growth media and 1x Anti-Anti (Gibco/Life Technologies, Carlsbad, CA). Cancer cell lines were cultured and maintained in a humidified environment at 37 °C and 5% CO2 in their respective media. Detailed description on the cell lines used for each screen

is available in Supplementary Tables 3.1 and 3.2. Cells were treated for 72 hrs, after which cell viability and growth were measured using CellTiter-Glo (Promega, Madison, WI). Cell viability scores were calculated by dividing the viability scores of the treatment by the control DMSO values.

3.3.2 Small Molecules

Dorsomorphin C and Ly2603618 were purchased from Selleckchem and dissolved in water and 100% DMSO, respectively. Dorsomorphin C was prepared as a stock of 100 mM, while Ly2603618 was prepared as a 28.65 mM stock.

3.3.3 MICL Screens

For Screen 1, 2778 HP20 fractions of marine organisms from MICL were screened at a single dose (~1.5 μM) against a panel of 16 (9 lung and 7 breast) cancer cell lines to determine fractions with antitumor properties. One hundred and seven HP20 fractions were chosen according to the following selection criteria: 1) all fractions with a standard deviation in viability of greater than 0.325; 2) Lung selective fractions (25% or less viable cells in three or more lung cancer cell lines and two or fewer breast cancer cell lines); 3) breast selective fractions (25% or less viable cells after treatment in two or more breast cancer cell lines and three or fewer lung cancer cell lines); 4) generally active nonuniversally toxic fractions (25% or less viability in a minimum of 5 and maximum of 13 cell lines); 5) relatively less active fractions (40% or less viability in a minimum of 9 and maximum of 13 cell lines). An additional 85 HP20 fractions from MICL that were not screened for were added to the selected 107 fractions based on chemo-taxonomic judgment of potential chemical similarity to the 107 fractions. These 192 HP20 fractions were then subjected to a second screening assayed at a single dose (~1.5 μM)

against a panel of 35 breast cancer and 37 lung cancer cell lines. This identified breast-selective fractions (fractions resulting in 25% or less cellular viability after treatment in 13 cell lines or more out of 35 breast cancer cell lines, and 12 cell lines or fewer lung cancer cell lines) and fractions effective against BL-CL (BL-CL vs Luminal/HER2+ breast cancer unpaired two-sample equal variance t-test < 0.05 with a positive average difference). Cell lines described as basal-like or claudin-low but being HER2+ were considered part of the Luminal/HER2+ group. LCMS (liquid crystal-mass spectroscopy) fractionation of the anti-BL-CL fractions following the MICL protocol [11,12] resulted in 20 subfractions each that were assayed for effectiveness against BL-CL in a panel of 33 breast cancer cell lines. Once a candidate subfraction was determined based on the results of all three screens, large scale isolation and the purification of the active compound of that fraction was pursued

3.3.4 Large-scale Isolation and Purification of Active Compound

Frozen PNG07-3-073 Topsentia sp. sponge (215 g, Supplementary Figure 3.1) was extracted three times with methanol. One half of the pooled methanol extract was fractionated on Diaion HP20SS resin, eluting with water/isopropanol mixtures in 25% increments, followed by 100% methanol to yield five fractions, FW and F1-F4, where F2 was the only fraction that exhibited tumoricidal properties. F2 (50/50 IPA/H2O, 98 mg) was subjected to C18 flash chromatography, eluting with 40-100% methanol in water in 10% increments, yielding 46 subfractions, of which only subfractions 22, 23, 24 and 25 showed tumoricidal activity. Bioactive fractions 22-25 were combined (65 mg) and further fractionated by HPLC using a Luna 5 µm phenylhexyl column (250 x 4.6 mm) and a gradient of acetonitrile (ACN) with 0.2 M NaCl (36% ACN increasing over 4 min to 43% ACN, held for

11 min, then decreased to 36% ACN over 2 min) to yield isolate 1 (sharp peak, RT=9.57 min, 13.4mg) and isolate 2 (broad peak, RT=10.2 min, 6.3mg). Salt was removed by loading samples onto pre-equilibrated Waters Sep-Pak C18 cartridges and flushing with three column volumes of 10% methanol, followed by compound elution with 100% methanol.

3.3.5 Dose Response Assays

Cell lines were plated as described above. Dorsomorphin C and Ly2603618 were serially diluted 1:3 starting from 90 μM to the lowest dose of 41.15 nM in RPMI media containing 5% FBS and 1x Anti-Anti and screened against a panel of 20 cell lines, along with the combination treatment of dorsomorphin C and Ly2603618. For the combination treatment, an equal molar concentration of each compound was used. TLT was serially diluted 1:2 starting from 104.4 μM to the lowest dose of 3.26 μM and screened against a panel of 30 cell lines. Cell viability was measured as described before. Doses were repeated in quadruplicates and averaged out for a single value. EC50 values were calculated from dose response curve data by plotting on GraphPad Prism 6.01 and using the equation Y=1/(1+10^((logEC50-X)*HillSlope) with a variable slope (Ymin = 0 and Ymax = 1). Plots were forced to start from the x-axis by plotting for an x-intercept point.

3.3.6 Cell Lysis and Western Blotting

Cell lines were washed once with ice-cold PBS (1x) and then lysed in a buffer containing 1% Triton X-100, 50mM HEPES, pH 7.4, 150mM NaCl, 1.5mM MgCl2, 1mM EGTA, 100mM NaF, 10mM Na pyrophosphate, 1mM Na3VO4, 10% glycerol, and protease inhibitors (P8340) added fresh from Sigma-Aldrich (St Louis, Missouri). Lysates were then incubated on ice for 15 min with agitation every 2

min, and then centrifuged at 14,000 RPMs in 4°C. Protein yield was quantified using the Bradford reagent (Amresco, Solon, OH) and denatured by boiling and SDS treatment (with beta-mercaptoethanol). Equivalent amounts of protein (approximately 30 µg) were resolved on 12% precast SDS-PAGE gels (Biorad, Hercules, CA) and transferred to Immun-blot PVDF membrane (Biorad, Hercules, CA). IgG HRP-linked Secondary antibodies were used from GE Lifesciences (Pittsburgh, PA). Western blots were developed using SuperSignal West Dura Substrate (Thermoscientific, Rockford, IL).

3.3.7 Immunostaining

Four BL-CL cell lines sensitive to topsentinol L trisulfate (HCC70, HCC1143, MDAMB468, MDAMB436) were treated with 105µM of TLT in 5% FBS RPMI media and 1x Anti-Anti for 6 hrs. Primary antibodies for GAPDH (#5174S), p38-T180/Y182 (#4511S), pChk1-S317 (#12302) and pAMPKα-T172 (#2535) were obtained from Cell Signaling Technology (Beverly, MA).

3.3.8 Reverse Phase Protein Array

Eight TLT-sensitive BL-CL cell lines (MDAMB157, MDAMB436, MDAMB468, MDAMB231, HCC38, HCC70, HCC1395, and HCC1143) were treated separately with TLT or DMSO at a concentration of 105µM (approximate average EC75 across all eight cell lines) for 6 hrs, after which they were lysed according to methodology detailed in above. Reverse phase protein array was performed at the University of Texas MD Anderson Cancer Center by the functional proteomics RPPA core facility according to their described methods and protocol [20,21]. Two hundred seventeen different antibodies of phosphorylated and non-phosphorylated proteins were stained for and quantified.

3.3.9 RNA Sequencing Data Acquisition

The same eight TLT-sensitive BL-CL cell lines were treated separately with TLT or DMSO for 6 hrs, after which total RNA was extracted using the RNeasy Mini Kit (Qiagen, Venlo, Netherlands) with on-column digestion of the genomic DNA, as described in the manufacturer's protocol. RNA sequencing was performed at the Huntsman Cancer Institute High Throughput Genomics Core Facility using 50-cycle, single-read sequencing (version 3) on an Illumina HiSeq instrument. To construct mRNA focused libraries from total RNA, the Illumina TruSeq RNA Sample Prep Kit (version 2) with oligo dT selection was used.

3.3.10 TLT Sensitivity Signature Generation and Analysis

To process the mRNA sequencing data, we used the TCGA mRNA-seq Pipeline [22]. RNA sequencing reads for the treated and control samples were aligned using MapSplice v12_07 [23], quantified using RSEM [24], and gene counts were normalized using upper quantile normalization. This was the same methodology used to normalize the PANCAN12 TCGA dataset, which we obtained from TCGA fully processed for use in this analysis [22]. To generate a TLT sensitivity signature, we used the DESeq2 package (version 1.4.5) in the Bioconductor framework (version 2.14.0, version 3.1.0 of R) to identify genes that were significantly deregulated (adjusted $p < 0.05$) between the treated and control samples [25,26]. One hundred forty-six genes were found to be significantly deregulated, out of which only 131 were found in the TCGA dataset. To use DEseq2, the reads had to be remapped using the Rsubread Bioconductor package. We used this package to map the reads to version hg19 of the human genome and to summarize the data to gene-level values [27]. We predicted TLT sensitivity for the PANCAN12 TCGA dataset [22] using the Bayesian binary regression algorithm version 2.0 (BinReg2.0) used as a MATLAB plug-in [28]. We used default parameters, except that our signature

used 131 genes and 1 metagene. The probability output from the binary regression model was subtracted from one, so that probabilities closer to one indicated higher probability of sensitivity to the drug as previously described [29]. Prior to making the predictions, the data were log2 transformed and DWD normalized [30] to reduce biases that can result from differences in batch processing and platforms.

3.3.11 Statistical Analysis

To identify candidate fractions significantly more effective against BL-CL than Luminal/HER2+ breast cancer, preliminary statistical analysis was performed using the unpaired two-sample equal variance t-test built into the Microsoft Excel program. Final statistical assessment was performed for the fractions from the sponge PNG07-3-073 by re-analyzing statistical significance test based on the normality of the data. Gaussian distribution of the data was checked for using three different tests built into the GraphPad Prism 6 software: the D'Agostino-Pearson omnibus test, the Shapiro-Wilk test and The Kolmogorov-Smirnov test (with the Dallal-Wilkinson-Lilliefor corrected P value). Dot plots were then created using Graphpad Prism 6.01 and a standard two-tailed Mann-Whitney U-test was used to test for statistical significance, with the exception of the dot plot diagrams for halistanol sulfate, dorsomorphin C, Ly2603618 and dorsomorphin C + Ly2603618 where an unpaired t-test with was used due to the normality of the data. To compare the difference of protein expression between treated cell lines and their DMSO controls and to test for the significance of the result, we used a two-tailed paired t-test.

3.4 Results

3.4.1 Identification of Topsentinol L Trisulfate as a Selective Inhibitor of BL-CL

The goal of this study is to find a novel inhibitor of BL-CL, describing the pathways effectively blocked by the compound, and projecting treatment efficacy across other cancer types. We aimed to achieve this through a stepwise approach by 1) screening MICL for fractions that exhibited tumoricidal properties, 2) selecting candidate fractions that displayed effectiveness against BL-CL, 3) separating the active compounds in the fractions, 4) identifying the active compound with anti-BL-CL properties, 5) describing the cell signaling effects of the compound on BL-CL, 6) projecting TLT sensitivity across human tumors of various cancer types using a gene-expression signature (Figure 3.1A).

To identify fractions with tumoricidal activity, we began by screening 2778 fractions from MICL against a panel of 16 cell lines (Figure 3.1B “Screen 1”). These fractions represent complex mixtures, and served as a starting point to identify promising hits [11,12]. From this screen, we selected 107 HP20 fractions based on differential tumoricidal activity among the 16 cell lines, eliminating all fractions that were universally toxic or that showed minimal anticancer activity. We then added an additional 85 previously-unscreened HP20 fractions from MICL based on chemical similarity to the 107 selected fractions, directed by chemo-taxonomic judgment of source organism [11,12]. Next, we screened these 192 HP20 fractions against a panel of 35 breast cancer and 37 lung cell lines to identify fractions effective against breast cancer in general, and BL-CL in particular (Screen 2). We selected 34 HP20 fractions based on their selectivity against breast cancer compared to lung cancer, with only seven of those fractions displaying significant subtype selectivity against BL-CL (Figure 3.1B “Screen 2”). These seven fractions were then fractionated further into 20 subfractions each (labeled M1-M20) using

LCMS for the purposes of additional active compound separation, and screened in two doses against a panel of 33 breast cancer cell lines (Figure 3.1B “Screen 3”). This screen identified five subfractions with significant selectivity against BL-CL, out of which three subfractions originated from the marine sponge PNG07-3-073 F2 fraction. We analyzed the results of all three screens retrospectively, and observed that the PNG07-3-073–F2 was initially identified as a candidate with increased tumoricidal activity against BL-CL (Figure 3.2A, Figure 3.1B). The HP20 fractionation of the sponge also resulted in four other fractions, FW, F1, F3 and F4; however, none exhibited sufficient tumoricidal activity and therefore did not proceed past the first screen. The F2 was the only fraction from the Topsentia sponge PNG07-3-073 to exhibit anti-BL-CL activity (Figure 3.1B). This activity was maintained after further fractionation of F2 via LC/MS into 20 subfractions. The M6 subfraction in particular displayed significant effectiveness against BL-CL (Figure 3.2B, Figure 3.1B).

Our next step was to proceed with the identification of the active compounds in the M6 subfraction with the aim of isolating the single compounds inducing this response (Figure 3.1A). For this purpose, a large amount of product was needed, and a scaled-up extraction of bulk PNG07-3-073 sponge ensued. This culminated in the purification of two isolates: isolate 1 and 2. 1D NMR analysis (Supplementary Table 3.3) identified isolate 1 as the previously reported metabolite halistanol sulfate [31] (Figure 3.2C, Supplementary Figure 3.2-3.3) and was validated using high-resolution electrospray ionization mass spectrometry (HRESIMS, low-resolution spectrum shown in Supplementary Figure 3.4). Isolate 2 was identified via 1D (Supplementary Figure 3.5-3.6) and 2D (Supplementary Figure 3.7-3.11) NMR analysis (Supplementary Table 3.3) as a previously uncharacterized sulfated sterol similar to the known compound topsentinol L but with three sulfate groups [32] (Figure 3.2D). The structure of the compound was corroborated by the data

obtained through HRESIMS (Low-resolution spectrum shown in Supplementary Figure 3.12). We named this compound topsentinol L trisulfate, or TLT (Figure 3.2D). Halistanol sulfate and TLT were then screened against a panel of 30 breast cancer cell lines, and tested for effectiveness against BL-CL. TLT showed significant tumoricidal activity against BL-CL breast cancer compared to other subtypes ($p = 0.0076$, Figure 3.2C, Figure 3.1B). Halistanol sulfate did not exhibit such activity ($p = 0.247$, Supplementary Figure 3.13). Through a multistep screening and fractionation process, we identified a novel sulfated sterol, TLT, which exhibits significant subtype selectivity against BL-CL.

3.4.2 Topsentinol L Trisulfate Treatment Inhibits AMPKα and CHK1 but Activates p38

Our next goal was to analyze and describe the signaling effects that are induced by TLT in cancer cells. For this purpose, we treated eight TLT-sensitive BL-CL cell lines with TLT or DMSO control and screened for 217 phosphorylated and nonphosphorylated protein changes using reverse phase protein array (RPPA) [20]. From this screen, we identified 21 proteins that exhibited a 15% or more upregulation or downregulation in protein level, with only eight of these proteins exhibiting statistically significant changes (Supplementary Table 3.4). To focus our research and narrow down our investigation, we studied the deregulation of three proteins, AMPK, CHK1 and p38, for the reasons outlined. AMPK phosphorylation recorded the biggest statistically significant change compared to DMSO control of all proteins, with 35% reduction in Thr172 phosphorylation, which is required for AMPK activation [33] ($p = 0.031$, Figure 3.3C). Interestingly, phosphorylation of ACC, a direct downstream effector of AMPK [34], was also significantly inhibited, recording a 26.5% reduction in Ser79, supporting the observation of AMPK inhibition (Supplementary Table 3.3, $p = 0.03$). We also observed significant

changes in phosphorylation of CHK1, recording a 16% downregulation in the nuclear localization mark Ser345 [35] ($p = 0.012$, Figure 3.3C). CHK1 has recently been suggested to represent a therapeutic target in triple negative breast cancer (TNBC) [36], therefore making its inhibition following TLT treatment a potential cause of treatment effectiveness. Upregulation of p38 phosphorylation was the most significant change observed upon treatment with TLT, with 23% increase in Thr180-Tyr182 phosphorylation ($p = 0.003$, Figure 3.3C). The activation of p38 has been shown to lead to the direct phosphorylation of BimEL and the induction of apoptosis [37].

In order to validate the observations of AMPK, p38, and CHK1 protein phosphorylation deregulation following TLT treatment in the RPPA screen, we analyzed phosphorylation levels by western blotting. The most consistent down-regulation observed was an inhibition of AMPK activation across all four cell lines (Figure 3.3D). CHK1 activity measured by the phosphorylation of the activation site of the protein, Ser317, was inhibited by TLT [38] (Figure 3.3D). In addition, the phosphorylation of p38 was also upregulated in three out of four cell lines, confirming previous results (Figure 3.3C-3D). These data describe the landscape of proteomic changes induced following TLT treatment in BL-CL cells.

3.4.3 Inhibition of AMPK and CHK1, Alone or in Combination is Effective Against BL-CL

Due to the consistent nature of the observation of AMPK inhibition (either the protein itself or its downstream effector ACC) and CHK1 (the inhibition of two separate activation marks Ser345 and Ser317), as well as the recent discovery of CHK1 treatment efficacy against TNBC [36], we decided to test the importance of the inhibiting AMPK and CHK1 in BL-CL. As such, we investigated the effects of AMPK, CHK1 and AMPK1+CHK1 small molecule targeted inhibition on a panel

of 20 breast cancer cell lines. We screened the panel with dorsomorphin C, an AMPK inhibitor [39], Ly2603618, a CHK1 inhibitor in phase two clinical trials [40], and the combination of both. Our results showed that either treatment strategy is significantly more effective against the BL-CL subtype than Luminal/HER2+ breast cancer (Figure 3.4). Dorsomorphin C was more than four times more effective against BL-CL (average EC50 = 9.33 μM) compared to Luminal/HER2+ breast cancer (average EC50 = 37.87 μM), which was a significant difference ($p = 0.011$, Figure 3.4A). Ly2603618 on the other hand was almost eight times more toxic against BL-CL (average EC50 = 0.72 μM) in comparison to Luminal/HER2 breast cancer (average EC50 = 5.73 μM), which was also a significant difference ($p = 0.001$, Figure 3.4B). Interestingly, the combination therapy was also significantly more effective against BL-CL ($p= 0.005$) (Figure 3.4C). These results validate the importance of the inhibitory effects of TLT on AMPK and CHK1 in BL-CL, and suggest the potential use of AMPK or CHK1 inhibition as a treatment.

3.4.4 TLT Sensitivity Signature Predicts Breast and Bladder Cancer Response in Human Tumors

Next, we sought to identify classes of solid tumors that are most sensitive to TLT using an unbiased computational approach. The gene-expression profiles of cancer cells are a valuable tool in the comprehension of transcriptional changes indicative of treatment. These profiles enable the identification of drug sensitivity across various cancer types. Such expression profiles may be used to characterize the genes whose expression is indicative of drug response [29]. Accordingly, we generated a TLT sensitivity signature that reflected the genomic changes in eight TLT-sensitive BL-CL cell lines (Figure 3.5A). We treated the cell lines with either TLT or DMSO control and used RNA-sequencing to profile the samples. We identified 131 genes that significantly upregulated or downregulated

and incorporated the expression values for these genes into a predictive signature (Figure 3.5A). We then used this signature to predict drug sensitivity for the tumors from the PANCAN12 gene-expression dataset, which contains expression profiles for 12 cancer types [22,41]. The outcome of this process is a probability for each tumor sample, indicating how likely each tumor would respond to TLT treatment. Breast (mean = 0.71) and bladder cancer (mean = 0.69) were predicted to be most sensitive to TLT (1.00 is highest possible sensitivity, and 0.00 is lowest), while glioblastoma was predicted to be least sensitive (mean = 0.16, Figure 3.5B). Low TLT sensitivity was also predicted for uterine corpus endometrial carcinoma (UCEC mean = 0.29) and kidney renal clear cell (KIRC mean = 0.35). Medium TLT sensitivity was recorded for the rest of the profiled cancer types, including colon adenocarcinoma (COAD mean = 0.42), lung adenocarcinoma (LUAD mean = 0.43) and ovarian serous cystadenocarcinoma (OV mean = 0.56) (Figure 3.5B). These results are in line with the in vitro observations of TLT effectiveness against breast cancer (BL-CL in particular) and suggest future investigation of TLT as an effective therapeutic lead against bladder cancer.

3.5 Discussion

We have identified and described a previously uncharacterized trisulfated sterol that we have named topsentinol L trisulfate and which exhibits increased tumoricidal activity against BL-CL. Interestingly, halistanol sulfate, another trisulfated sterol isolated from the same marine organism as TLT, did not exhibit similar activity against BL-CL (Supplementary Figure 3.13). This could potentially be attributed to the differences in the side chains of these two compounds, which are otherwise structurally similar (Figure 3.2C-D).

Furthermore, we describe the treatment effect of TLT on BL-CL, highlighting the particular changes in the activation of AMPK, CHK1 and p38. AMPK is a

heterotrimeric serine/threonine kinase complex that is regulated by adenylate levels in the cell and functions as part of an evolutionarily conserved energy-sensing pathway [42,43]. The effective result of AMPK activation is the avoidance of bioenergetic catastrophe and cell death through the conservation of cellular energy [43]. Interestingly, the role of AMPK in cancer is complex, as AMPK can exert pro- or antitumor effects based on cell context. AMPK is central to a tumor suppressor network, the LKB1-AMPK-TSC-mTOR signaling cascade, known to regulate cell growth and proliferation in response to stress [44]. Conversely, retaining continuous activation of AMPK leading to an enhanced ability to adapt to metabolic stress may function to promote tumor survival and growth. For example, the activation of AMPK in response to stresses such as hypoxia and nutrient deprivation provides cancers cells with the metabolic flexibility needed for survival [43]. These dueling roles of AMPK highlight the complexity and dichotomy of the kinase's role in cancer cells. AMPK agonists acting as anticancer agents have been suggested through the use of the therapeutic biguanides: metformin and phenformin. Metformin is currently used to treat type II diabetes and has been associated with a significantly lower cancer incidence in patients relative to those using other medications to manage their diabetes [39,45]. However, recent work has indicated that the antitumorigenic effects of metformin and another known AMPK agonist, AICAR, are due to AMPK-independent effects [46]. Interestingly, other studies have implicated AMPK as a mediator of cellular proliferation and survival, showing the promising effect of AMPK inhibition as a cancer therapy [47,48]. We observe similar effects against breast cancer, and particularly the BL-CL subtype which exhibits higher sensitivity against dorsomorphin C than Luminal/HER2+ breast cancer (Figure 3.4A). This observation is in line with the AMPK inhibitory effects induced in BL-CL breast cancer when treated with TLT (Figure 3.3C-D).

Another aspect of the inhibitory effects promoted by TLT treatment was the downregulation of CHK1 activation. Upon cellular exposure to various genotoxic stresses, CHK1 is activated by ATR-mediated phosphorylation following DNA-damage leading to the phosphorylation of cdc25. CHK1 assumes the role of the major cell-cycle checkpoint kinase mediating S- and G2-arrest [36]. In BL-CL, the rationale of CHK1 targeted therapy is supported by the documented evidence of alterations in the DNA damage repair machinery through either the high rate of BRCA or p53 mutations [6,7,9]. Therefore, another loss of a DNA damage repair component may lead to the cell's inability to properly fix chromosomal damage and enter apoptosis. Indeed, Albiges, et al. have shown that CHK1 is potential therapeutic target in TNBC, with CHK1 inhibition observed to induce mitotic cell death in TNBC cell lines [36]. In our work, we complement this finding by recording the selectivity of CHK1 inhibition against BL-CL, which is concordant with the TNBC subtype (Figure 3.4B). The inhibitory effects of TLT on AMPK and CHK1 shed light on the potential therapeutic benefit of AMPK and/or CHK1 inhibition on BL-CL. However, further work is required to validate these findings. Although dorsomorphin C is a potent AMPK inhibitor, studies have shown this compound to exhibit high affinity towards other proteins such as BMP and ALK [49].

Finally, our work describes the projected efficacy of TLT against a variety of human tumors, highlighting the optimal effect of the compound against breast and bladder cancer. In a recent TCGA study characterizing the molecular landscape of urothelial bladder carcinoma, a p53 mutation rate of 49% was recorded in the samples tested [50], drawing a similarity to the common observation of p53 mutation in BL-CL. More interestingly, among the key pathway nodes deregulated in bladder cancer, the LKB1/STK11-TSC-mTOR node was among the most commonly deregulated. LKB1, the deactivator of AMPK, was recorded to contain copy number alternations (CNAs) in 11% of all cases. TSC1 and TSC2 recorded

CNAs in 16% and 9% of all cases, as well as inactivating mutations in 8% and 2%, respectively [50]. Thus, one hypothesis is that the inhibitory effect of TLT on CHK1 and AMPK (and subsequently the LKB1-AMPK-TSC-mTOR node) could lead to an equally effective response against bladder cancer. Further work is needed to elucidate the exact mechanism of action of TLT and its projected effectiveness against bladder cancer.

In this study, we have described the discovery and identification of a previously unreported sulfated sterol, as well as its signaling effect on BL-CL. We have described two potential therapeutic targets of BL-CL that can be exploited for the benefit of treatment efficacy. This lays the groundwork necessary for the exploration of AMPK and CHK1 as potential targets of BL-CL treatment, with a need to further characterize and delineate TLT's role as an investigational anti-BL-CL compound.

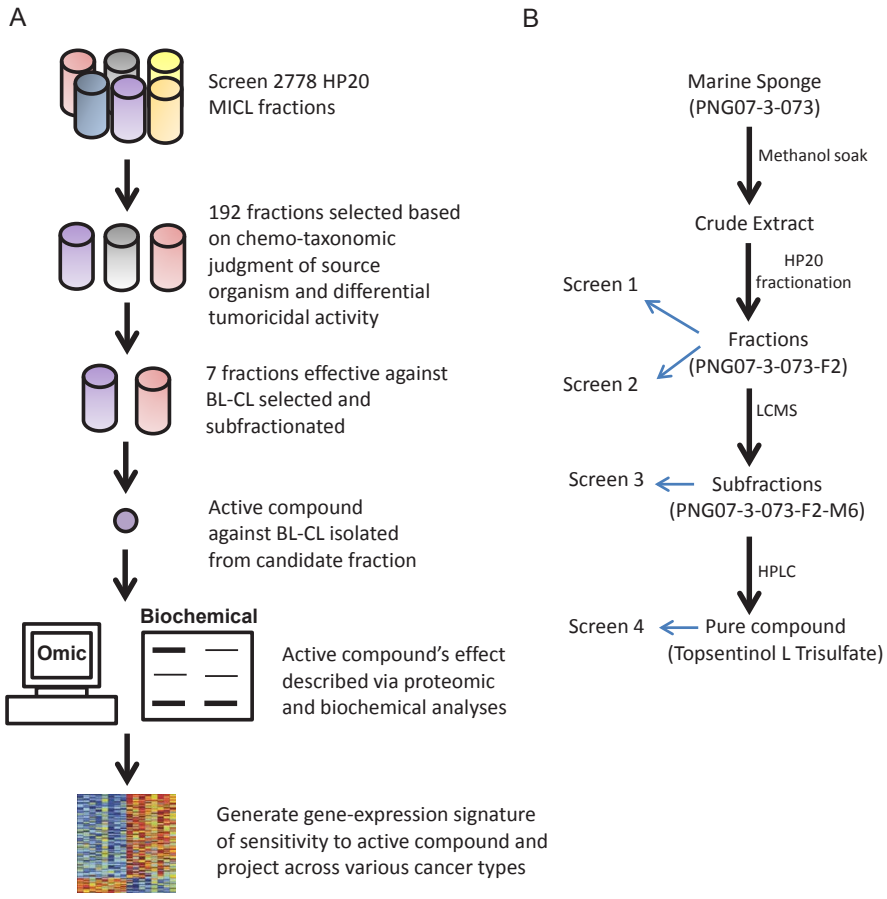

Figure 3.1: The overall design of the step-wise drug screen. (A) 2778 HP20 fractions were first screened.
One hundred ninety-two HP20 fractions were selected based on tumoricidal properties and chemo-taxonomic judgment of source organism. These fractions were then screened to identify BL-CL selective inhibitors. Seven candidate fractions were identified and further subfractionated. The subfractions were in turn screened for anti-BL-CL properties. After a candidate anti-BL-CL subfraction was identified, the active compound of the fraction was isolated, and its effect on BL-CL analyzed through proteomic and biochemical methods. A gene-expression signature of sensitivity to the active compound was then generated and used to project compound sensitivity across various cancer types. (B) The path towards identifying TLT. Marine sponge PNG07-3-073 was diced and soaked in methanol to obtain a crude extract, which was fractionated on HP20SS resin. Among the five fractions obtained, only the F2 fraction exhibited tumoricidal activity (Screen 1). This activity was amplified against BL-CL (screen 2). PNG07-3-073-F2 was then further fractionated, and the subfractions investigated for anti-BL-CL activity, where the M6 fraction was identified as being BL-CL selective (Screen 3). Large-scale isolation of PNG07-3-073 ensued, culminating in the purification of TLT and its identification as the active compound in PNG07-3-073 responsible for anti-BL-CL effects (Screen 4).

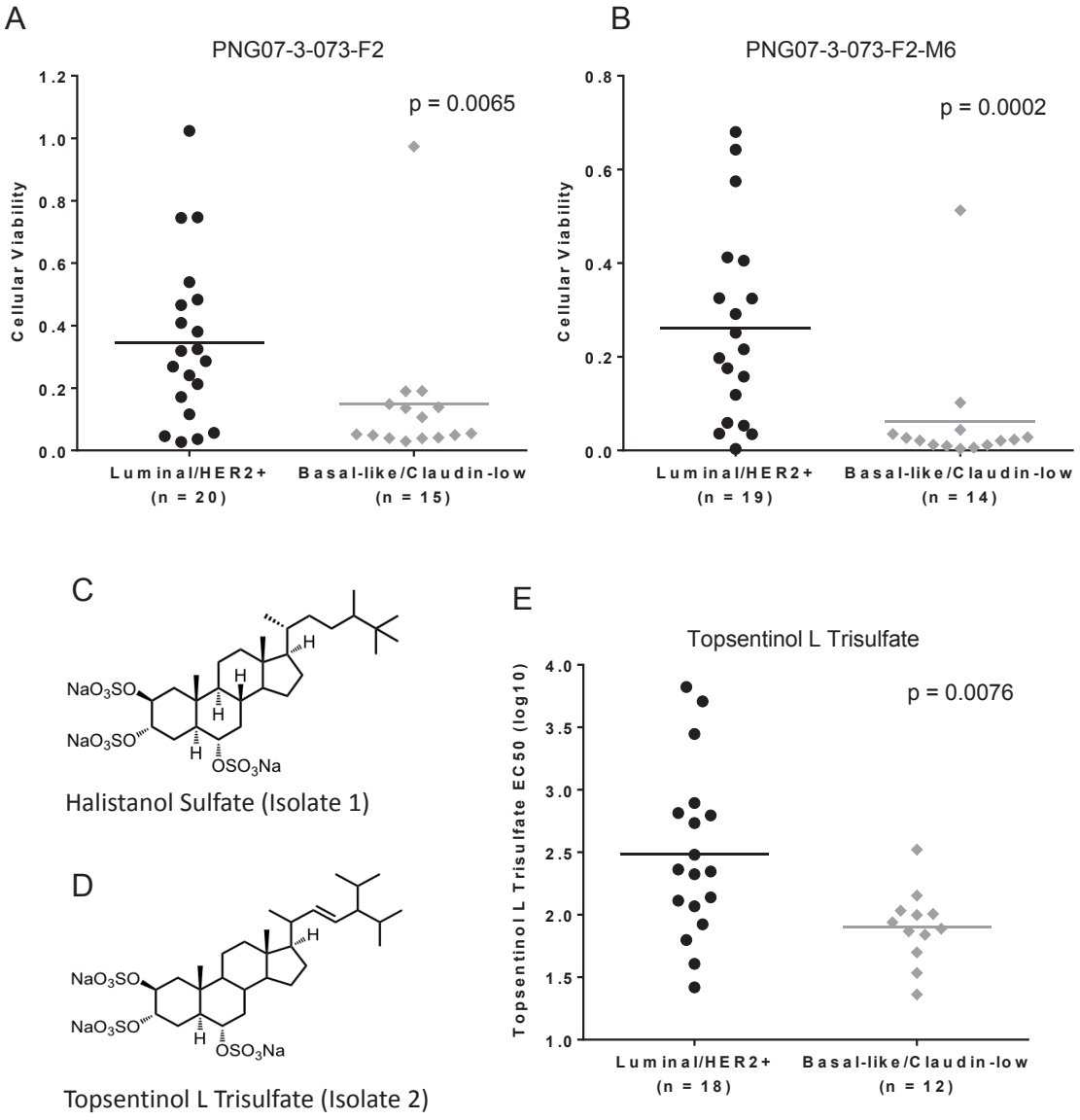

Figure 3.2: Topsentinol L trisulfate, isolated from the marine sponge Topsentia sp. (PNG07-3-073), is selective against BL-CL.
Cell lines were divided accordingly and scatter dot diagrams plotted. Every dot represents a cell line, with the y value representing the cell line's viability or compound EC50 posttreatment. The horizontal line indicates the mean for every group. BL-CL cell lines exhibit significantly lower cell viability when treated with (A) PNG07-3-073-F2 and (B) PNG07-3-073-F2-M6 than Luminal/HER2+ cell lines. (C) Chemical structure of halistanol sulfate. (D) Chemical structure of topsentinol L trisulfate. (E) Response to topsentinol L trisulfate treatment as measured by compound EC50. BL-CL cell lines are significantly more sensitive to TLT than Luminal/HER2+ cell lines.

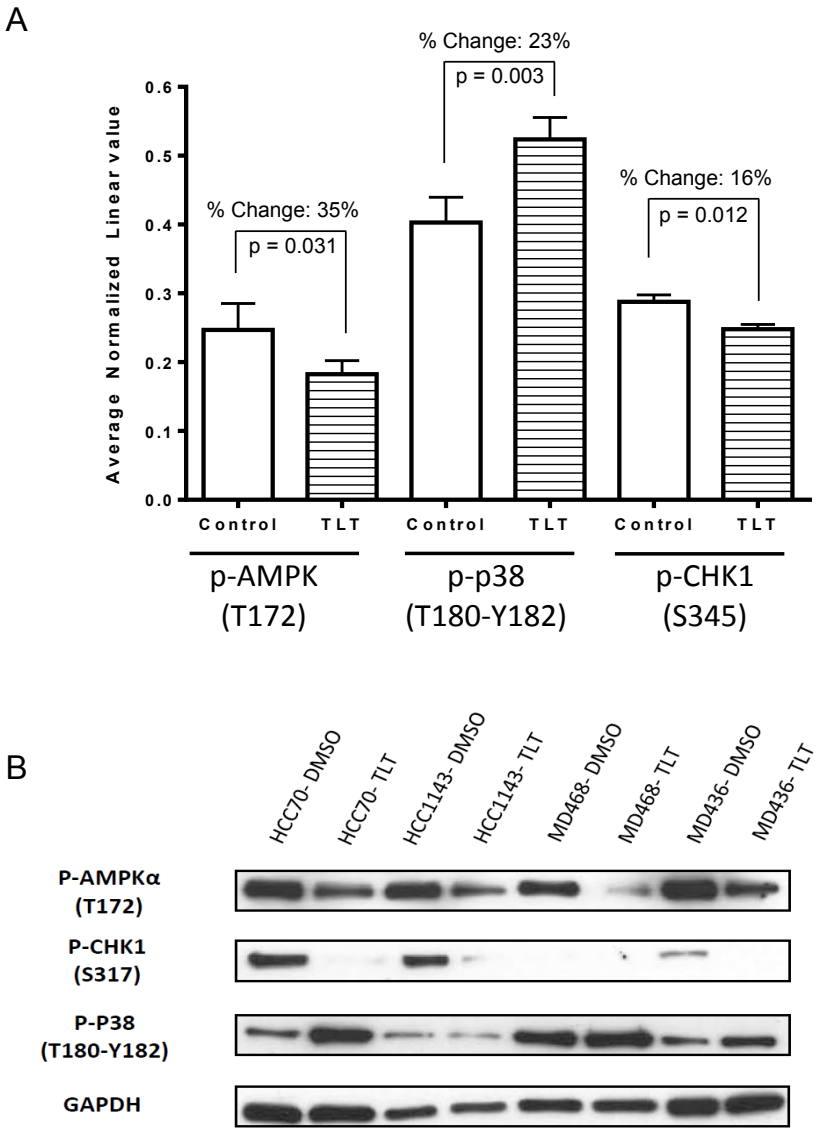

Figure 3.3: TLT inhibits AMPK and CHK1 but activates p38.
(A) A panel of eight BL-CL cell lines were treated with TLT at a 105μM dose (approximate average EC75 dose across all eight lines) for 6 hrs, and compared to DMSO control via RPPA that investigated 217 proteins. Eight proteins displayed 15% or more significant deregulation in protein levels, among which, AMPK, CHK1 and p38 are displayed here in bar graphs. Error bars represent SEM. (B) Observations made for p38, AMPK and CHK1 in the RPPA experiment were validated by western blotting. A panel of four BL-CL cell lines were treated similarly with TLT at a 105μM dose for 6 hrs, and compared to DMSO control. TLT treatment inhibits AMPK and CHK1, and activates p38.

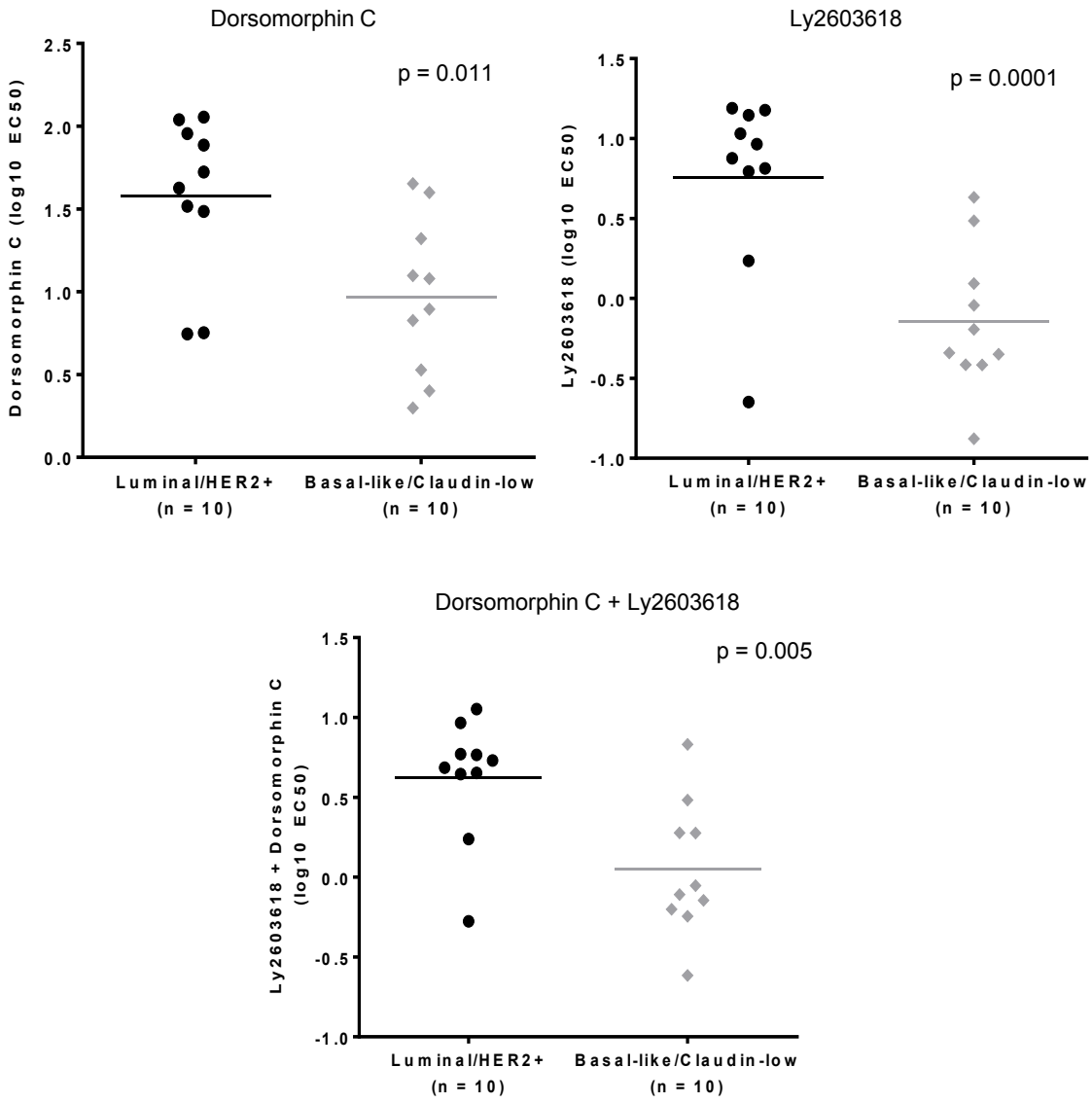

Figure 3.4: Singular or dual inhibition of AMPK and CHK1 is selective against BL-CL.
(A) Cell lines were divided accordingly and scatter dot diagrams of treatment EC50 values plotted. Every dot represents a cell line, with the y value representing the cell line's treatment EC50 and the horizontal line indicating the mean for each group. BL-CL cell lines are significantly more sensitive to (A) AMPK inhibition through dorsomorphin C, (B) CHK1 inhibition through Ly2603618 and (C) the combined inhibition of both AMPK and CHK1 through concurrent treatment of dorsomorphin C and Ly2603618.

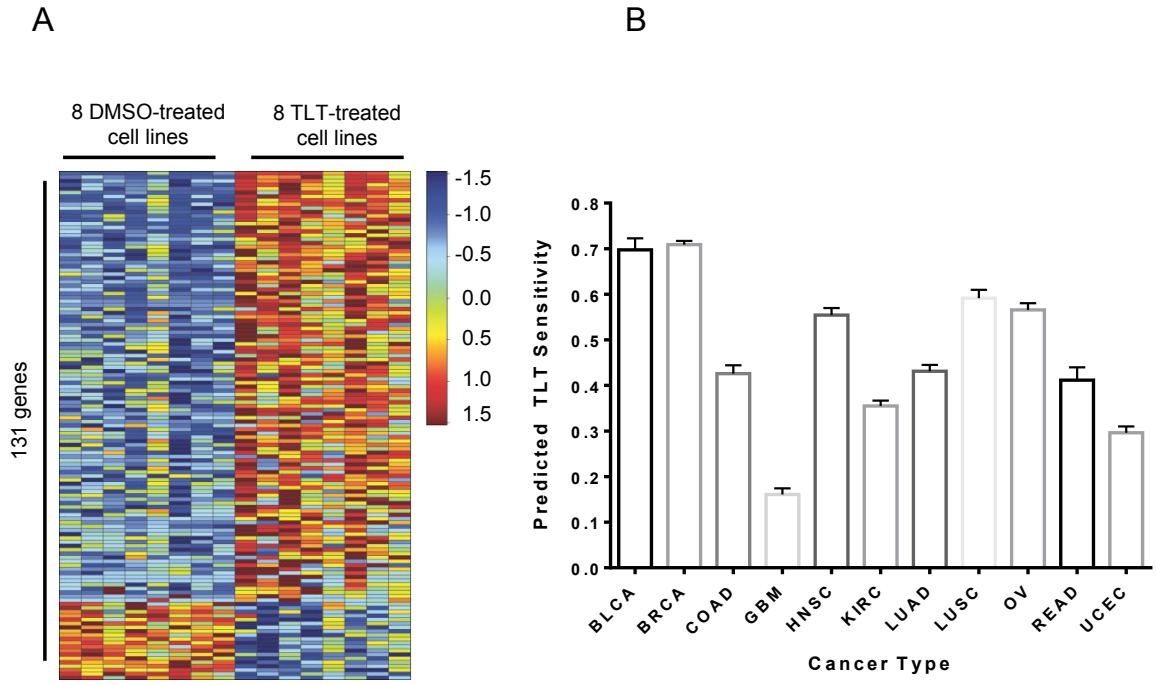

Figure 3.5: TLT sensitivity is predicted in breast and bladder cancer using gene-expression signature analysis.
(A) The gene-expression signature for TLT sensitivity was generated by treating eight BL-CL cell lines with either TLT or DMSO. The heatmap columns are the eight cell lines making up eight controls on the left (treated with DMSO) and eight treated samples on the right (treated with TLT). Each row represents a gene that is part of the signature. There are a total of 131 genes making up the signature. Red indicates upregulation while blue indicates downregulation of the gene. (B) The TLT sensitivity signature was used to project the sensitivity of 12 different cancers. Results are shown in a bar graph where the x axis represents the 12 cancer types assayed and the y axis represents the predicted score of TLT sensitivity (minimum = 0, maximum = 1). Each column portrays the mean of the TLT sensitivity scores across the samples in a particular cancer type. The error bars indicate SEM. Breast and bladder cancer were predicted to be the most sensitive to TLT treatment, with glioblastoma being the least sensitive. Legend = BLCA: bladder urothelial carcinoma. BRCA: breast invasive carcinoma. COAD: colon adenocarcinoma. GBM: glioblastoma multiforme. HNSC: head and neck squamous cell carcinoma. KIRC: kidney renal clear cell carcinoma. LUAD: lung adenocarcinoma. LUSC: lung squamous cell carcinoma. OV: ovarian serous cystadenocarcinoma. READ: rectum adenocarcinoma. UCEC: uterine corpus endometrial carcinoma.

Supplementary Figure 3.1: Image of the marine invertebrate Topsentia sp. sponge labeled PNG07-3-073.
The sponge specimen PNG07-3-073 was identified as Topsentia sp. (OTU UU1273), order Halichondrida, family Halichondriidae. The creamy white sponge is massive with thick fistular processes, a firm texture and slightly hispid surface. The ectosome is not detachable, consisting of a thin paratangential layer of spicules with protruding choanosomal spicules. The interior of the sponge is densely spiculous and completely disorganized with plumose bundles of spicules just below the surface, spongin not visibly present. The spicules are fusiform oxea in a range of sizes and widths, generally in categories: ~1125-1325 × 42-48μm, 715-1050 × 25μm, 525-825 × 15μm. Topsentia sp. (OTU UU1273) does not compare entirely to previously described species of Topsentia and likely represents an undescribed species. The sponge was collected by SCUBA November 21, 2007 from New Britain, Papua New Guinea (S 05° 19.680', E 150° 17.674') and immediately frozen. The specimen has been described in SpongeMaps, available at the following link: http://www.spongemaps.org/#!Topsentia-sp-OTU-UU1273-demosponge/zoom/c21kz/imagel3v

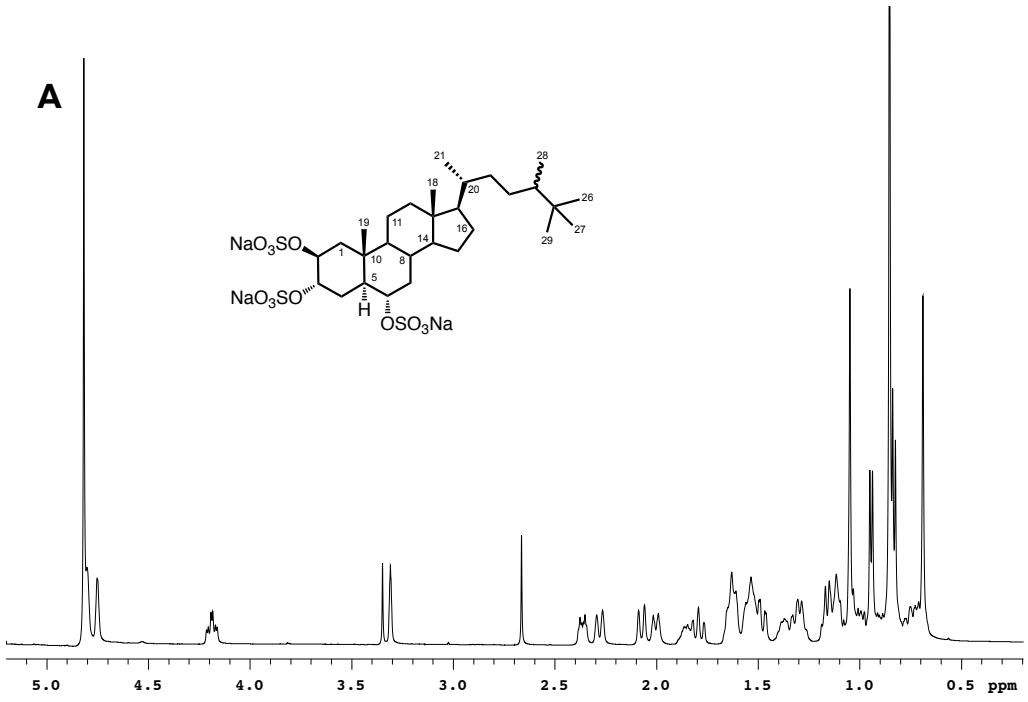

Supplementary Figure 3.2: 1D NMR spectra for halistanol sulfate in CD3OD 1H spectrum.

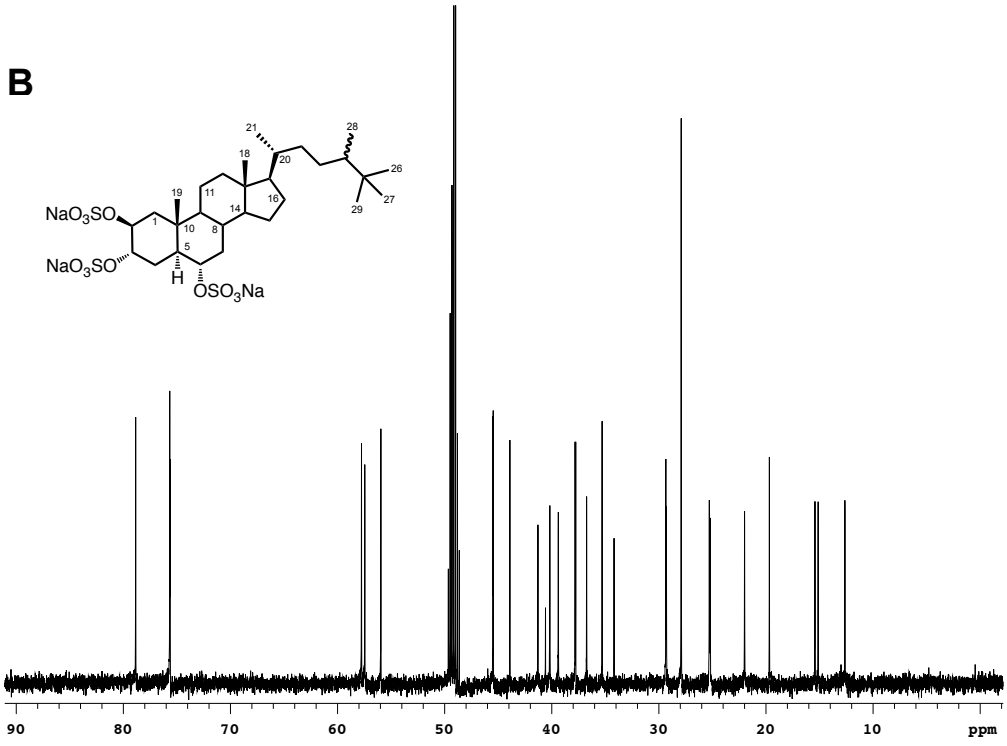

Supplementary Figure 3.3: 1D NMR spectra for halistanol sulfate in CD3OD 13C spectrum.

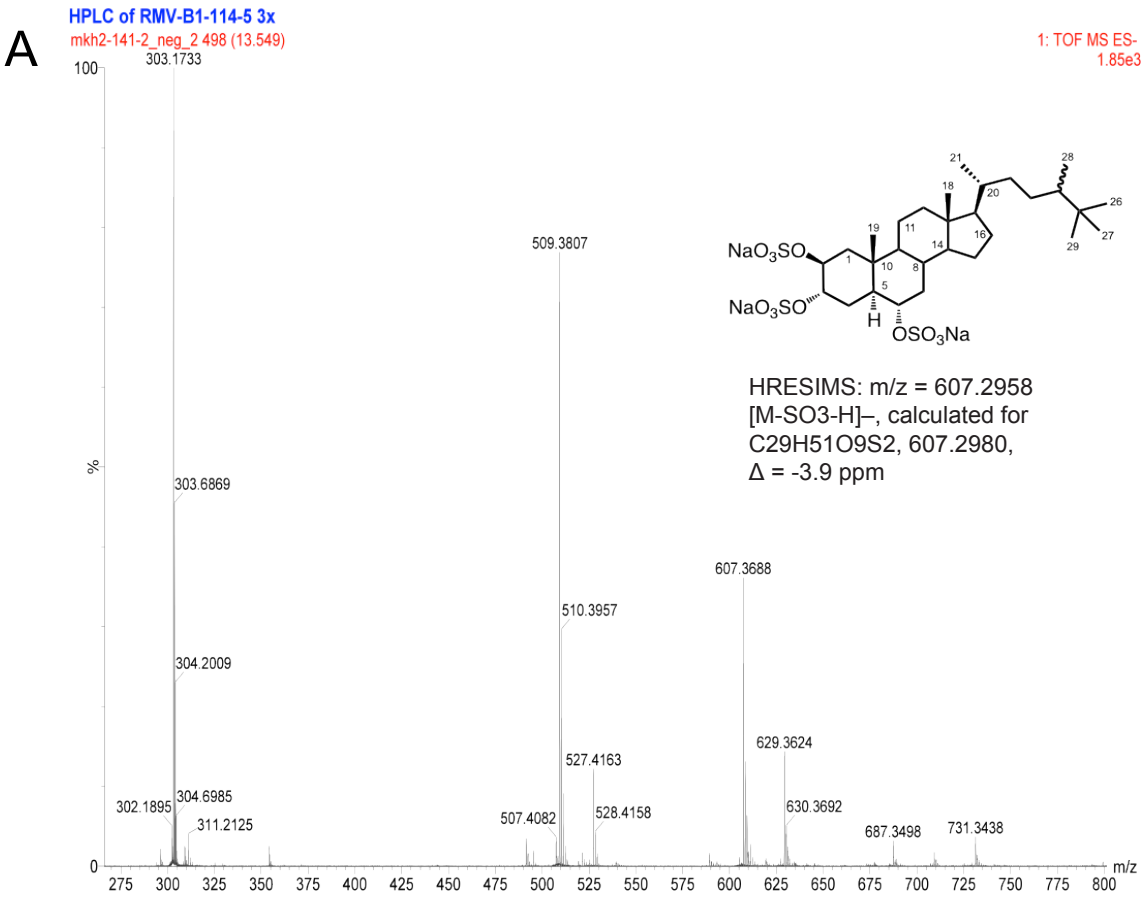

Supplementary Figure 3.4: Low-resolution mass spectra for (A) halistanol sulfate.

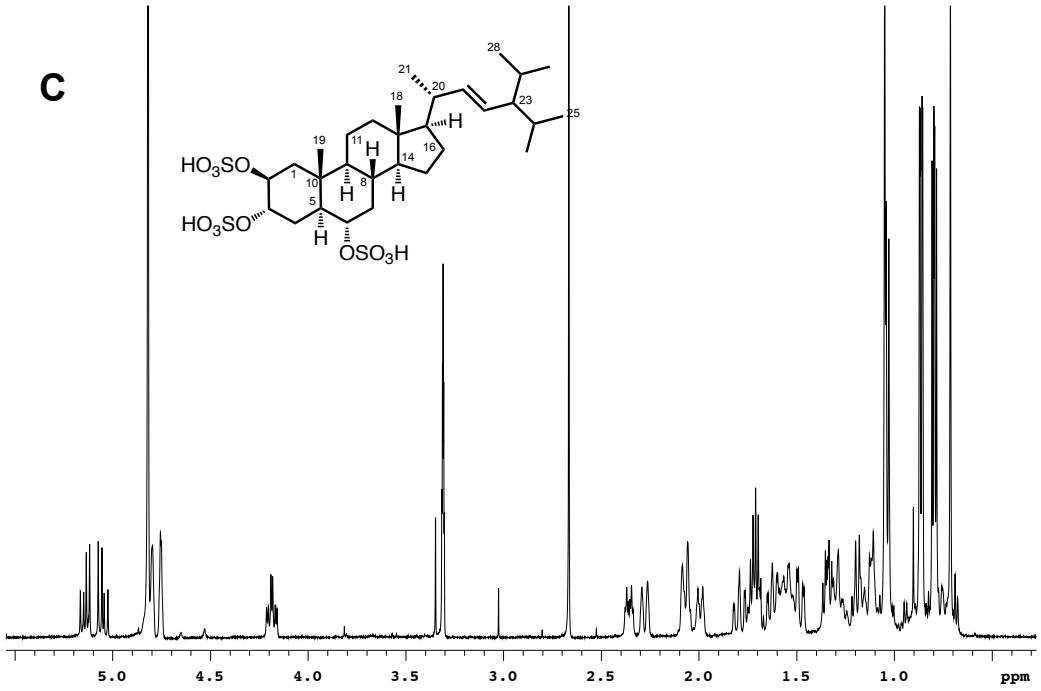

Supplementary Figure 3.5: 1D NMR spectra for topsentinol L trisulfate in CD3OD 1H spectrum.

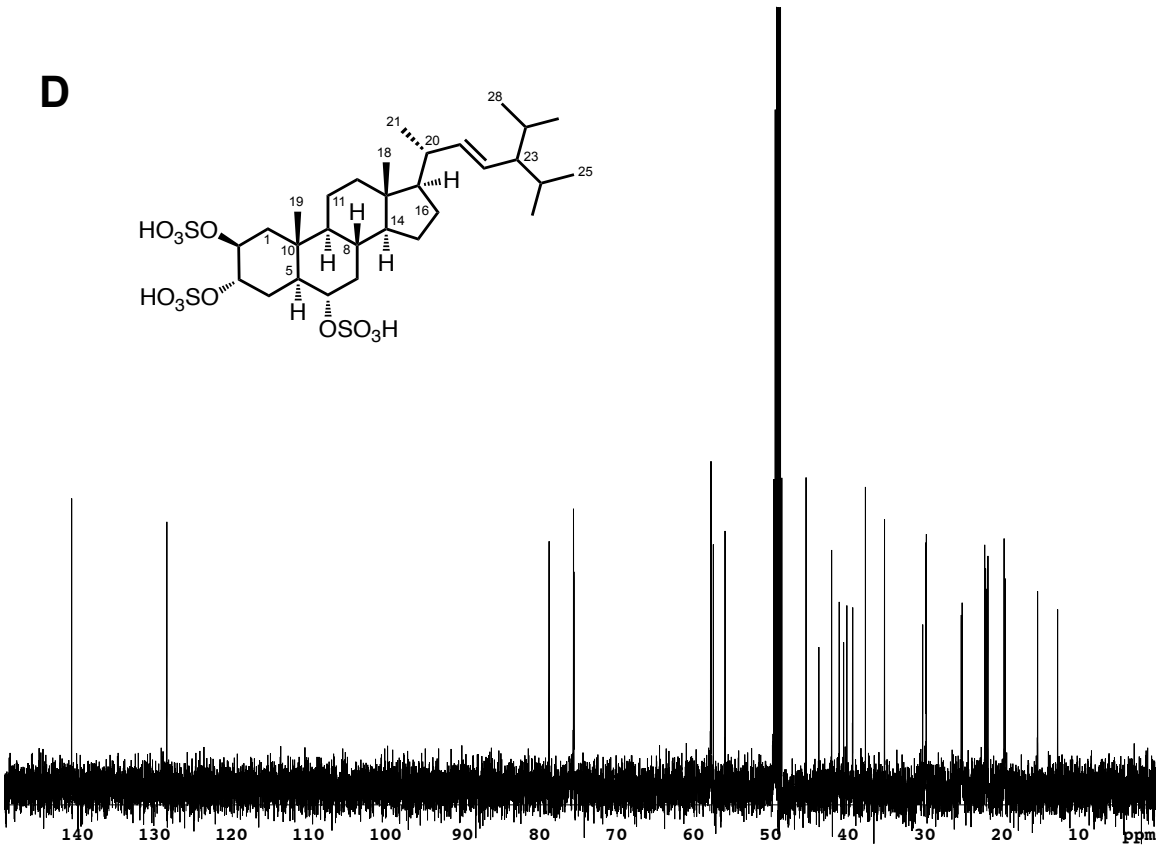

Supplementary Figure 3.6: 1D NMR spectra for topsentinol L trisulfate in CD3OD 13C spectrum.

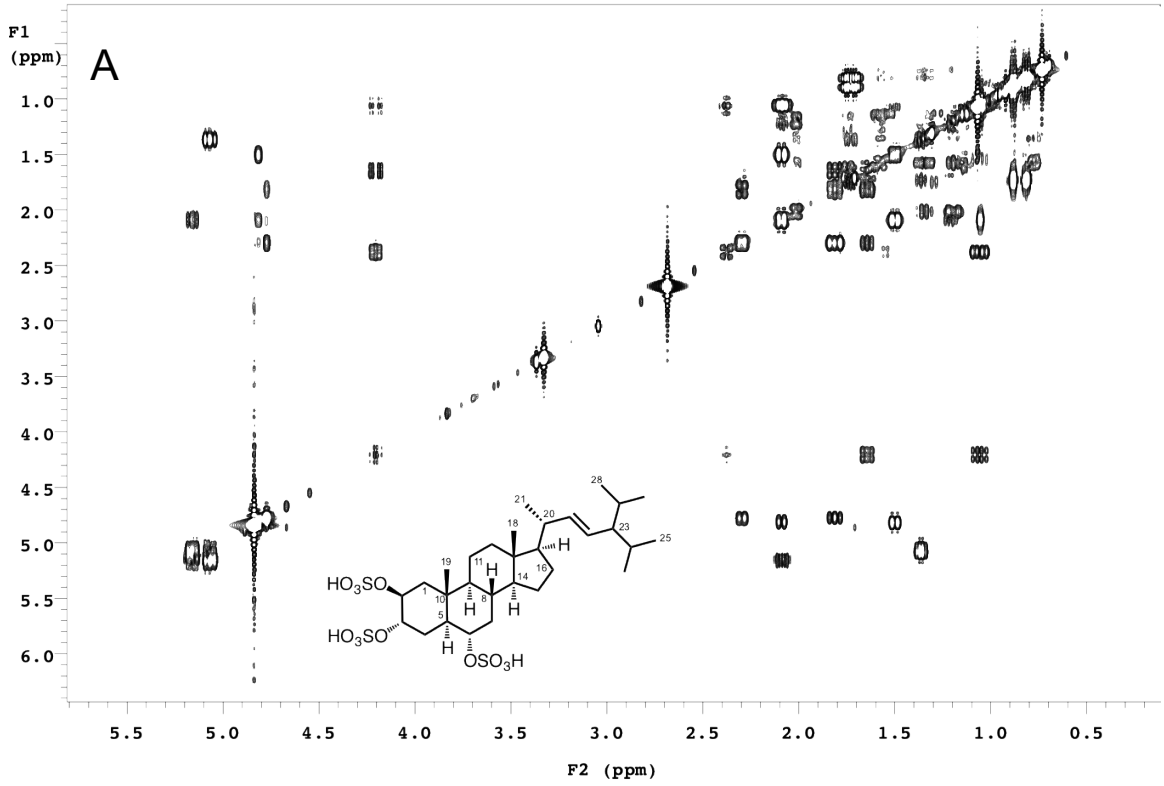

Supplementary Figure 3.7: 2D NMR spectra for topsentinol L trisulfate in CD3OD gCOSY spectrum.

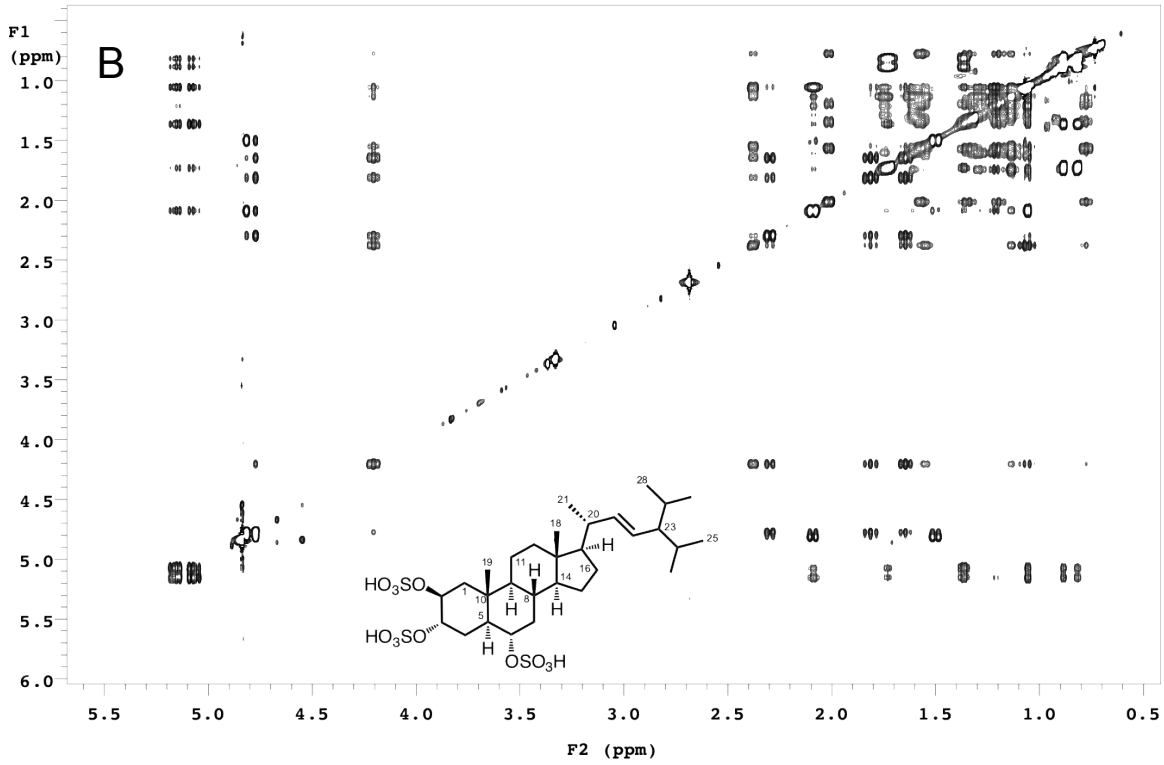

Supplementary Figure 3.8: 2D NMR spectra for topsentinol L trisulfate in CD3OD zTOCSY spectrum.

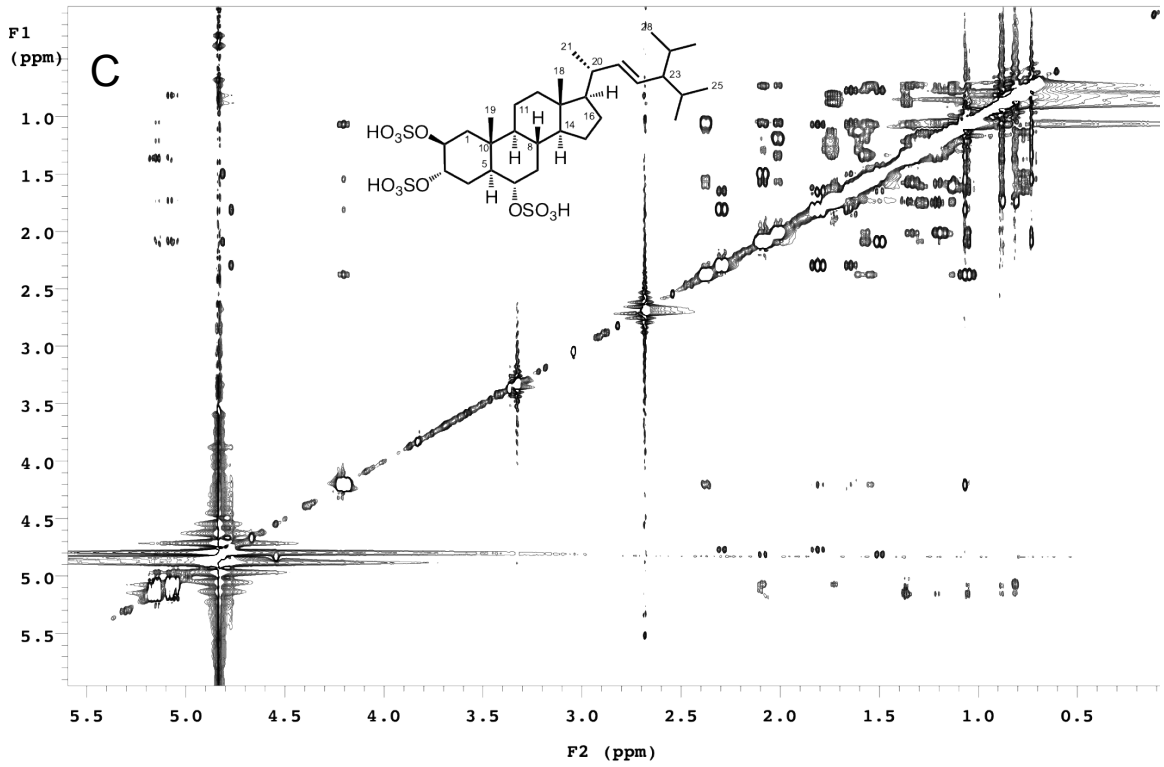

Supplementary Figure 3.9: 2D NMR spectra for topsentinol L trisulfate in CD3OD ROESY spectrum.

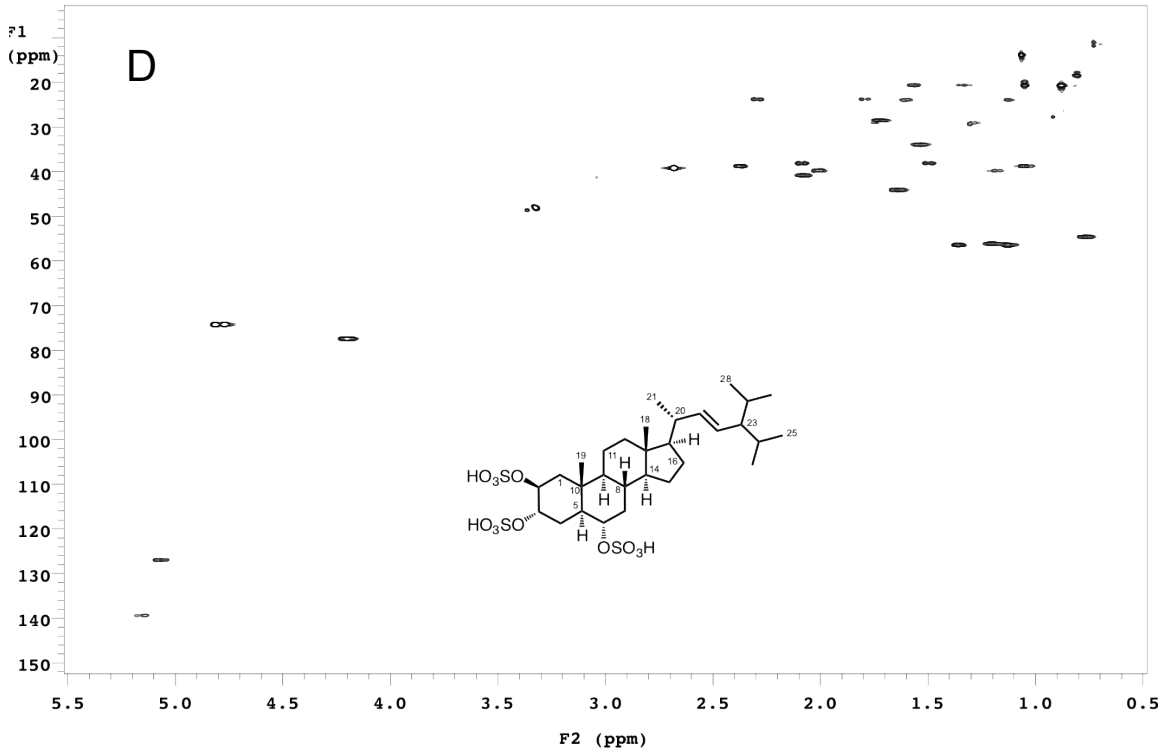

Supplementary Figure 3.10: 2D NMR spectra for topsentinol L trisulfate in CD3OD gHSQC spectrum.

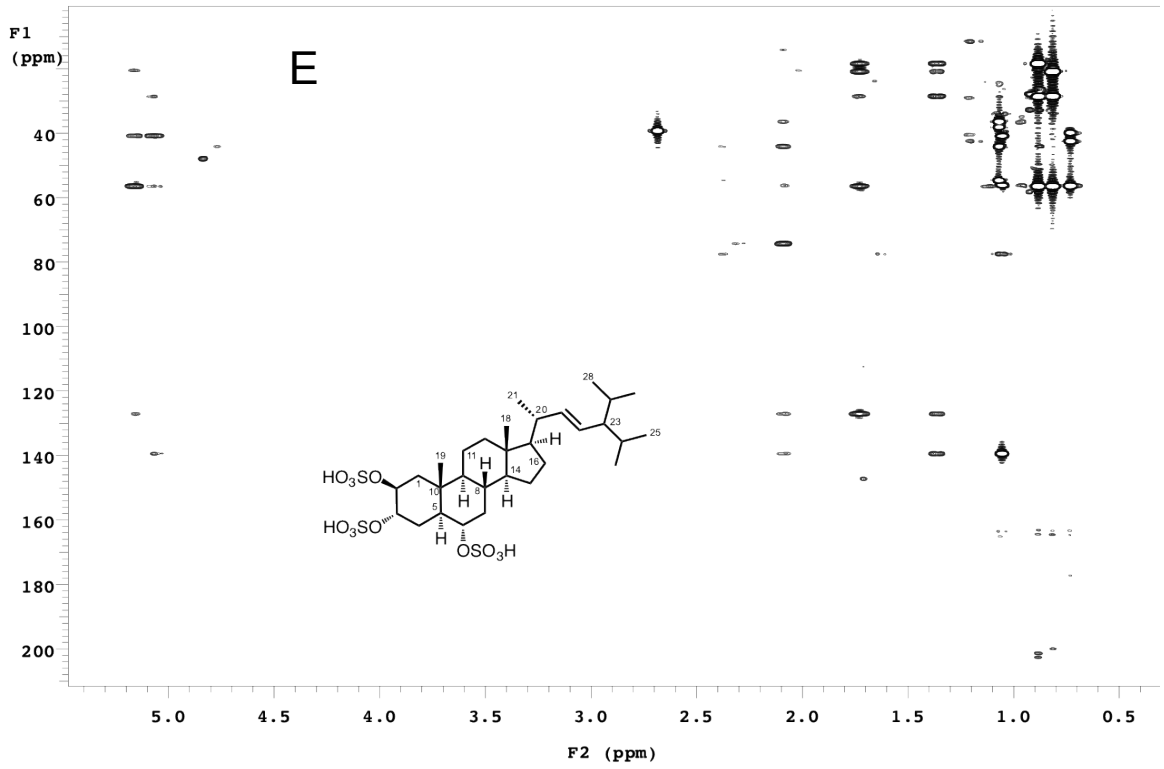

Supplementary Figure 3.11: 2D NMR spectra for topsentinol L trisulfate in CD3OD gHMBC spectrum.

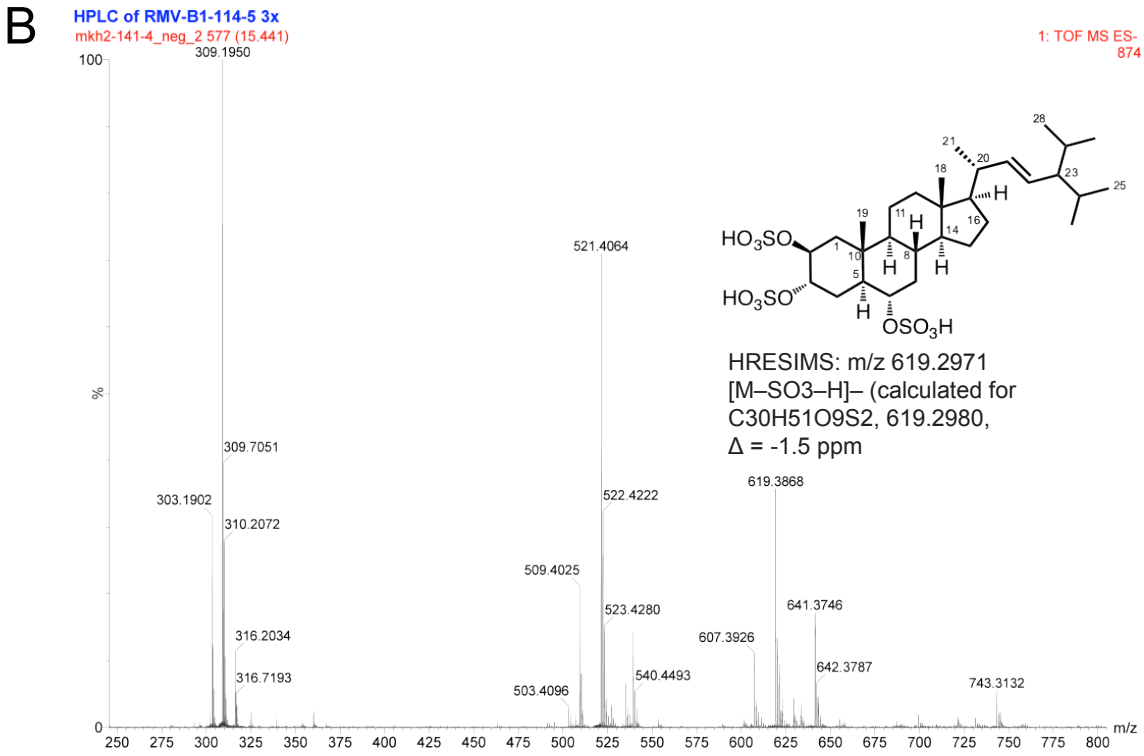

Supplementary Figure 3.12: Low-resolution mass spectra for (B) topsentinol L trisulfate.

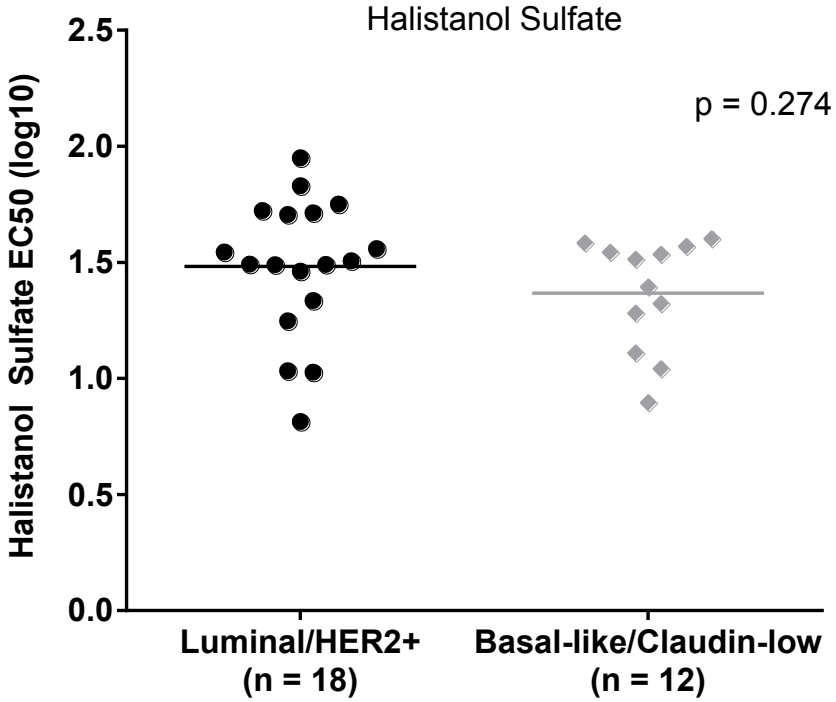

Supplementary Figure 3.13: Halistanol sulfate is not selective against BL-CL in comparison to Luminal/HER2+ breast cancer.
The cell lines of the investigated breast cancer panel were divided accordingly and scatter dot plot diagrams of halistanol sulfate EC50 values plotted. Every dot represents a cell line, with the y value representing the cell line's halistanol sulfate compound EC50 and the horizontal line indicating the mean value for every group. There is no significant difference between the response of BL-CL and Luminal/HER2+ cell lines to halistanol sulfate.

Supplementary Table 3.1

Characteristics of the breast cancer cell lines used in the study for all screens and drug response assays.

Breast Cancer Cell Line	ER	PR	HER2	Gene-expression Subtype	Media	Screen 1	Screen 2	Screen 3	Screen 4	AMPKi/CHKi Screen
AU565	-	-	+	luminal/HER2 positive	RPMI		x	x	x	x
BT20	-	-	-	basal	DMEM		x	x	x	
BT474	+	+	+	luminal/HER2 positive	DMEM	x	x	x	x	x
BT483	+	+	-	luminal	RPMI		x	x	x	x
BT549	-	-	-	claudin low	RPMI	x	x	x		
Cama-1	+	-	-	luminal	DMEM		x	x	x	
HCC1143	-	-	-	basal	RPMI		x	x	x	x
HCC1395	-	-	-	Basal	RPMI		x	x	x	
HCC1419	-	-	+	luminal/HER2 positive	RPMI		x	x	x	x
HCC1500	+	+	-	Basal	RPMI		x			
HCC1569	-	-	+	basal/HER2 positive	RPMI		x	x	x	
HCC1599	-	-	-	basal	RPMI		x	x		
HCC1806	-	-	-	basal	RPMI		x	x	x	x
HCC1937	-	-	-	basal	RPMI		x	x	x	x
HCC1954	-	-	+	basal/HER2 positive	RPMI		x	x	x	
HCC2218	-	-	+	luminal	RPMI		x	x	x	
HCC38	-	-	-	claudin low	RPMI		x	x	x	x
HCC70	-	-	-	basal	RPMI		x	x	x	x
Hs578T	-	-	-	claudin low	DMEM	x	x	x	x	x
JIMT-1	-	-	+	basal/HER2 positive	DMEM		x	x	x	
MCF7	+	+	-	luminal	DMEM	x	x	x	x	x
MD134VI	+	-	-	luminal	RPMI		x	x	x	
MD157	-	-	-	claudin low	DMEM		x	x	x	x
MD175VII	+	-	-	luminal	RPMI		x	x	x	x
MD231	-	-	-	claudin low	RPMI	x	x	x	x	x
MD415	+	-	-	luminal	RPMI		x	x	x	x
MD436	-	-	-	claudin low	RPMI		x	x	x	x
MD453	-	-	-	luminal	RPMI		x	x	x	
MD468	-	-	-	basal	RPMI		x	x	x	x
MDAMB361	+	-	+	luminal/HER2 positive	DMEM	x	x	x		
SKBR3	-	-	+	luminal/HER2 positive	RPMI		x	x	x	x
T47D	+	+	-	luminal	RPMI	x	x	x	x	
UACC812	-	-	+	luminal/HER2 positive	DMEM		x	x	x	x
ZR75-1	+	-	-	luminal	RPMI		x	x	x	x
ZR75-30	+	-	+	luminal/HER2 positive	RPMI		x			

Supplementary Table 3.2

Characteristics of the lung cancer cell lines used in the study for all screens and drug response assays.

Lung Cancer Cell Line	Subtype	K-Ras Mut	P53 Mut	EGFR Mut	Media	Screen 1	Screen 2
A549	Adenocarcinoma	G12S	x	x	F12K		x
CALU3	Adenocarcinoma	x	M237I	x	EMEM		x
H1155	Large cell	Q61H	R273H	x	ACL-4		x
H1355	Adenocarcinoma	G13C	E285K	Q1159H	ACL-4		x
H1373	Adenocarcinoma	G12C	E339*	Intron	RPMI		x
H1395	Adenocarcinoma	x	x	x	RPMI		x
H1437	Adenocarcinoma	x	R267P	x	RPMI		x
H1563	Adenocarcinoma	x	x	x	RPMI	x	x
H1581	Large cell	x	Q144*	x	ACL-4	x	x
H1650	Adenocarcinoma	x	V225_splic	ELREA746del	RPMI	x	x
H1651	Adenocarcinoma	x	C176Y	x	ACL-4		x
H1693	Adenocarcinoma	x	Q331_splic	x	RPMI		x
H1703	Adenocarcinoma	x	A307_splic	x	RPMI		x
H1792	Adenocarcinoma	G12C	E224_splic	x	RPMI		x
H1793	Adenocarcinoma	x	R209*	C311F	HITES		x
H1944	Adenocarcinoma	G13D	x	x	RPMI	x	x
H1975	Adenocarcinoma	x	x	T790M, L858R	RPMI	x	x
H2009	Adenocarcinoma	G12A	R273L	Intron	HITES		x
H2030	Adenocarcinoma	G12C	G262V	x	RPMI		x
H2085	Adenocarcinoma	x	ND	ND	ACL-4		x
H2122	Adenocarcinoma	G12C	C176F, Q16	x	RPMI		x
H2126	Adenocarcinoma	x	E62*	x	ACL-4		x
H23	Adenocarcinoma	G12C	M246I	x	RPMI	x	x
H2405	Adenocarcinoma	x	x	x	ACL-4		x
H322	Adenocarcinoma	x	R248L	x	RPMI		x
H358	Adenocarcinoma	G12C	x	x	RPMI		x
H441	Adenocarcinoma	G12V	R158L	x	RPMI		x
H460	Large cell	Q61H	x	x	RPMI		x
H520	Squamous	x	W146*	x	RPMI	x	x
H522	Adenocarcinoma	x	P191fs FRA	x	RPMI		x
H661	Large cell	x	R158L, S21	x	RPMI	x	x
H838	Adenocarcinoma	x	x	x	RPMI		x
HCC4006	Adenocarcinoma	x	x	ELR746del INFRAME	RPMI	x	x
SKLU1	Adenocarcinoma	G12D	H193R	x	EMEM		x
SKMES1	Squamous	x	E298*	x	EMEM		x
SW1573	Squamous	G12C	Intron	x	RPMI		x

Supplementary Table 3.3

13C and 1H chemical shifts of halistanol sulfate and topsentinol L trisulfate in CD3OD.

	Halistanol sulfate (mkh2-141-2)		Topsentinol L trisulfate (mkh2-141-4)	
Position	δ_C (mult.)	δ_H (mult., *J* in Hz)	δ_C (mult.)	δ_H (mult., *J* in Hz)
1	39.4	2.07 (br d, 14.3)	39.4	2.07 (m)
		1.48 (dd, 15.4, 2.9)		1.48 (dd, 14.9, 3.7)
2	75.7	4.80 (s)	75.7	4.80 (s)
3	75.6	4.75 (s)	75.6	4.75 (br d, 22.3)
4	25.2	2.28 (br d, 14.6)	25.2	2.28 (br d, 14.5)
		1.79 (br t, 13.4)		1.78 (m)
5	45.5	1.63 (m)	45.5	1.62 (m)
6	78.9	4.19 (td, 11.1, 4.4)	78.9	4.19 (td, 11.1, 4.4)
7	40.2	2.37 (dt, 12.2, 4.3)	40.2	2.36 (dt, 12.1, 4.3)
		1.05 (m)		1.04 (m)
8	35.3	1.53 (m)	35.3	1.53 (m)
9	56.0	0.76 (m)	56.0	0.75 (m)
10	37.8		37.8	
11	22.0	1.54 (m)	22.0	1.55 (m)
		1.31 (m)		1.31 (m)
12	41.3	2.00 (br d, 12.4)	41.2	2.00 (dt, 12.4, 2.9)
		1.15 (m)		1.17 (m)
13	43.9		43.8	
14	57.8	1.11 (m)	57.8	1.11 (m)
15	25.3	1.63 (m)	25.3	1.59 (m)
		1.11 (m)		1.11 (m)
16	29.3	1.86 (m)	30.3	1.73 (m)
		1.29 (m)		1.29 (m)
17	57.5	1.16 (m)	57.5	1.19 (m)
18	15.4	1.05 (s)	15.4	1.05 (s)
19	12.6	0.69 (s)	12.8	0.71 (s)
20	37.8	1.38 (m)	42.2	2.06 (m)
21	19.7	0.94 (d)	21.9	1.05 (d, 7.2)
22	36.8	1.56 (m)	140.8	5.14 (dd, 15.2, 8.5)
		0.90 (m)		NA
23	29.4	1.63 (m)	128.5	5.05 (dd, 15.6, 9.5)
		0.71 (m)		NA
24	45.5	0.99 (m)	57.8	1.34 (m)
25	34.2		29.9 [a]	1.70 (m) [a]
26	27.9	0.86 (s)	22.3 [a]	0.86 (dd, 6.6, 1.6) [a]
27	27.9	0.86 (s)	19.8 [a]	0.80 (dd, 6.7, 4.7) [a]
28	15.1	0.83 (d)	29.9 [b]	1.70 (m) [b]
29	27.9	0.86 (s)	22.2 [b]	0.86 (dd, 6.6, 1.6) [b]
30	NA	NA	19.6 [b]	0.80 (dd, 6.7, 4.7) [b]

[a] Chemical shifts cannot be distinguished from those denoted by [b].

Supplementary Table 3.4

RPPA results of the eight BL-CL cell lines treated with DMSO or TLT.

Protein	Paired TTEST	DMSO Av	TLT Av	Mean diff DMSO-M4	% Change
AMPK-alpha_pT172	0.030926158	0.2468539	0.18237	0.06448569	-35.360163
14-3-3-epsilon	0.127055041	0.0924194	0.08764	0.004775493	-5.448744719
14-3-3-zeta	0.611359948	0.6997833	0.69274	0.007044538	-1.016911279
4E-BP1	0.88102686	0.2872652	0.286	0.001265921	-0.442630957
4E-BP1_pS65	0.688000793	0.6132918	0.60668	0.006608546	-1.089290952
4E-BP1_pT37_T46	0.052849589	0.7249001	0.83875	-0.11385355	13.57413446
53BP1	0.129295665	0.4471605	0.50738	-0.060216947	11.86827429
A-Raf	0.021802658	0.3242939	0.30103	0.023259764	-7.726620108
MAPK_pT202_Y204	0.063897497	0.3657461	0.27199	0.09375541	-34.47007848
ACC1	0.057831968	0.7090081	0.66169	0.047320333	-7.151459425
ACVRL1	0.204285214	0.0932188	0.09812	-0.004902111	4.995992268
ADAR1	0.722298854	0.1220255	0.12328	-0.001252066	1.015647984
Akt	0.019548209	0.572984	0.52345	0.04953045	-9.462243974
Akt_pS473	0.956418547	0.3849057	0.38686	-0.001955655	0.505518217
Akt_pT308	0.848831423	1.0898163	1.07076	0.019051852	-1.779275781
AMPK-alpha	0.494529968	0.8115008	0.82971	-0.01821201	2.194977551
FAK_pY397	0.080659613	0.0997996	0.08071	0.019094485	-23.65957935
ACC_pS79	0.023981823	0.6414503	0.51904	0.122410764	-23.5840916
Annexin-VII	0.479745507	0.1808896	0.19652	-0.015631946	7.954316733
AR	0.086105524	0.1613788	0.15309	0.008291424	-5.416139865
ARHI	0.374227021	0.0561487	0.0545	0.001644846	-3.017852599
ATM	0.310104666	0.1761461	0.17153	0.004614255	-2.690027967
ATM_pS1981	0.937022455	0.0777696	0.07816	-0.000390239	0.499282649
ATP5H	0.186610373	0.0743909	0.07776	-0.003372651	4.337059112
ATR	0.92837797	0.2607643	0.26007	0.000696483	-0.26780838
b-Catenin	0.584632507	0.6792402	0.71601	-0.036766439	5.134930087
b-Catenin_pT41_S45	0.070481607	0.1303322	0.13996	-0.009625835	6.877656406
B-Raf	0.032395628	1.009608	0.94963	0.059981572	-6.316333569
B-Raf_pS445	0.778696211	0.1716865	0.17297	-0.001285076	0.742940326
Bad_pS112	0.010420165	0.4945067	0.55515	-0.060640319	10.9232895
Bak	0.008721632	0.1909752	0.2054	-0.0144239	7.022377178
BAP1	0.259977565	0.2223549	0.21511	0.007244081	-3.367604315
Bax	0.343854359	0.3507281	0.36731	-0.016583733	4.514891461
Bcl-xL	0.13933645	0.5464368	0.57938	-0.032944392	5.68613386
Bcl2	0.422689711	0.0737728	0.07546	-0.001686947	2.235559768
Beclin	0.302512426	0.1887283	0.22117	-0.032440994	14.66794427
Bid	0.654051893	0.2214305	0.22455	-0.003117031	1.388138801
Bim	0.601368016	0.5163407	0.53035	-0.014011711	2.641962346
BRCA2	0.634796435	0.1778776	0.18588	-0.008002506	4.305198123
GAPDH	0.076587901	0.511228	0.41902	0.092207104	-22.00536928
c-Kit	0.137841447	0.1486842	0.15822	-0.009531557	6.024403154
c-Met	0.100343269	0.149599	0.14234	0.007259813	-5.100362748
c-Met_pY1234_Y1235	0.607157419	0.1791378	0.1818	-0.002660777	1.463584969
c-Myc	0.823539509	0.3123089	0.3083	0.00400808	-1.300054814

Supplementary Table 3.4 (continued)

Protein	Paired TTEST	DMSO Av	TLT Av	Mean diff DMSO-M4	% Change
C-Raf	0.00569841	0.2922268	0.26106	0.031170474	-11.94013341
C-Raf_pS338	0.181233222	0.4905809	0.45703	0.033551782	-7.341279215
Caspase-7-cleaved	0.199719195	0.0678278	0.07255	-0.004718936	6.504683391
Caspase-8	0.111844814	0.3088891	0.29177	0.017117839	-5.866869961
Caveolin-1	0.330102248	0.454963	0.44035	0.014615083	-3.31898519
CD29	0.347436034	0.031597	0.03009	0.001504719	-5.00034688
CD31	0.027495297	0.0240145	0.02141	0.002608377	-12.18521243
CD49b	0.000681184	0.090206	0.08321	0.006999799	-8.412591597
CDK1	0.527951409	0.2966172	0.30303	-0.006412135	2.116011117
Chk1	0.517023385	0.4436631	0.43806	0.005598172	-1.277931995
Stat3_pY705	0.061361639	0.288247	0.23968	0.048567263	-20.26340212
Chk2	0.900777361	0.3054057	0.30321	0.002196345	-0.724366013
Chk2_pT68	0.234845145	0.1516815	0.15712	-0.005434188	3.458717341
Claudin-7	0.838258667	0.5496062	0.53524	0.014368512	-2.684510622
Collagen-VI	0.581827632	0.1085949	0.09859	0.010000297	-10.14284249
Complex-II-Subunit	0.019357592	0.4883395	0.5321	-0.043759206	8.223889209
Cox-IV	0.21180139	0.0470478	0.04401	0.003040435	-6.908917587
p70-S6K_pT389	0.031044202	0.1669332	0.14084	0.026097196	-18.53020434
Cyclin-B1	0.047649153	1.5024802	1.70111	-0.19862495	11.67622972
Cyclin-D1	0.255149632	0.3947857	0.37585	0.018939256	-5.039094233
Cyclin-E1	0.471229306	0.3046325	0.2948	0.009828166	-3.333793248
Cyclophilin-F	0.588089846	1.2412809	1.12366	0.117620772	-10.4676463
DJ1	0.057596359	0.3065183	0.31909	-0.012574353	3.940658557
Dvl3	0.305796393	0.3631395	0.35437	0.008770662	-2.475009209
E-Cadherin	0.414543231	0.2309039	0.26116	-0.030252555	11.58407426
E2F1	0.465992121	0.0490497	0.05045	-0.001399862	2.774776277
eEF2	0.024329272	0.4482607	0.42437	0.023888806	-5.629214761
eEF2K	0.019692069	0.5732332	0.5177	0.055530627	-10.72635653
EGFR	0.694306782	0.6800515	0.66891	0.011142733	-1.665807521
Smac	0.20574698	0.4343177	0.36964	0.064677673	-17.4974742
EGFR_pY1173	0.30499704	0.1638452	0.17395	-0.010102281	5.80766297
eIF4E	0.125804471	0.8195001	0.79346	0.026037641	-3.28152156
eIF4G	0.878724419	1.035565	1.03183	0.003731644	-0.361651783
ER-alpha	0.504178772	0.0388962	0.0377	0.001192711	-3.163397879
ER-alpha_pS118	0.634911633	0.3953871	0.39946	-0.004070958	1.019120408
ERCC1	0.007891293	0.1646311	0.19196	-0.02732517	14.23510243
Ets-1	0.436109849	0.2073012	0.20972	-0.002419888	1.153860178
FAK	0.00596371	0.3746999	0.35153	0.023166155	-6.590023246
Chk1_pS345	0.012431443	0.2876721	0.24789	0.039780631	-16.0476008
FASN	0.010279931	0.7383777	0.68099	0.057383377	-8.426410979
Fibronectin	0.287511878	0.0348751	0.03279	0.002080442	-6.34384711
FoxM1	0.021099513	0.466201	0.42671	0.039490719	-9.254691723
FoxO3a	0.551797236	0.1353121	0.1374	-0.002085824	1.518089719
FoxO3a_pS318_S321	0.943894769	0.5589604	0.56027	-0.001312249	0.234216082
G6PD	0.228099421	0.0796185	0.07617	0.003448534	-4.52742041

Supplementary Table 3.4 (continued)

Protein	Paired TTEST	DMSO Av	TLT Av	Mean diff DMSO-M4	% Change
Gab2	0.129420955	0.2553089	0.24282	0.012488801	-5.143232028
EGFR_pY1068	0.28897535	0.0780788	0.09203	-0.013946575	15.15514849
GATA3	0.444543139	0.2890905	0.27977	0.009317527	-3.330389022
GCN5L2	0.581933997	0.4024414	0.41069	-0.008251661	2.009204067
GPBB	0.693848285	0.2242394	0.23134	-0.00710235	3.070067796
GSK-3ab	0.107780308	0.8094326	0.82645	-0.017016942	2.059041866
GSK-3ab_pS21_S9	0.550735827	0.6241206	0.64794	-0.023816819	3.675790205
GSK-3b_pS9	0.177310106	0.4761323	0.5083	-0.03216499	6.327988207
Gys	0.995834943	0.518761	0.51881	-5.10903E-05	0.009847553
Gys_pS641	0.541992189	0.3732588	0.36622	0.007043452	-1.923308627
HER2	0.263192338	0.0281805	0.02605	0.002128034	-8.16827614
NDRG1_pT346	0.168014205	0.3168807	0.37585	-0.05897111	15.68998963
HER3	0.192076665	0.2256087	0.20685	0.018756371	-9.06751822
HER3_pY1289	0.334961404	0.3471657	0.33777	0.009395071	-2.781494189
Heregulin	0.356306262	0.158463	0.16414	-0.005672826	3.456177062
HIAP	0.418473854	0.4569881	0.44928	0.00770568	-1.715108173
Histone-H3	0.859920263	0.1358833	0.13816	-0.002276057	1.647415041
IGF1R-beta	0.633604069	0.2032754	0.20619	-0.002917845	1.415102345
HER2_pY1248	0.104377998	0.0403153	0.04791	-0.0075911	15.8456832
INPP4b	0.224786181	0.1661943	0.16219	0.004006157	-2.470067174
IRS1	0.149211343	0.6053276	0.58946	0.015868518	-2.692047293
JAB1	0.551441944	0.0690752	0.06787	0.001201038	-1.769508052
JNK_pT183_Y185	0.622517253	0.1801214	0.18676	-0.006641022	3.555867298
JNK2	0.620583516	0.4413883	0.43619	0.005199641	-1.192062542
Lck	0.404041823	0.1615087	0.15269	0.008820444	-5.776766198
Annexin-I	0.202592026	0.2944506	0.35136	-0.056913782	16.19793713
Mcl-1	0.869330062	0.3021391	0.30475	-0.002608929	0.856093758
MDM2_pS166	0.184798884	0.4228332	0.43978	-0.016949566	3.854077221
MEK1	0.749093243	0.4931058	0.48759	0.005517333	-1.131555193
MEK1_pS217_S221	0.330871457	0.4264982	0.40648	0.020019075	-4.924994372
MEK2	0.046725637	0.262228	0.24935	0.012881695	-5.166185233
Merlin	0.110425164	0.6224777	0.57406	0.048420054	-8.434701674
MIG6	0.65818707	0.2714421	0.26646	0.004981295	-1.869428612
MSH2	0.232864132	0.7096262	0.69032	0.019305584	-2.796611216
MSH6	0.353124034	0.8008488	0.8208	-0.019953461	2.43097042
mTOR	0.10247673	1.0000496	0.97459	0.025457724	-2.612141883
mTOR_pS2448	0.535634771	0.5736505	0.58052	-0.006872585	1.183860668
Myosin-11	0.130662479	0.2516351	0.24104	0.010593952	-4.3950794
Myosin-IIa_pS1943	0.136330833	0.5590272	0.52052	0.038505586	-7.397499919
N-Cadherin	0.115979527	0.108239	0.0995	0.008736554	-8.780236006
N-Ras	0.424040717	0.0373128	0.03559	0.001720188	-4.83299624
NAPSIN-A	0.000244622	0.1888714	0.1789	0.009967334	-5.571328945
c-Jun_pS73	0.039255625	0.2882244	0.34707	-0.058847805	16.95549391
NF-kB-p65_pS536	0.700093069	0.5674735	0.54107	0.026404604	-4.880082075
Notch1	0.661226615	0.6396916	0.65434	-0.01464397	2.237990814

Supplementary Table 3.4 (continued)

Protein	Paired TTEST	DMSO Av	TLT Av	Mean diff DMSO-M4	% Change
p16INK4a	0.089057378	0.2589195	0.24097	0.017949144	-7.448692453
p21	0.072152138	0.589791	0.68726	-0.09746523	14.18179013
p27-Kip-1	0.101448071	0.1353413	0.12438	0.010959469	-8.811151583
p27_pT157	0.628732156	0.4132618	0.42135	-0.008085064	1.918861914
p27_pT198	0.015523921	0.380493	0.4207	-0.040209916	9.557793229
p38-alpha	0.00774209	0.3541716	0.32024	0.033932183	-10.59587949
p38	0.03267437	0.8570567	0.8278	0.029257917	-3.534423672
p38_pT180_Y182	0.002755169	0.4029123	0.52386	-0.120951629	23.08836548
p53	0.314234566	0.0975719	0.09485	0.002724253	-2.872240696
Snail	0.021853524	0.2435867	0.32022	-0.076637945	23.93255874
p70-S6K1	0.172006967	0.2027094	0.1965	0.006210831	-3.160751165
PAI-1	0.360871698	0.7728393	0.79675	-0.02391276	3.001280111
PARP-cleaved	0.118830095	0.0705842	0.06733	0.00325635	-4.836555963
PARP1	0.967407249	2.6880892	2.69449	-0.006399885	0.237517567
Paxillin	0.906536745	0.5151816	0.51694	-0.001762799	0.341003507
PCNA	0.06253059	0.2458135	0.23039	0.015419488	-6.692659587
Pdcd-1L1	0.112960284	0.1537748	0.21549	-0.061714605	28.63927851
Pdcd4	0.2306148	0.4398906	0.47403	-0.034134929	7.201073805
PDGFR-beta	0.638238272	0.7599954	0.79413	-0.034136002	4.298533004
PDK1	0.004328426	0.1989206	0.17397	0.024949699	-14.34130609
PDK1_pS241	0.010023724	0.4803055	0.44315	0.037151425	-8.38341026
PEA-15	0.575925151	0.4603699	0.4734	-0.013030284	2.752488295
PEA-15_pS116	0.07112505	0.4775941	0.51308	-0.035485327	6.91614747
PI3K-p110-alpha	0.045315699	0.3424673	0.32277	0.019699858	-6.103421879
PI3K-p85	0.209222646	0.2749676	0.27946	-0.004493387	1.607876193
PKC-alpha	0.896269303	0.7304674	0.7277	0.002768541	-0.380451526
PKC-alpha_pS657	0.795719345	0.4284552	0.43106	-0.002602363	0.603716011
PKC-beta-II_pS660	0.425784911	0.7686049	0.80879	-0.040182907	4.968287878
PKC-delta_pS664	0.045976568	0.3448394	0.36918	-0.024340036	6.593008843
PMS2	0.025956644	0.801951	0.74703	0.054920915	-7.351901528
Porin	0.243883965	0.0857229	0.08904	-0.003322	3.730702144
PR	0.663238212	0.1169763	0.11619	0.000789801	-0.679769967
PRAS40_pT246	0.365275156	0.8290985	0.86475	-0.035650351	4.122624665
PREX1	0.101304994	0.1049792	0.09812	0.006861336	-6.992955773
PTEN	0.782392774	0.1851321	0.18314	0.001988066	-1.085520762
Rab11	0.858096277	0.0879305	0.08734	0.000591986	-0.677806514
Rab25	0.332786784	0.1389058	0.13712	0.001783779	-1.300869619
Rad50	0.960424116	0.4113952	0.41097	0.000428285	-0.104213934
Rad51	0.024369829	0.1550382	0.13781	0.017233102	-12.50541433
Raptor	0.79377184	0.762859	0.75543	0.007433942	-0.984074094
Rb	0.533730146	0.2241153	0.2198	0.004313551	-1.962473631
Rb_pS807_S811	0.457540895	1.1841248	1.11809	0.066029881	-5.90557026
RBM15	0.957138438	0.4360402	0.43545	0.000592611	-0.13609247
Rictor	0.689051732	0.6479663	0.6408	0.007167023	-1.11845059
Rictor_pT1135	0.017269911	0.6853876	0.62371	0.061679537	-9.889167527

Supplementary Table 3.4 (continued)

Protein	Paired TTEST	DMSO Av	TLT Av	Mean diff DMSO-M4	% Change
RSK	0.147394136	0.4682432	0.45481	0.013431948	-2.953301246
S6_pS235_S236	0.09647995	1.2531184	1.40306	-0.149946424	10.68706343
S6_pS240_S244	0.118730496	0.8496313	0.94022	-0.090591207	9.635081836
SCD	0.759737499	0.0673423	0.06663	0.000707615	-1.061931555
SETD2	0.041455038	0.1748269	0.16728	0.007542015	-4.508486479
SF2	0.082190928	0.0562108	0.05337	0.002836706	-5.314761793
Shc_pY317	0.413441153	0.3421638	0.33226	0.009902927	-2.980467043
TAZ	0.293525898	0.4116032	0.58673	-0.175121832	29.8473411
Smad1	0.109784621	0.2190075	0.20699	0.012015241	-5.804681259
Smad3	0.042150885	0.5352521	0.5145	0.020756397	-4.034318757
Smad4	0.109781972	0.1975331	0.18686	0.01066866	-5.709304748
14-3-3-beta	0.297467434	0.1205898	0.17484	-0.054254273	31.03008862
Src	0.921787018	0.2637837	0.26281	0.000976124	-0.371421462
Src_pY416	0.208694232	0.1672131	0.15217	0.015041977	-9.884909758
Src_pY527	0.10778136	0.700054	0.642	0.05805016	-9.042026273
IGFBP2	0.004643877	0.1284908	0.19396	-0.065470005	33.7542394
Stat5a	0.004748425	0.5811547	0.52104	0.060117804	-11.53810864
Stathmin-1	0.452980835	0.1374042	0.14212	-0.004714313	3.317171496
Syk	0.804047646	0.2295709	0.22859	0.000979491	-0.428489726
Cox2	0.267016058	0.1049197	0.17838	-0.073460635	41.18203035
TFRC	0.45006093	0.5982809	0.62051	-0.022225227	3.581790061
TIGAR	0.203513955	0.4447832	0.43667	0.008111844	-1.857654354
Transglutaminase	0.347628428	0.3099899	0.31823	-0.008237679	2.588612494
TSC1	0.724792685	0.6995556	0.70621	-0.006652592	0.942015755
TTF1	0.072765875	0.4216622	0.40529	0.016367572	-4.038438288
Tuberin	0.007348867	1.2912628	1.17141	0.119849468	-10.23118546
Tuberin_pT1462	0.472275507	0.3208728	0.30659	0.014281069	-4.658009245
TWIST	0.026724298	0.0787599	0.07013	0.00863235	-12.30950185
Tyro3	0.148506776	0.2903453	0.26374	0.026606514	-10.08820479
UBAC1	0.084205337	0.4482809	0.42428	0.023999931	-5.656613047
UGT1A	0.129590932	0.0798728	0.07732	0.002550457	-3.298473152
UQCRC2	0.968988613	0.097701	0.09758	0.000124445	-0.127535891
VEGFR-2	0.399973553	0.4634747	0.45786	0.005619443	-1.227340541
XRCC1	0.599402963	0.4539372	0.45771	-0.003775075	0.824770285
YAP	0.389819715	0.3792817	0.38599	-0.006706443	1.737473896
YAP_pS127	0.786380304	0.7320844	0.73928	-0.007192785	0.972948256
YB1	0.055196453	0.6676773	0.7363	-0.068626495	9.320405293
YB1_pS102	0.019015082	0.6649866	0.78032	-0.11532871	14.77975748

3.7 References

1. Perou CM, Sorlie T, Eisen MB, van de Rijn M, Jeffrey SS, et al. (2000) Molecular portraits of human breast tumours. Nature 406: 747-752.

2. Sorlie T, Perou CM, Tibshirani R, Aas T, Geisler S, et al. (2001) Gene expression patterns of breast carcinomas distinguish tumor subclasses with clinical implications. Proc Natl Acad Sci U S A 98: 10869-10874.

3. Prat A, Parker JS, Karginova O, Fan C, Livasy C, et al. (2010) Phenotypic and molecular characterization of the claudin-low intrinsic subtype of breast cancer. Breast Cancer Res 12: R68.

4. Prat A, Perou CM (2011) Deconstructing the molecular portraits of breast cancer. Mol Oncol 5: 5-23.

5. Rouzier R, Perou CM, Symmans WF, Ibrahim N, Cristofanilli M, et al. (2005) Breast cancer molecular subtypes respond differently to preoperative chemotherapy. Clin Cancer Res 11: 5678-5685.

6. Perou CM (2010) Molecular stratification of triple-negative breast cancers. Oncologist 15 Suppl 5: 39-48.

7. Eroles P, Bosch A, Perez-Fidalgo JA, Lluch A (2012) Molecular biology in breast cancer: intrinsic subtypes and signaling pathways. Cancer Treat Rev 38: 698-707.

8. Parker JS, Mullins M, Cheang MC, Leung S, Voduc D, et al. (2009) Supervised risk predictor of breast cancer based on intrinsic subtypes. J Clin Oncol 27: 1160-1167.

9. Perou CM, Borresen-Dale AL (2011) Systems biology and genomics of breast cancer. Cold Spring Harb Perspect Biol 3.

10. Herschkowitz JI, Simin K, Weigman VJ, Mikaelian I, Usary J, et al. (2007) Identification of conserved gene expression features between murine mammary carcinoma models and human breast tumors. Genome Biol 8: R76.

11. Bugni TS, Richards B, Bhoite L, Cimbora D, Harper MK, et al. (2008) Marine natural product libraries for high-throughput screening and rapid drug discovery. J Nat Prod 71: 1095-1098.

12. Bugni TS, Harper MK, McCulloch MWB, Reppart J, Ireland CM (2008) Fractionated marine invertebrate extract libraries for drug discovery. Molecules 13: 1372-1383.

13. Newman DJ, Cragg GM (2012) Natural products as sources of new drugs over the 30 years from 1981 to 2010. J Nat Prod 75: 311-335.

14. Mayer AM, Glaser KB, Cuevas C, Jacobs RS, Kem W, et al. (2010) The odyssey of marine pharmaceuticals: a current pipeline perspective. Trends Pharmacol Sci 31: 255-265.

15. Ortholand JY, Ganesan A (2004) Natural products and combinatorial chemistry: back to the future. Curr Opin Chem Biol 8: 271-280.

16. Bindseil KU, Jakupovic J, Wolf D, Lavayre J, Leboul J, et al. (2001) Pure compound libraries; a new perspective for natural product based drug discovery. Drug Discov Today 6: 840-847.

17. Grabowski K, Baringhaus KH, Schneider G (2008) Scaffold diversity of natural products: inspiration for combinatorial library design. Nat Prod Rep 25: 892-904.

18. Veber DF, Johnson SR, Cheng HY, Smith BR, Ward KW, et al. (2002) Molecular properties that influence the oral bioavailability of drug candidates. J Med Chem 45: 2615-2623.

19. Molinski TF, Dalisay DS, Lievens SL, Saludes JP (2009) Drug development from marine natural products. Nat Rev Drug Discov 8: 69-85.

20. Tibes R, Qiu Y, Lu Y, Hennessy B, Andreeff M, et al. (2006) Reverse phase protein array: validation of a novel proteomic technology and utility for analysis of primary leukemia specimens and hematopoietic stem cells. Mol Cancer Ther 5: 2512-2521.

21. Iadevaia S, Lu Y, Morales FC, Mills GB, Ram PT (2010) Identification of optimal drug combinations targeting cellular networks: integrating phospho-proteomics and computational network analysis. Cancer Res 70: 6704-6714.

22. Cancer Genome Atlas Research N, Weinstein JN, Collisson EA, Mills GB, Shaw KR, et al. (2013) The Cancer Genome Atlas Pan-Cancer analysis project. Nat Genet 45: 1113-1120.

23. Wang K, Singh D, Zeng Z, Coleman SJ, Huang Y, et al. (2010) MapSplice: accurate mapping of RNA-seq reads for splice junction discovery. Nucleic Acids Res 38: e178.

24. Li B, Dewey CN (2011) RSEM: accurate transcript quantification from RNA-Seq data with or without a reference genome. BMC Bioinformatics 12: 323.

25. Love MI, Huber W, Anders S (2014) Moderated estimation of fold change and dispersion for RNA-Seq data with DESeq2. BioRxiv. http://dx.doi.org/10.1101/002832

26. R Development Core Team. (2014) R: A Language and Environment for Statistical Computing. Vienna, Austria: R Foundation for Statistical Computing.

27. Liao Y, Smyth GK, Shi W (2013) The subread aligner: fast, accurate and scalable read mapping by seed-and-vote. Nucleic Acids Res 41: e108.

28. West M, Blanchette C, Dressman H, Huang E, Ishida S, et al. (2001) Predicting the clinical status of human breast cancer by using gene expression profiles. Proc Natl Acad Sci U S A 98: 11462-11467.

29. Cohen AL, Soldi R, Zhang H, Gustafson AM, Wilcox R, et al. (2011) A pharmacogenomic method for individualized prediction of drug sensitivity. Mol Syst Biol 7: 513.

30. Benito M, Parker J, Du Q, Wu J, Xiang D, et al. (2004) Adjustment of systematic microarray data biases. Bioinformatics 20: 105-114.

31. Fusetani N, Matsunaga S, Konosu S (1981) Bioactive marine metabolites II. Halistanol sulfate, as antimicrobial novel steroid sulfate from the marine sponge Halichondria cf. moorei Bergquist. Tetrahedron Lett 22.

32. Dai J, Sorribas A, Yoshida WY, Kelly M, Williams PG (2010) Topsentinols, 24-isopropyl steroids from the marine sponge Topsentia sp. J Nat Prod 73: 1597-1600.

33. Lizcano JM, Goransson O, Toth R, Deak M, Morrice NA, et al. (2004) LKB1 is a master kinase that activates 13 kinases of the AMPK subfamily, including MARK/PAR-1. EMBO J 23: 833-843.

34. Ha J, Daniel S, Broyles SS, Kim KH (1994) Critical phosphorylation sites for acetyl-CoA carboxylase activity. J Biol Chem 269: 22162-22168.

35. Jiang K, Pereira E, Maxfield M, Russell B, Goudelock DM, et al. (2003) Regulation of Chk1 includes chromatin association and 14-3-3 binding following phosphorylation on Ser-345. J Biol Chem 278: 25207-25217.

36. Albiges L, Goubar A, Scott V, Vicier C, Lefebvre C, et al. (2014) Chk1 as a new therapeutic target in triple-negative breast cancer. Breast 23: 250-258.

37. Cai B, Chang SH, Becker EB, Bonni A, Xia Z (2006) p38 MAP kinase mediates apoptosis through phosphorylation of BimEL at Ser-65. J Biol Chem 281: 25215-25222.

38. Martin SA, Ouchi T (2008) Cellular commitment to reentry into the cell cycle after stalled DNA is determined by site-specific phosphorylation of Chk1 and PTEN. Mol Cancer Ther 7: 2509-2516.

39. Zhou G, Myers R, Li Y, Chen Y, Shen X, et al. (2001) Role of AMP-activated protein kinase in mechanism of metformin action. J Clin Invest 108: 1167-1174.

40. McNeely S, Beckmann R, Bence Lin AK (2014) CHEK again: revisiting the development of CHK1 inhibitors for cancer therapy. Pharmacol Ther 142: 1-10.

41. Omberg L, Ellrott K, Yuan Y, Kandoth C, Wong C, et al. (2013) Enabling transparent and collaborative computational analysis of 12 tumor types within The Cancer Genome Atlas. Nat Genet 45: 1121-1126.

42. Hardie DG, Carling D, Gamblin SJ (2011) AMP-activated protein kinase: also regulated by ADP? Trends Biochem Sci 36: 470-477.

43. Faubert B, Vincent EE, Poffenberger MC, Jones RG (2014) The AMP-activated protein kinase (AMPK) and cancer: many faces of a metabolic regulator. Cancer Lett.

44. Shackelford DB, Shaw RJ (2009) The LKB1-AMPK pathway: metabolism and growth control in tumour suppression. Nat Rev Cancer 9: 563-575.

45. Pierotti MA, Berrino F, Gariboldi M, Melani C, Mogavero A, et al. (2013) Targeting metabolism for cancer treatment and prevention: metformin, an old drug with multi-faceted effects. Oncogene 32: 1475-1487.

46. Liu X, Chhipa RR, Pooya S, Wortman M, Yachyshin S, et al. (2014) Discrete mechanisms of mTOR and cell cycle regulation by AMPK agonists independent of AMPK. Proc Natl Acad Sci U S A 111: E435-444.

47. Rios M, Foretz M, Viollet B, Prieto A, Fraga M, et al. (2013) AMPK activation by oncogenesis is required to maintain cancer cell proliferation in astrocytic tumors. Cancer Res 73: 2628-2638.

48. Park HU, Suy S, Danner M, Dailey V, Zhang Y, et al. (2009) AMP-activated protein kinase promotes human prostate cancer cell growth and survival. Mol Cancer Ther 8: 733-741.

49. Yu PB, Hong CC, Sachidanandan C, Babitt JL, Deng DY, et al. (2008) Dorsomorphin inhibits BMP signals required for embryogenesis and iron metabolism. Nat Chem Biol 4: 33-41.

50. Cancer Genome Atlas Research N (2014) Comprehensive molecular characterization of urothelial bladder carcinoma. Nature 507: 315-322.

CHAPTER 4

DISCUSSION

4.1 Summary of Findings

This dissertation work identifies two novel therapeutic strategies personalized against two different complex cancer phenotypes using genomic classification and high-throughput drug screening. In Chapter 2, we showed the importance of incorporating global assessment of RAS pathway activity as means to classify the RAS-active NSCLC subtype. This allowed the grouping of NSCLC according to global activation status of the RAS pathway (independent of histological subtyping and RAS mutation) and permitting the identification of EGFR and MEK co-inhibition as a personalized treatment against this molecular subpopulation. Furthermore, this study provided strong evidence on the limitations of tailoring targeted therapeutics to tumors expressing particular mutations, as KRAS mutation status, 1) failed to predict EGFR+MEK co-inhibition treatment response, 2) did not account for RAS-active NSCLC without a KRAS mutation, 3) left out a large population of NSCLC tumor cells with wild-type KRAS sensitive to the treatment. Through the use of a RAS gene-expression signature as a predictor of RAS pathway activation, we were able to classify NSCLC cells based on their RAS pathway activity profile. This allowed the identification of a therapy particularly effective against NSCLC cells with an active RAS pathway, independent of KRAS mutation status. Indeed, the signature succeeded as a biomarker of response to co-inhibition of EGFR and MEK where KRAS mutation status failed.

In Chapter 3, we addressed the need for therapeutic options in the BL-CL complex cancer phenotype by identifying a novel natural product personalized against this molecular subtype. To identify BL-CL tumor cells, we classified breast cancer cell lines genomically by utilizing the intrinsic molecular subtyping of breast cancer, based on gene-expression profiles [1]. This chapter describes a step-wise process of drug screening crude fractions and isolating the active compounds to identify a novel therapeutic leads personalized against BL-CL. This study identified

a previously uncharacterized sulfated sterol, TLT, capable of inhibiting both AMPK and CHK, a targeting strategy that was also identified to be particularly effective against BL-CL. Furthermore, following the generation of a TLT sensitivity gene-expression signature and the projection across a dataset of diverse human tumors, bladder cancer predicted to be as equally sensitive to TLT as breast cancer. Indeed, bladder cancer harbors frequent deregulation in the AMPK and CHK1 pathways. In summary, the results described in these chapters highlight the importance of the incorporation of cancer genomics and personalized medicine in cancer drug discovery as means to identify effective treatments against complex cancer phenotypes.

4.2 Personalized Medicine in Cancer Should Not Exclusively Depend on Mutations

The landscape of small molecule therapy in cancer has been revolutionized dramatically over the last decade. This coincided with a move from a one-size-fits-all strategy that emphasized cytotoxic chemotherapy to a more personalized medicine approach that focuses on the identifying molecularly targeted drugs that exploit the particular genetic vulnerabilities of cancer cells [2]. Currently, the field of personalized medicine in cancer is strongly dependent on the identification of single gene modifications as predictive biomarkers of therapy response. This approach involves tailoring targeted therapeutics to particular aberrant modifications of single genes that include translocation, copy number increase and mutations [3]. The ABL inhibitor imatinib is widely regarded as the pioneer drug that validated the concept of designing a small molecule to treat a specified patient population [2]. Indeed, when imatinib was given to chronic myeloid leukaemia patients (in which the malignancy is driven by the BCR-ABL translocation), the recorded improvement in survival was dramatic [4,5]. Further success was observed with

the initial pioneering study linking the HER2 monoclonal antibody trastuzumab to breast tumors overexpressing HER2 [6,7]. Mutations haven taken center stage since then, with the observations that EGFR and ALK-MET inhibitors in NSCLC, and the BRAF inhibitor vemurafenib were particularly effective against tumors harboring mutations in those proteins [8-10]. Indeed, today we recognize that the successful use of targeted therapy in cancer is reliant on predictive biomarkers of response for the purposes of patient selection. As such, in the era of personalized cancer medicine, companion diagnostics have become crucial in tailoring the ideal therapeutic to a particular patient [3]. This is particularly the case for cancers that are driven by complex signaling pathways that are difficult to target, such as RAS-active NSCLC. Problems arise when trying to characterize RAS pathway activation based solely on the mutation status of the RAS protein. This is due to the fact that the presence of mutated RAS does not necessarily indicate an oncogenic addiction to the RAS pathway. Indeed, previous observations have shown that KRAS dependency is widely variable in KRAS mutant cancer cell lines. Therefore, cancer cells may harbor an activating mutation in RAS, but not necessarily be addicted and dependent on the continual signaling of the pathway [11]. This has been observed in cancer cells carrying an activating mutation in KRAS but still exhibiting low overall RAS pathway activation, an observation recorded in Chapter 2 of this dissertation and by the work of others [12]. Furthermore, the lack of an activation mutation on RAS does not imply that the network is off as additional components of the network such as EGFR, PDGFR and IGFR that are upstream of RAS can be activated, leading to the initiation of RAS pathway signal transduction [13-17]. Thus, focusing on a single protein of a large network composed of many components might limit the ability to accurately reflect activity [18]. Indeed, this is observed in Chapter 2 where we identify a panel of KRAS wild-type cancer lines characterized by an activated RAS pathway through gene-expression profiling of

pathway activation. It will be critical in future clinical trials to identify those tumors that are RAS-active, independent of the mechanism of RAS activation. By using mutation analysis alone, one overlooks a large population of tumors that do not carry particular mutations yet harbor activated oncogenic pathways. Therefore, the benefit of a particular treatment is lost on a large population of patients. As an example, there are currently clinical trials recruiting patients for EGFR + MEK inhibitor combinations based solely on RAS mutation status. The results presented in Chapter 2 suggest that using mutation status as a biomarker for that treatment 1) fails as a biomarker of response in NSCLC and 2) does not provide optimal selection of responsive patients by leaving out patients diagnosed with KRAS wild type NSCLC tumors with an active RAS pathway. Through a more comprehensive genomic characterization of patients with deregulated pathway independent of the mechanism of activation, it may be possible to optimize selection of patients for clinical trial inclusion.

4.3 Identifying Compounds Effective Against Tumor Subpopulations

The ultimate goal of drug discovery in cancer is to eradicate malignant cells while minimizing adverse effects on normal cells. The main strategy to achieve this goal involves exploiting differences in the activity or expression of the molecular targets driving cancer-specific cellular phenotypes in cancer cells as compared to normal cells. However, this is complicated by the inherent genomic heterogeneity of cancer. This creates diversity in the molecular drivers among tumors and makes the treatment of cancer require a much larger repertoire of drugs than the majority of other diseases [19].

Various drug discovery approaches have been used to build the armamentarium necessary to treat cancer, ranging from hypothesis-driven

screening (targeting identified oncogenic drivers such as EGFR or HER2), to phenotype screening (identifying drugs effective against cellular phenotypes without regard for mechanism). Given our growing understanding of the molecular characteristics and weaknesses of cancer, pursuing hypothesis-driven targeted therapies has been a scientifically and logically appealing method [19]. This is reflected by the current predominant use of that approach in the field of cancer drug discovery. However, this target-based discovery in oncology has witnessed many challenges and limitations. Despite the large number of targeted agents approved and in clinical development, there have been very few instances of “magic bullets,” where a single target drives the cancer phenotype, as exemplified by imatinib’s exquisite effectiveness against BCR–ABL-driven chronic myeloid leukaemia [20]. Often, the signaling mediators targeted are nodes in complex signaling networks in which redundancy, compensatory crosstalk and feedback loops tend to reduce the predicted impact of a single targeted inhibitor. This contributes to the high failure rate of targeted therapeutics owing to insufficient efficacy in clinical trials [21]. On the other hand, phenotypic screening in general avoids oversimplified reductionist assumptions regarding molecular targets and instead focuses on functional effects; compounds that are discovered in phenotypic assays may be more likely to show clinical efficacy [19,22] . Indeed, the goal of this dissertation is to identify therapeutic leads effective against particular complex cancer phenotypes first and foremost, and then identify their mechanism of action. Through this top-down approach, we are able to identify therapeutic leads, and the tumor subpopulation they are most effective against. This is particularly possible with the use of genomic classification of tumors, which allows the segregation of the heterogeneous cancers into groups with similar molecular characteristics. Indeed, we show this in Chapters 2 and 3 where we classify a RAS-active phenotype from NSCLC, and the BL-CL phenotype in breast cancer. For both these molecular subpopulations, we identified effective

therapeutic leads tailored specifically against them. Clinically, the ideal patient population has theoretically been identified, and effective therapeutics described. Further work is necessary to validate the findings, as discussed in the next section of this chapter.

4.4 Future Directions

The incorporation of gene expression molecular classification of cancer makes up the cornerstone of the work described in this dissertation. The ultimate goal of such classification is the identification of treatments personalized against particular molecular subtypes. Chapter 2 describes the use of a RAS gene expression signature as a biomarker of pathway activity and classifier of RAS-active NSCLC. Chapter 3 utilizes the gene expression signature classification system pioneered by Perou et al. to subtype breast cancer tumors based on molecular attributes [1,23]. This dissertation shows the successful implementation of such an approach in cancer drug discovery in a research setting; however, this method was not investigated as a possible clinic tool. One way to address this would be to obtain a panel of patient NSCLC samples and analyze them for RAS pathway activation using the same methodology described in Chapter 2. This would then be followed by concurrent treatment with EGFR and MEK inhibitors, for the purpose of correlating treatment effectiveness to RAS pathway activation in the context of patient tumors. A similar approach could be used for the observation recorded in Chapter 3 regarding BL-CL breast cancer sensitivity to TLT and AMPK/CHK1 inhibitors. Patient breast cancer samples can be classified according to the intrinsic molecular subtypes patient breast cancer samples, and the BL-CL samples examined for TLT and AMPK/CHK1 inhibitor sensitivity. However, future work will still need to validate the in vitro cell culture findings in preclinical in vivo models of NSCLC and breast cancer. To validate the findings of Chapter 2 in a

mouse model, it would be necessary to use a model of lung cancer development that generates KRAS mutant and wild-type tumors. One such model would be the 4-(methylnitrosamino)-1-(3-pyridyl)-1-butanone (NNK) lung carcinogenesis murine model. NNK reproducibly induces pulmonary adenocarcinomas in laboratory rodents through KRAS mutation or the activation of EGFR, AKT and MAPK pathways [24,25]. To validate the Chapter 3 findings, the EF1α-PyMT10C breast carcinogenesis mouse model could be used since it is able to generate both luminal and basal-like tumors in nearly equal ratios [26]. For both these models, tumors could be biopsied and analyzed for molecular classification. Treatment would follow, and the results analyzed for the observation of the same correlation between BL-CL and RAS-active NSCLC sensitivity to EGFR+MEK and TLT or AMPK/CHK1 inhibition, respectively.

The challenges of incorporating gene expression profiling in the clinic have been mitigated by the recent advances and successes of incorporating microarray diagnostics. Indeed, gene-expression signatures have recently made their way into the clinical and commercial sectors, laying the ground for the introduction of future gene expression signatures into the clinic [27]. One example is the FDA-approved microarray-based gene expression profiling signature Mammaprint®, which uses frozen archived tissue as source material or tissue core sampled on fresh specimens preserved in RNA later to score the low/high risk of tumor metastasis [27-29]. Therefore, the application of a gene-expression signature as a genomic biomarker of RAS pathway activation as described in Chapter 2 is both promising and feasible in the clinic. Overall, our results show the significant correlation between RAS pathway activity and response to EGFR+MEK inhibition, and the predictive power of our signature which is independent of other factors such as cancer subtype of mutations in key pathway components. In the clinic, the RAS-gene expression signature could be used to assess RAS pathway activation

status in a patient's tumor. If the tumor has high pathway activity, that patient may be a candidate to receive EGFR+MEK dual inhibition. Indeed, the clinical potential of our study is supported by the validation of our observed correlation of RAS pathway activation and EGFR+MEK dual inhibition using FDA-approved inhibitors trametinib and erlotinib [30,31].

Furthermore, a practical application of classifying breast tumors based on their molecular subtypes has recently made its way into the clinic in the form of the FDA-approved PAM50 gene signature. This signature measures the expression levels of 50 genes in surgically resected breast tumors with the purpose of classifying them according to one of the four intrinsic subtypes (Luminal A, Luminal B, HER2-enriched, and Basal-like) [32,33]. In addition to identifying a tumor's intrinsic subtype, the PAM50 signature generates a personalized score estimating patient probability of cancer recurrence by weighting the molecular subtype correlations, a subset of proliferation genes, and tumor size. This signature uses multiplexed fluorescently-labeled probe pairs to measure gene expression in frozen or formalin-fixed paraffin-embedded (FFPE) tissues [33]. The availability of this signature in the clinic makes it feasible to subtype breast cancer tumors molecularly, in order to identify Basal-like tumors and tailor effective treatments.

The discovery and identification of TLT in Chapter 3 is an exciting finding. This sulfated sterol, isolated from the marine topsentia species sponge, exhibits preferential tumoricidal effectiveness against BL-CL breast cancer, in comparison to Luminal and HER2+ tumors. Mechanistically, TLT was observed to inhibit both AMPK and CHK1 effectively. The importance of inhibiting AMPK and CHK1 in BL-CL breast cancer was validated by investigating the effects of AMPK, CHK1 and AMPK1+CHK1 small molecule targeted inhibition on a panel of breast cancer cell lines. Twenty breast cancer cell lines were treated with dorsomorphin C, an AMPK inhibitor [34], Ly2603618, a CHK1 inhibitor in phase 2 clinical trials [35],

and the combination of both together. Results showed that treating BL-CL breast cancer with either treatment strategy is significantly more effective against the subtype than Luminal/HER2+ breast cancer. This validates the importance of the inhibitory effects of TLT on AMPK and CHK1 in BL-CL breast cancer, and suggests the potential use of AMPK or CHK1 inhibition as a treatment for BL-CL breast cancer. However, further work is required to strengthen these findings. Although dorsomorphin c is a potent AMPK inhibitor, this compound has been shown to have high affinity towards other proteins such as BMP and ALK [36]. Unfortunately, no exclusive inhibitor of AMPK exists currently. As such, future work will have to investigate the importance of AMPK signaling in BL-CL by knocking down AMPK using siRNA or shRNA.

Clinically, there are no available AMPK inhibitors. However, the CHK1 inhibitor used in the work described in Chapter 3, Ly2603618, is in phase 2 clinical trials and could be a treatment option in the near future. PAM50 molecular subtyping of patient tumors could be used to tailor CHK1 inhibitor therapy to those diagnosed with Basal breast cancers. Alternatively, CHK1 targeted therapy could be tailored to patients diagnosed with triple negative breast cancers, which frequently overlap with BL-CL breast cancers [37,38].

In conclusion, the work presented in this dissertation discusses the feasibility of incorporating cancer genomics in cancer drug discovery for the purpose of identifying personalized medicine treatment strategies. Particularly, this approach has been successful in identifying novel treatment options for two complex cancer phenotypes that have been difficult to treat and identify therapeutic leads for. The findings lay the foundation for future studies regarding the potential of EGFR+MEK co-inhibition as a treatment for RAS-active NSCLC, and TLT or AMPK/CHK1 inhibition as a candidate therapy against BL-CL.

4.5 References

1. Perou CM, Borresen-Dale AL (2011) Systems biology and genomics of breast cancer. Cold Spring Harb Perspect Biol 3.

2. Hoelder S, Clarke PA, Workman P (2012) Discovery of small molecule cancer drugs: successes, challenges and opportunities. Mol Oncol 6: 155-176.

3. Gonzalez de Castro D, Clarke PA, Al-Lazikani B, Workman P (2013) Personalized cancer medicine: molecular diagnostics, predictive biomarkers, and drug resistance. Clin Pharmacol Ther 93: 252-259.

4. O'Brien SG, Guilhot F, Larson RA, Gathmann I, Baccarani M, et al. (2003) Imatinib compared with interferon and low-dose cytarabine for newly diagnosed chronic-phase chronic myeloid leukemia. N Engl J Med 348: 994-1004.

5. Druker BJ, Guilhot F, O'Brien SG, Gathmann I, Kantarjian H, et al. (2006) Five-year follow-up of patients receiving imatinib for chronic myeloid leukemia. N Engl J Med 355: 2408-2417.

6. Romond EH, Perez EA, Bryant J, Suman VJ, Geyer CE, Jr., et al. (2005) Trastuzumab plus adjuvant chemotherapy for operable HER2-positive breast cancer. N Engl J Med 353: 1673-1684.

7. Slamon DJ, Leyland-Jones B, Shak S, Fuchs H, Paton V, et al. (2001) Use of chemotherapy plus a monoclonal antibody against HER2 for metastatic breast cancer that overexpresses HER2. N Engl J Med 344: 783-792.

8. Kwak EL, Bang YJ, Camidge DR, Shaw AT, Solomon B, et al. (2010) Anaplastic lymphoma kinase inhibition in non-small-cell lung cancer. N Engl J Med 363: 1693-1703.

9. Chapman PB, Hauschild A, Robert C, Haanen JB, Ascierto P, et al. (2011) Improved survival with vemurafenib in melanoma with BRAF V600E mutation. N Engl J Med 364: 2507-2516.

10. Rosell R, Carcereny E, Gervais R, Vergnenegre A, Massuti B, et al. (2012) Erlotinib versus standard chemotherapy as first-line treatment for European patients with advanced EGFR mutation-positive non-small-cell lung cancer (EURTAC): a multicentre, open-label, randomised phase 3 trial. Lancet Oncol 13: 239-246.

11. Singh A, Greninger P, Rhodes D, Koopman L, Violette S, et al. (2009) A gene expression signature associated with "K-RAS addiction" reveals regulators of EMT and tumor cell survival. Cancer Cell 15: 489-500.

12. Loboda A, Nebozhyn M, Klinghoffer R, Frazier J, Chastain M, et al. (2010) A gene expression signature of RAS pathway dependence predicts response to

PI3K and RAS pathway inhibitors and expands the population of RAS pathway activated tumors. BMC Med Genomics 3: 26.

13. Ono M, Kuwano M (2006) Molecular mechanisms of epidermal growth factor receptor (EGFR) activation and response to gefitinib and other EGFR-targeting drugs. Clin Cancer Res 12: 7242-7251.

14. Chan TW, Pollak M, Huynh H (2001) Inhibition of insulin-like growth factor signaling pathways in mammary gland by pure antiestrogen ICI 182,780. Clin Cancer Res 7: 2545-2554.

15. Innocenti M, Tenca P, Frittoli E, Faretta M, Tocchetti A, et al. (2002) Mechanisms through which Sos-1 coordinates the activation of RAS and RAC. J Cell Biol 156: 125-136.

16. Bazenet C, Kazlauskas A (1993) The PDGF receptor a subunit activates p21r- and triggers DNA synthesis without interacting with rasGAP. Oncogene 9: 517-525.

17. Repasky GA, Chenette EJ, Der CJ (2004) Renewing the conspiracy theory debate: does RAF function alone to mediate RAS oncogenesis? Trends Cell Biol 14: 639-647.

18. Downward J (2006) Cancer biology: signatures guide drug choice. Nature 439: 274-275.

19. Moffat JG, Rudolph J, Bailey D (2014) Phenotypic screening in cancer drug discovery - past, present and future. Nat Rev Drug Discov 13: 588-602.

20. Capdeville R, Buchdunger E, Zimmermann J, Matter A (2002) Glivec (STI571, imatinib), a rationally developed, targeted anticancer drug. Nat Rev Drug Discov 1: 493-502.

21. Williams R (2013) Discontinued drugs in 2012: oncology drugs. Expert Opin Investig Drugs 22: 1627-1644.

22. Ellis LM, Fidler IJ (2010) Finding the tumor copycat. Therapy fails, patients don’t. Nat Med 16: 974-975.

23. Perou CM, Sorlie T, Eisen MB, van de Rijn M, Jeffrey SS, et al. (2000) Molecular portraits of human breast tumours. Nature 406: 747-752.

24. Zheng HC, Takano Y (2011) NNK-Induced Lung tumors: a review of animal model. J Oncol 2011: 635379.

25. Granville CA, Warfel N, Tsurutani J, Hollander MC, Robertson M, et al. (2007) Identification of a highly effective rapamycin schedule that markedly reduces the size, multiplicity, and phenotypic progression of tobacco carcinogen-induced

murine lung tumors. Clin Cancer Res 13: 2281-2289.

26. Smith BA, Shelton DN, Kieffer C, Milash B, Usary J, et al. (2012) Targeting the PyMT oncogene to diverse mammary cell populations enhances tumor heterogeneity and generates rare breast cancer subtypes. Genes Cancer 3: 550-563.

27. Arpino G, Generali D, Sapino A, Del Matro L, Frassoldati A, et al. (2013) Gene expression profiling in breast cancer: a clinical perspective. Breast 22: 109-120.

28. van de Vijver MJ, He YD, van't Veer LJ, Dai H, Hart AA, et al. (2002) A gene-expression signature as a predictor of survival in breast cancer. N Engl J Med 347: 1999-2009.

29. van 't Veer LJ, Dai H, van de Vijver MJ, He YD, Hart AA, et al. (2002) Gene expression profiling predicts clinical outcome of breast cancer. Nature 415: 530-536.

30. United States Food and Drug Administration. (2013) Trametinib.

31. United States Food and Drug Administration. (2013) Erlotinib.

32. Parker JS, Mullins M, Cheang MC, Leung S, Voduc D, et al. (2009) Supervised risk predictor of breast cancer based on intrinsic subtypes. J Clin Oncol 27: 1160-1167.

33. Nielsen T, Wallden B, Schaper C, Ferree S, Liu S, et al. (2014) Analytical validation of the PAM50-based prosigna breast cancer prognostic gene signature assay and nCounter analysis system using formalin-fixed paraffin-embedded breast tumor specimens. BMC Cancer 14: 177.

34. Zhou G, Myers R, Li Y, Chen Y, Shen X, et al. (2001) Role of AMP-activated protein kinase in mechanism of metformin action. J Clin Invest 108: 1167-1174.

35. McNeely S, Beckmann R, Bence Lin AK (2014) CHEK again: revisiting the development of CHK1 inhibitors for cancer therapy. Pharmacol Ther 142: 1-10.

36. Yu PB, Hong CC, Sachidanandan C, Babitt JL, Deng DY, et al. (2008) Dorsomorphin inhibits BMP signals required for embryogenesis and iron metabolism. Nat Chem Biol 4: 33-41.

37. Albiges L, Goubar A, Scott V, Vicier C, Lefebvre C, et al. (2014) Chk1 as a new therapeutic target in triple-negative breast cancer. Breast 23: 250-258.

38. Eroles P, Bosch A, Perez-Fidalgo JA, Lluch A (2012) Molecular biology in breast cancer: intrinsic subtypes and signaling pathways. Cancer Treat Rev 38: 698-707.